TÉCNICO LISBOA

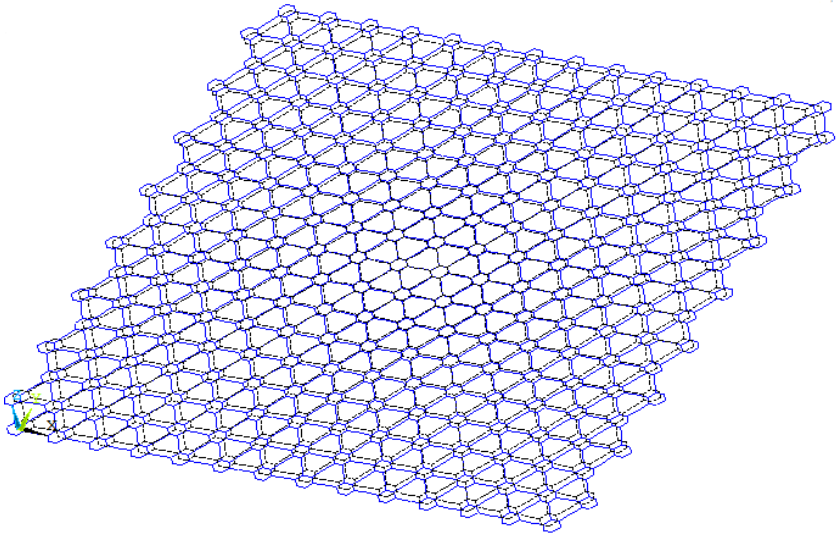

Nanomaterials for Aerospace Applications: the Mechanical Behavior of Graphyne

Ricardo Miguel Carneiro do Couto

Thesis to obtain the Master of Science Degree in

Aerospace Engineering

Supervisor: Prof. Nuno Miguel Rosa Pereira Silvestre

Examination Committee

Chairperson: Prof. Filipe Szolnoky Ramos Pinto Cunha
Supervisor: Prof. Nuno Miguel Rosa Pereira Silvestre
Member of the Committee: Prof. Augusto Manuel Moura Moita de Deus

November 2015

Acknowledgements

I would like to thank my supervisor, Prof. Nuno Silvestre, for introducing and guiding me through the journey it was doing this thesis.

I also would like to express my gratitude to every professor who gave me the amount of wisdom I could never possess, weren't the time they spent teaching me along my master course at Instituto Superior Técnico.

Finally, and most important of all, I must be grateful for having a family who always supported me during my academic course. Furthermore, I shall be grateful for being so lucky during my whole life.

Abstract

Graphyne is an allotrope of carbon with excellent mechanical, electrical and optical properties, and its vastness of applications is yet to be unveiled. For this reason, the scientific community has been providing a great deal of attention during the last few years, especially in its characterization. Regarding the mechanical characterization, the present work aims to develop a reliable finite element model to simulate graphyne sheets. First, the covalent bonds and interatomic van der Waals forces are simulated through the use of beam and bar finite elements, respectively. The results extracted from two models (with and without van der Waals forces) are then compared to better understand the influence of different kinds of interatomic forces on the mechanical properties of graphyne. Then, the elastic properties of graphyne sheets (Young's moduli, Poisson's ratio, shear moduli and bulk modulus) are evaluated using finite element method for the first time. Finally, this thesis also includes for the first time the finite element simulation of a graphyne sheet under the influence of temperature. The results obtained from all simulations are subjected to comparison with previously obtained results from other works available in the literature, achieved through molecular dynamics and density functional theory simulations. The present model is able to correctly simulate the mechanical behavior of graphyne and successfully obtain its elastic properties.

Keywords:

Finite Element Analysis, Graphyne, Mechanical Properties, Temperature

Resumo

O grafino é um alótropo do carbono com excelentes propriedades mecânicas, eléctricas e ópticas, e a vastidão de aplicações que este pode ter, ainda está por desvendar. Por esta razão, a comunidade científica tem-lhe prestado bastante atenção nos últimos anos, especialmente no que diz respeito à sua caracterização. Considerando a caracterização mecânica, o presente trabalho tem como objectivo o desenvolvimento de um modelo de elementos finitos fidedigno para a simulação de folhas de grafino. Em primeiro lugar, as ligações covalentes e as forças de van der Waals são simuladas através de elementos finitos de viga e barra, respectivamente. Os resultados extraídos dos dois modelos (com e sem forças de van der Waals) são então comparados para que melhor se compreenda a influência que diferentes tipos de forças interatómicas produzem nas propriedades mecânicas do grafino. Posteriormente, as propriedades elásticas das folhas de grafino (módulo de Young, coeficiente de Poisson, módulo de corte e o módulo de expansão volumétrica) são avaliadas através de um método de elementos finitos, pela primeira vez. Finalmente, a tese incluirá também pela primeira vez a simulação pelo método dos elementos finitos de uma folha de grafino sob a influência da temperatura. Os resultados obtidos em todas as simulações são então comparados com resultados previamente obtidos noutros trabalhos disponíveis na literatura, conseguidos por simulações de dinâmica molecular e teoria de densidade funcional. O presente modelo é capaz de simular correctamente o comportamento mecânico do grafino e obter as propriedades elásticas deste.

Palavras Chave:

Análise de Elementos Finitos, Grafino, Propriedades Mecânicas, Temperatura

Index

List of Figures

List of Tables

List of Acronyms and Abbreviations

APDL – Ansys Parametric Design Language
AIREBO – Adaptive Intermolecular Reactive Empirical Bond Order
BN – Boron Nitride
BC – Boundary Conditions
CNT – Carbon Nanotube
DFT – Density Functional Theory
DMLG – Disordered Multilayers of Graphene
FEM – Finite Elements Method
FET – Field-Effect Transistor
FKM – Di-Polymer of Vinylidene Fluoride and Hexafluoropropylene
GC – Glass-like Carbon
GO – Graphene Oxide
GNT – Graphyne Nanotube
LAMMPS – Large-scale Atomic/Molecular Massively Parallel Simulator
LCBOP – Long-range Carbon Bond-order Potential
MD – Molecular Dynamics
MM – Molecular Mechanics
MWCNT – Multi-walled Carbon Nanotube
NFC – Nanofibrillated Cellulose
QHA – Quasi-Harmonic Approximation
REBO – Reactive Empirical Bond Order
RGO – Reduced Graphene Oxide
SWCNT – Single-walled Carbon Nanotube
TEC – Thermal Expansion Coefficient
UV – Ultraviolet
vdW – van der Waals
vdW-DF – van der Waals-density functional correlation

List of Symbols

$\boldsymbol{A}$ – Cross-Sectional Area

$\boldsymbol{a}$ – Transverse Displacement on zigzag direction

$\boldsymbol{b}$ – Transverse Displacement on armchair direction

$\boldsymbol{c}$ – Axial Displacement on zigzag direction

$\boldsymbol{d}$ – Axial Displacement on armchair direction

$\boldsymbol{d}$ – Bond Diameter

$\boldsymbol{D^{ij}}$ – Well-Depth of Interaction

$\boldsymbol{E_x}$ – Young's Modulus on armchair direction

$\boldsymbol{E_y}$ – Young's Modulus on zigzag direction

$\boldsymbol{E^{Total}}$ – Total Bond Interaction Young's Modulus

$\boldsymbol{E^{w}}$ – van der Waals Interaction Young's Modulus

$\boldsymbol{E^{\alpha}}$ – Bond-Stretching Interaction Young's Modulus

$\boldsymbol{E^{\beta}}$ – Bond-Angle Variance Interaction Young's Modulus

$\boldsymbol{E_b^T}$ – Bond-Angle Variance Interaction Young's Modulus at Temperature T

$\boldsymbol{E_s^T}$ – Bond-Stretching Variance Interaction Young's Modulus at Temperature T

$\boldsymbol{F}$ – Unit Force

$\boldsymbol{G_{xy}}$ – In-Plane Shear Modulus

$\boldsymbol{H_i}$ – Initial Sheet Height

$\boldsymbol{H_f}$ – Sheet Height after Biaxial Tensile Test

$\boldsymbol{I, J}$ – Area Moment of Inertia

$\boldsymbol{K}$ – In-Plane Bulk Modulus

$\boldsymbol{K^{\theta}}$ – Angle-Variance Force Constant

$\boldsymbol{K^{\rho}}$ – Stretching Force Constant

$\boldsymbol{K_{ij}^T}$ – Bond Stretching Force Constant at Temperature T

$\boldsymbol{K_{ijk}^T}$ – Bond Bending Force Constant at Temperature T

$\boldsymbol{L}$ – Interatomic Bond Length

$\boldsymbol{L_i}$ – Initial Sheet Length

$\boldsymbol{L_f}$ – Sheet Length after Biaxial Tensile Test

r^T – Bond Length at Temperature T

$r^T_{\overline{ij-jk}}$ – Mean Bond Length

Z^* – Nuclear Effective Charges

γ – Shear Strain

ε – Extensional Strain

Θ – Undeformed Bond Angle

θ – Average Stress

ϑ – Poisson's Ratio

ρ – Distance of van der Waals Bonds on Graphene

ρ_c – Distance of Crossed van der Waals Bonds on Acetylene Links

ρ_p – Distance of Parallel van der Waals Bonds on Acetylene Links

ρ^{ij} – Distance for van der Waals Interaction

σ – Tensile Stress

Δ – Relative Change in Area

ΔA – Area Variation

1 Introduction

1.1 Nanomaterials and their applications

Providing the basis for life on our planet, carbon is found in many known life forms. Its numerous hybridizations (sp, sp^2, sp^3) possessing strong chemical bonds display a rich variety of arrangements allied to the ability to bind to itself as it does to almost all elements. Besides the well-known crystalline forms carbon can take, as diamond and graphite, it also has numerous allotropes, namely, graphene, fullerenes, carbon nanotubes and several structures of graphyne (Katsnelson 2007). These allotropes have shown distinct mechanical (Roman and Cranford 2014, McCarthy et al. 2014), electronic (Mak et al. 2012, Lazic and Crljen 2015), optical (Bhattachary et al. 2015) and chemical properties (Ren et al. 2015) over the last years.

Graphene has been found to be one of the strongest materials ever tested while being only a monoatomic layer of carbon atoms in a honeycomb lattice (Lee et al. 2008). This carbon allotrope sheets can be rolled-up to later form fullerenes and nanotubes. Nanotubes can be made with a single wall, thus being named as single-walled nanotubes, or several, being named as multi-walled nanotubes. They have shown evidence of an enormous amount of tensile strength (Lee et al. 2008) and excellent conduction of heat and electricity (Haskins et al. 2011).

After the discovery of graphene, plenty of two-dimensional materials were and still are proposed and simulated, experimentally or computationally. Graphene/boron nitride (Peng and De 2012), graphene oxide (Peng and De 2013), aluminum nitride monolayers (Peng et al. 2013) and hydrogenated graphene are some of the examples.

As for graphyne, it was predicted to exist, but it's still hard to synthesize. However this material has a vastness of possibilities in terms of distinct structures. It's a one atom thick material much like graphene, but unlike graphene, this carbon allotrope can have between 33 and 100% acetylenic linkages in its composition. Among the most known geometries of graphyne are α, β and γ-graphyne. The aforementioned linkages have great influence both on its mechanical properties and heat conduction. In matter of electrical properties, this material displayed a band gap in the semiconductor range and this band gap can be changed through mechanical strain (Narita et al. 1998, Kang et al. 2011).

With such discoveries on the abovementioned carbon allotropes, extensive studies were and still are being proposed in order to better explore their properties and future applications, either by experimental or computational means, until they can be synthesized in larger quantities.

Regarding current aerospace applications, some of these allotropes are already being mixed with polymers to form composites with enhanced mechanical, electric and thermal properties. Njuguna and Pielichowski (2003) investigated experimentally the mechanical, thermal, electronic and optical properties of polymer nanocomposites. They have found that single-walled carbon nanotubes (SWCNTs) composites display high flexibility coupled with high resistance to torsion, as can be seen at Fig. 1.1. In terms of heat release rates, the combination of CNTs on organoclays resulted in improved values for this

parameter. As for the remaining properties, evidence of improvements were shown through the research, proving CNT composites allow the optimization of aerospace structures.

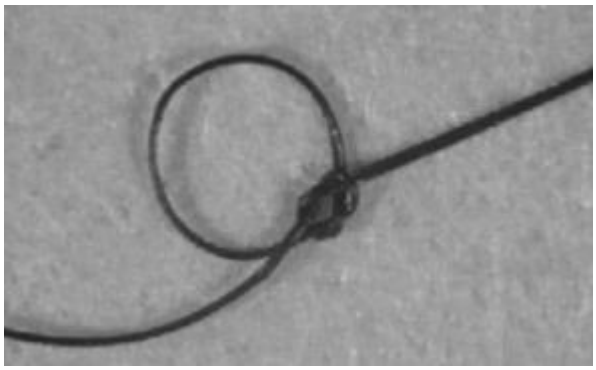

Figure 1.1 - Tying knot of SWCNT of about 15 nm in radius (Njuguna and Pielichowski 2003)

In 2008, Park et al. choose the experimental approach to study the effect of dispersing SWCNTs in a solvent or a polymer solution. The resultant nanocomposites exhibited excellent electroactive properties as well as good mechanical reinforcement. Balasubramanian (2012) dispersed graphene oxide (GO) over a poly ether sulphone matrix in order to test the mechanical properties and electromagnetic shielding effectiveness of the obtained nanocomposites. With a small quantity of GO (2%), Balasubramanian (2012) successfully enhanced the mechanical properties and at the same time improved the shielding effectivenes of the nanocomposite. Tate et al. (2013) manufactured ablative nanocomposites by incorporating multiwall carbon nanotubes (MWCNT) into phenolic resin. Their objective was to observe the thermal protection such nanocomposites can provide. After testing, Tate et al. (2013) obtained a decrease on mass loss percentage with only a small addition of MWCNT. Also, the insulation performance on the manufactured nanocomposite was improved. In the present year, Monetta et al. (2015) mixed graphene nanoflakes with epoxy resin, to form a coating which was expected to show superior corrosion protection and barrier properties. Fig 1.2 display one of the aforementioned expectations, which suggests a minor improvement of barrier properties of this coating. Furthermore, Monetta et al. (2015) concluded that graphene had an impressive effect on the corrosion performance of the nanocomposites.

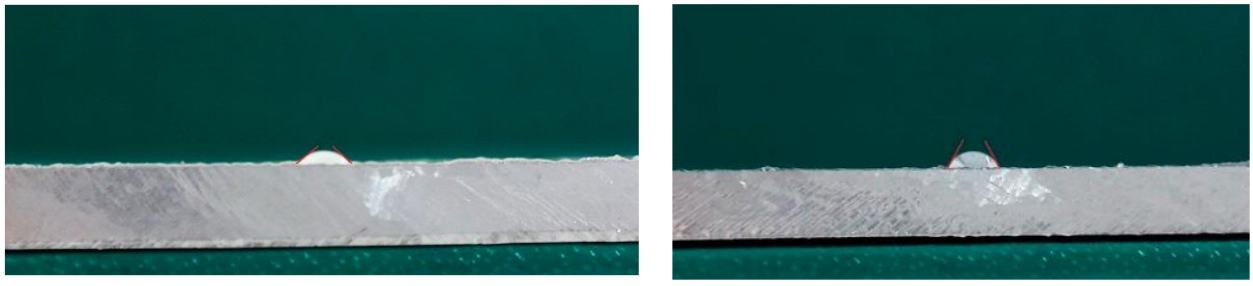

Figure 1.2 - (left) Contact angle of water drops over unfilled water epoxy resin and (right) graphene/epoxy resin (Monetta et al. 2015)

1.1.1 Graphene

Being one of the many recently discovered allotropes of carbon, graphene is nothing more than a single atomic layer form of carbon, previously isolated from graphite through a process of mechanical exfoliation. This shows how simple is graphene to make and how hard is to find. Such process can be done by simply writing with a graphite pencil on a paper, however producing many sheets of varying thicknesses. Therefore, one cannot harness extensively the produced graphene sheets. Bearing this in mind a group in Manchester, led by Andre Geim (Novoselov, Geim et al. 2004) solved this problem smoothly rubbing a graphite crystal on an oxidized silicon wafer, thus extracting mono layered graphene flakes. Further on, several methods were devised in order to improve the quality of extracted material, to detect and subsequently analyze graphene sheets (Bunch 2008, Sundaram 2011).

Graphene is made of a hexagonal structure of atoms, each one forming three covalent bonds with the nearest neighbor carbon atoms (Bunch 2008). Within the graphene sheet the carbon atoms are arranged in an open honeycomb lattice. Being an aromatic system, it's similar to benzene rings with the hydrogen atoms substituted by carbon atoms from neighboring rings. Such chemical structure can be seen on the image from Fig. 1.3.

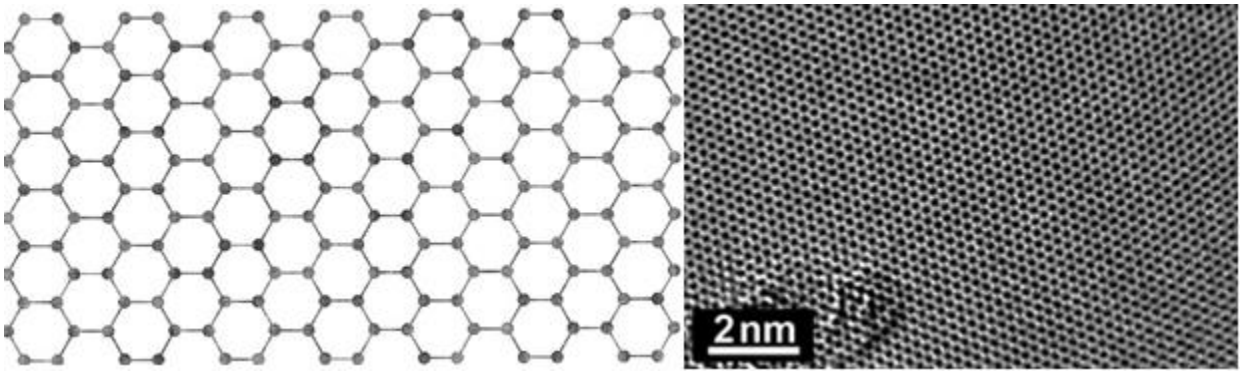

Figure 1.3: Graphene structure

Graphene has showed several applications, based on its mechanical, electrical and optical properties, extensively investigated theoretically for the last 60 years. (Novoselov, Geim et al. 2009).

As for biological engineering, it is foreseen graphene won't see any applications on this field before 2030, as it must undergo a battery of tests to make sure it's a biocompatible material. Overcoming this obstacle may revolutionize this area with new bioelectric sensory devices able to measure glucose, hemoglobin and cholesterol levels. Also, it can be turned into an engineered antibiotic in the future (Graphenea 2015, The University of Manchester 2015).

In terms of energy storage, graphene found his way in future super capacitors or batteries, which should be charged faster than current ones and increase its longevity, while being lighter and smaller. This enhancements shall be provided by incorporating graphene as an anode in lithium ion batteries. To light up the interest on this kind of application, it is claimed that such graphene storage equipment will be commercially available within the next 5 or 10 years (Graphenea 2015).

In addition to this, since graphene shows good electric conductivity and better light absorption than current photovoltaic cells (Mak et al. 2012), it can be used subsequently as a better and potentially cheaper option.

The only downside of graphene in terms of its electrical properties is the lack of band gap, without it, it's impossible to create an On/Off switch to interrupt the conduction of electrical energy when it's not needed. However, this problem is solved, accordingly to (Roman and Cranford 2014) with the successfully fabrication of graphdiyne.

Focusing now on its optical properties, graphene will be soon applied on touchscreens, both LCDs and OLEDs. For a material to find its way on this kind of optoelectronic applications, it must transmit at least 90% of light while providing good electrical properties, therefore low electrical resistivity. In the case of graphene it achieves an astounding value of 97.7% in terms of light transmission.

Knowing that current touchscreens are made of indium tin oxide, which is a brittle material, enables graphene, due to its flexibility and the aforementioned properties, to notoriously surpass the currently used materials.

Another very interesting application from graphene or in this case, graphene oxide, can be found on its ability to completely seal containers. In the form of thin layered membranes, this super permeable material can totally block gasses such as helium, which is the hardest gas to stop leaking from a container, and still lets water evaporate through, unimpeded (Bunch 2008).

Such discovery may in the future enhance the easiness on purifying or filtrate water, for example, or as barrier membranes between fluids, whether they are liquid or in gaseous form. Furthermore, graphene oxide may be used as a coating on food and pharmaceutical packaging in order to stop the transfer of water and oxygen, hence increasing its durability.

Besides the aforementioned coating possibilities, it's being developed by The University of Manchester (2015) a graphene paint to apply on other materials with the intent of protecting it from chemical attacks, weather elements and even air.

Sporting goods are already benefiting from graphene-based composites, mainly in tennis and it's expected to extend its applications to ski, cycling and so forth.

After many discoveries and achievements using pristine graphene, some derivatives of it have been predicted. One of them is graphone, which was firstly predicted by Zhou et al. in 2009 . This is a semi hydrogenated derivate of graphene, and it wasn't synthesized until now. Hence, its properties were examined through MD simulation (Peng et al. 2014) and DFT calculations (Zhou and Sun 2012), on this last article, Zhou and Sun (2012) also proposed a strategy to fabricate semi hydrogenated graphene sheets.

In terms of application and according to the analyses results, graphone seems to be suited to use in field-effect transistors (FETs), as Fiori et al. (2010) found. In the same study, graphane was also targeted, and like graphone it can be used to produce FETs.

Graphane is a 100% hydrogenated sheet of graphene, opposed to graphone which was only 50% hydrogenated. This material was first predicted by Sluiter and Kawazoe in 2003. In contrast to graphone, graphane has been already synthesize, and such achievement was attained by Elias et al. (2009).

Graphone can also see use in hydrogen storage, through the doping of lithium on the system, as Hussain et al. unveiled by DFT and MD simulations (Hussain et al. 2012). This graphene derivative also shows promise in biosensing applications (Tan et al. 2013).

This is just a small of ever-growing list of applications suited for graphene and some of its derivatives.

1.1.2 Fullerenes

A fullerene is a hollow molecule of carbon, mostly known in the shape of a sphere, called buckyball or a cylinder, called nanotube.

In 1985, Sir Harold W. Kroto et al. (1985) discovered a cagelike molecule composed of 60 carbon atoms coupled via single and double bonds. Reassembling a football, this molecule has 12 pentagonal and 20 hexagonal faces. Such discovery granted the Nobel Prize to those noble people for their pioneering efforts. Later on, more precisely in 1991, Iijima Sumio identified and synthesized the carbon nanotubes (CNTs). The image present in Fig. 1.4 shows the structures of a single walled carbon nanotube (SWCNT) and a buckyball.

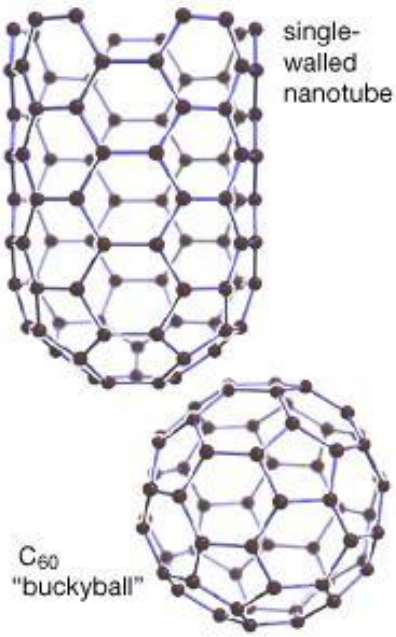

Figure 1.4: Examples of fullerenes structure (Encyclopedia Britannica 2015)

The discovery of fullerenes, especially CNTs, lately unveiled a new chapter of nanoscience and nanotechnology as they provide excellent conduction of heat and electricity while possessing an enormous amount of tensile strength. In terms of practical applications, as of now, are hard to determine

with accuracy, as fullerenes either exist in earth (Buseck et al. 1992) and in outer space (Cami and Peeters 2010), but are still hard to control and synthesize in efficient ways.

Therefore, researchers directed their efforts in order to identify the source of CNTs exceptional properties and how to apply them in future macroscale nanocomposites through experimental, analytical, DFT, MD and molecular mechanics (MM) simulations.

The Young's modulus of a SWCNT was determined experimentally to be in terapascal (TPa) range by Treacy et al. (1996), Wong et al. (1997) and Krishnan et al. (1998). In 2003, Li and Chou investigated the elastic properties of CNTs under a combined structural mechanics and MM approach view. Xing et al. in 2004, using a MD approach, attained a value of Young's modulus for SWCNTs, once again in the TPa range.

Many studies were also made in order to understand how multi walled carbon nanotubes (MWCNTs) can enlarge the already wide range of possibilities given by fullerenes. The image in Fig. 1.5 shows the main structural differences between SWCNTs and MWCNTs.

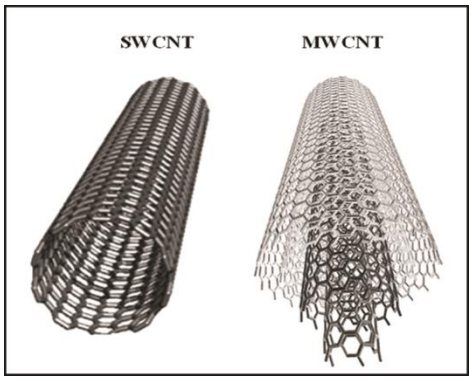

Figure 1.5: Schematics of different CNTs (Choudhary and Gupta 2011)

McCarthy et al. using an extensive series of MD simulations and an analytical shear-lag model, shown that given the same size initial intra-wall defect, MWCNTs with inter-wall coupling were stronger than SWCNTs. Furthermore, if designed carefully, i.e. with a suitable diameter, number of walls and irradiation dosage, MWCNT-based composites should have better performance than composites containing SWCNT (McCarthy et al. 2014).

Seidel et al. addressed the effects of having MWCNTs inside the fiber in a composite, also called fuzzy fibers, under analytic hierarchical mechanical and electrostatic composite cylinders methods. Obtaining the effective mechanical and electrostatic properties of the nanocomposites, the author concluded that is of utter importance to control the alignment of the fibers and the fuzzy fiber mixture ratio in order to achieve unidirectional ply properties for stiffening and sensing applications, not forgetting the electrical conductivity (Seidel et al. 2014).

In addition to the abovementioned possibilities of applying CNTs, in 2010, Kateb et al. (2010) proposed a technique to apply this allotrope in nanomedicine, more specifically, on a way to deliver a drug into microglia which seeks to immunize the brain against cancer.

Nowadays, MWCNTs are being used as structural composites and in lithium ion batteries (Rasmussen et al. 2014, Pushparaj et al. 2007). This allotrope of carbon, can be found in final products such as conductive polymers and composites, aerospace structural parts, sporting goods and even sensors (Rasmussen et al. 2014, Choudhary and Gupta 2011). According to a market research report (Pr Web 2013) released in 2013, CNTs are the fastest growing segment in nanomaterial technology market around the world.

The examples presented above are only some of the possibilities of present and future application of CNTs. With the increasing interest given by the scientific community not only on fullerenes, but also on other carbon allotropes, soon enough we shall see graphene, graphynes and CNTs being manufactured in large scale.

1.1.3 Graphyne N

Graphyne, graphdiyne, graphyne 3, 4 and 5 are allotropes of carbon, all belonging to a family called graphyne N; these structures are one atom thick planar sheets of sp and sp^2 of bonded carbon atoms arranged in a crystal lattice (Peng et al. 2014). The main difference between them, is the extent of acetylene links in between the honeycomb arranged carbon atoms. The next Fig. 1.6 clarifies the previous sentence explanation.

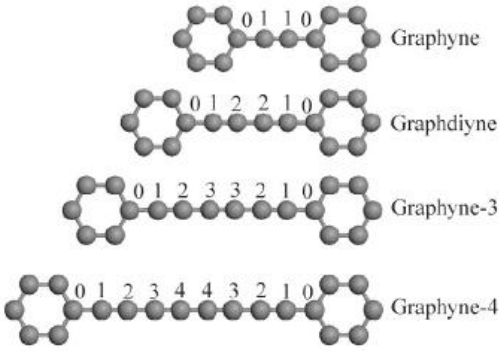

Figure 1.6: Acetylene linkages (Jing et al. 2013)

Due to their unique chemical structure, most of the allotropes from Graphyne N family are more suited for applications that does not require amazing mechanical properties. The previous sentence is supported by theoretical analyzes since the 1980s as such materials are still hard to synthesize to this day (Jing et al. 2013, Yang and Xu 2012, Peng et al. 2014).

Graphyne, having the same hexagonal symmetry as graphene, has one-third of the C-C bonds in the graphene replaced with one acetylene unit, as predicted by Baughman et al. (1987). Although having a fixed amount of C-C bonds, there are several structures of graphyne, being the most known, graphyne-α, β, γ and 6,6,12-graphyne. These are the most well-known structures, which can be observed on the images standing at Fig. 1.7.

This allotrope, after several analyzes applying both molecular dynamics and density functional theory has shown good mechanical properties, in terms of Young modulus, fracture stresses and strains (Yang and Xu 2012, Cranford and Buehler 2011, Zhang et al. 2012).

According to (Peng et al. 2014) only molecular fragments of graphyne has been synthesized up to now, such small samples couldn't be subjected to extensive studies in order to find the experimental properties of the material, either mechanical, electrical or others, thus one must rely solely on theoretical data. While not being stable yet in finite form (flake), this allotrope has its edges terminated with hydrogen atoms in order to satisfy the bonding requirements of the carbon atoms at the borders of the flake.

Like graphene, this allotrope's mechanical properties suggest it can be used as a nanofiller in certain composite materials, therefore enhancing the matrix in order to reduce the disparity between the usually brittle and strong fiber against the ductile but weak matrix. Such mixing should also disperse the anisotropic behavior of graphyne.

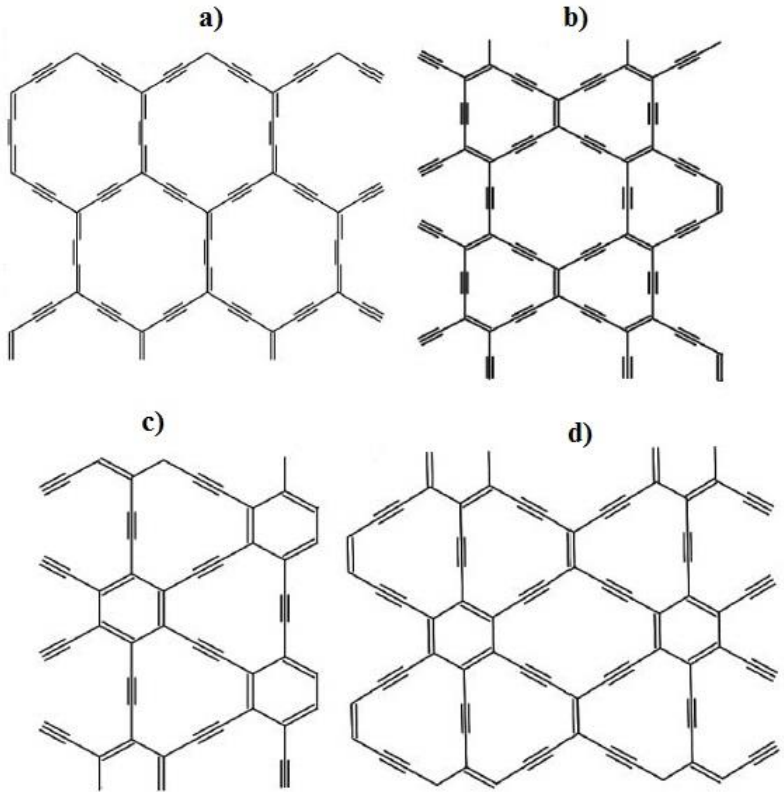

Figure 1.7: Structures of graphyne: a) α-graphyne, b) β-graphyne, c) γ-graphyne d) 6,6,12-graphyne (Zhang et al. 2012)

Regarding its electronic properties, it has been shown through first principle calculations that graphyne ribbons with finite width have band gaps in the semiconductor range (Pan et al. 2011). The band gap can be altered if mechanical strain is applied, another study has shown (Kang et al. 2011). However, structural modifications of graphyne through the adsorption on Cu, Ni and Co surfaces help modulate the energy gap, as it was found by (Lazic and Crljen 2015) applying a DFT method with the

novel nonlocal van der Waals-density functional correlation (vdW-DF). These authors also found the binding of graphyne to the abovementioned metal surfaces is stronger than that of graphene, which makes graphyne more suitable for the building of future nanoelectronic components.

Given the computational studies performed whose foresee a tunable band gap, the future looks bright in terms of electronic applications of graphyne. Since graphyne semiconductor properties are determined onto fabrication, it becomes clearly an advantage comparing to conventional transistors, which have their properties determined during the chemical doping process. Hence, graphyne semiconductor properties will be determined by the sheets size upon fabrication.

Regarding its large elastic strain region, coupled with its electronic properties, one may figure the future implementing of graphyne on sensors that can be useful in a wide range of possibilities, including temperature sensing.

Lately has been found by Hu et al. (2015), from a MD perspective, that graphyne nanotubes (GNTs) has an unprecedentedly low thermal conductivity, even lower than any values displayed by other carbon nanotubes (CNTs), being defected, doped or chemically functionalized. This low thermal conductivity persist even if the tubes are infinitely long and/or have large diameters, up to 18nm. Such discovery may be valuable for future applications, such as thermo electrics devices for energy conversion.

On the branch of optical applications, recently was found by Bhattachary et al. (2015) through the systematical substitution of boron (B) and nitrogen (N) into the structure of the graphyne family that this allotrope displays characteristic optical properties, comparing to other carbon-based structures. Due to the presence of BN, the optical band gap is tuned, and BN doped graphyne exhibits a strong absorption peak in a wide UV-region for perpendicular polarization. Hence, graphyne shall find usage in future UV light protection.

With the development of reactive empirical bond order (REBO) potential energy expressions for hydrocarbons (Brenner et al. 2002) and later the long-range carbon bond-order potential (LCBOP) by Los et al. (2005), the mechanical, electrical and vibrational properties of both graphene and graphyne started to be able to be analyzed in depth. Zakharchenko et al. (2009) applied the improved LCBOPII method to prove within their computational model, that graphene doesn't always expands with the increase in temperature. Later, Shao et al. (2012), making good use of DFT method, compared the behavior of the mechanical properties of graphene and graphyne, to find a resembling way of reacting to the change of temperature on both materials. This research also found that the closer to 0K the carbon allotrope got, the higher its mechanical properties become.

Such discoveries, even if only through computational methods, may in the future be a great contribute to aeronautics, as long-range aircrafts spend most of their flight time at negative temperatures (in Celsius degrees range). However this field seems to have a great potential to developments, since it has been newly found.

Much like graphene, this allotrope can be used to desalinize water, as Xue et al. (2013) predicted through MD simulations and first principles modeling. Xue et al. (2013) also found a 100% rejection of

ions in sea water, using pristine graphyne. Ergo, graphyne shall provide a new solution to alleviate the shortage of fresh water around the globe.

Focusing now on a softer material called graphdiyne, which was first predicted by Haley et al. (1997) and belongs to the graphyne family, it's one of the carbon allotropes where mechanical properties are not worth mentioning, since they're far less interesting than those of graphyne or graphene (Yang and Xu 2012). Nevertheless, its stiffness is nearly 30% that of graphyne with a noticeably reduced strength according to (Cranford and Buehler 2012, Pei 2012). The weaker mechanical behavior of graphdiyne is due to the larger acetylenic linkage which results in weaker bonding. The image in Fig. 1.8 exhibits the atomic scheme of graphdiyne.

However, given its other interesting properties, graphdiyne is considered separately from the rest of the graphyne family.

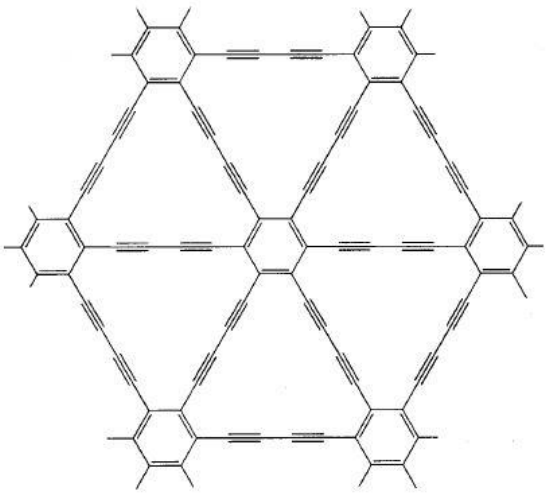

Figure 1.8: Chemical structure of Graphdiyne (Haley et al. 1997)

As for electronic properties, graphdiyne can have its band gap varied proportionally to externally applied strain, similarly to graphyne, though the band gap is quite different (Pei 2012). Pei also reported the band gap on graphdiyne is in the semiconduction range, making this allotrope quite suitable for electronic applications. Such results were obtained through computational simulations, although graphdiyne has already been synthetized successfully (Li et al. 2009, Li et al. 2011), in small sizes.

After it was synthesized on copper substrates, graphdiyne went through analyzes applying full atomistic MD, in order to once more find its mechanical properties, but now as a composite (Ramon and Cranford 2014). Cranford et al. concluded that graphdiyne can enhance Cu performance in a synergetic way, by combining Cu with layers of graphdiyne. The resulting composite also has its failure strain increased substantially, by confining the Cu crystal during deformation.

Another significant difference between graphyne and graphdiyne lies in the discovery of Xue et al. (2013), where this last allotrope is impermeable to water and ions due to its small pore size. Thus, graphdiyne shouldn't be used as a desalinator or a mean to purify water.

Since graphdiyne show evidence of low effective electron mass (Pei 2012), the electrons should move fast, even if a small potential field is applied. Therefore, one of the limitations of silicon based transistors is outclassed by graphdiyne. Such limitation lies in the fact that the maximum switching frequency on current transistors is limited by the velocity of the electrons across the transistor channel relative to the length of the channel. Hence, graphdiyne should be used on transistors in a near future.

In terms of sensors, knowing this carbon allotrope has a desired electromechanical coupling, we're not far from glimpsing its application on several mechanically and electronically driven systems. For example, thermal control systems. Regarding the abovementioned doping of graphdiyne using boron and nitrogen, one can fabricate patterned sheets with different properties. These patterns, can later be used to control large amounts of current flow by harnessing the electrons flow through the sheets.

1.2 Scope and Objectives

As it was shown before, graphyne has been a nanomaterial of great interest amongst the scientific community since the beginning of the 21st century. Unlike graphene, it shows an orthotropic behavior, mostly due to the acetylene links in between the graphene hexagons. Graphyne isn't limited to single or double bonds connecting its atoms, and depending on the structure, it can have triple bonds. Moreover this allotrope is not limited to the hexagonal pattern exhibited by graphene. The more the percentage in acetylenic linkages, the weaker in terms of mechanical properties the material gets. This is the main reason why graphdiyne, graphyne-3 and other allotropes with longer chains of acetylene, from the graphyne family, are not targeted as much as graphyne is on extensive studies to understand its mechanical properties. With the very scarce production of graphyne (Peng et al. 2014), one must rely mostly on computational methods to address the issue at hand, i.e. the analysis of graphyne mechanical properties.

Therefore, the scope of this thesis is the study of graphyne from the mechanical viewpoint. In the recent past, some authors applied DFT calculations (Cranford and Buehler 2011, Peng et al. 2012) or made their approach through MD simulations (Yang and Xu 2012, Zhang et al. 2012) with the purpose of finding the ultimate stress, strain and stiffness, of several types of graphyne. The efforts in this thesis will be directed towards the calculation of some of such properties using the finite element method (FEM). In resume, the following three objectives are assumed:

1) To develop a consistent finite element model to simulate the mechanical behavior of graphyne.
2) To calibrate this finite element model with results available in literature and obtained from either MD or DFT calculations.
3) To assess the influence of non-bonded forces (van der Waals forces) and temperature on the elastic properties of graphyne.

Regarding that many possible structures of graphyne could be assumed, γ-graphyne will be adopted for the present study. Hereafter, we shall designate γ-graphyne simply as graphyne. Hence, this work

seeks to provide a new path to analyze this promising carbon allotrope. To the author's knowledge, this is the first work on the application of FE method to study graphyne mechanical properties.

1.3 Organization of Contents

The present Chapter includes an overview of the latest discovered allotropes of carbon, a brief description of their vastness of applications, whether they are mechanical, electrical or optical. Some examples of their present and future applications, both as a 2D sheet or integrated in composites, are shown not only in high technology devices, but also on everyday objects. Chapter 2 addresses the last breakthroughs regarding graphene, the wide graphyne family and fullerenes, and what methods are used to achieve such features. In this chapter, some results obtained by other researchers are presented as they can provide a useful comparison with the results of this work, later obtained in Chapters 4 and 5.

Chapter 3 presents the development of a computational model of a graphyne sheet, which is explained in-depth. Moreover, several particular issues of the model, such as the element type, boundary conditions and interatomic forces, will also be addressed in detail. This will enable the computation of graphyne's elastic properties, after which follows the same process but now with the effect of van der Waals forces applied on the sheet. With all the conditions set on the model, uniaxial tensile tests, shear test and biaxial tensile test are carried on the graphyne sheet during Chapter 4. Having obtained the results from the abovementioned calculations, a comparison between these results and values found in literature will enable the check for consistency of this model. At the end of this chapter, the results are expected to bring enlightenment about how much van der Waals forces affect the mechanical behavior of a graphyne sheet in terms of its elastic properties. In Chapter 5, the same model used for previous calculations is adapted, this time to simulate the influence of temperature on graphyne's mechanical properties. With it, one seeks to build, for the first time, a successful FEM model able to simulate graphyne's elastic properties in a given range of temperatures and then compare its results with few other results available in literature, achieved by other authors through MD and FDT models.

At the end of this document, some main conclusions regarding the presented results will be presented and some proposals for future developments will be given.

2 Mechanical Behavior of Carbon Nanomaterials – Literature Review

The following chapter sums up many of the latest discoveries on the carbon allotropes referred at Chapter 1. While the last chapter was mainly focused on applications for such materials, the present chapter is directed towards the state of the art regarding the applied methods and obtained results on the mechanical properties of graphene, fullerenes and graphyne. Sections 2.1 and 2.2 revolve around graphene and fullerenes, while section 2.3 strictly speaks about graphyne's mechanical properties.

Although the main issue of this thesis is the achievement of graphyne's mechanical properties, one should not overlook how other carbon allotropes have been studied up to now, as they may provide ways to analyze several structures of carbon.

2.1 Graphene

The scientific community has showed great interest on the mechanical properties of graphene. With the discovery of new methods to synthesize graphene composites (Ren et al. 2015) and new possibilities of mixing graphene with other materials (Dang and Seppälä 2015, Wei et al. 2015), more and more analysis are done either through computational and/or experimental methods.

This year, Baimova et al. (2015) studied the mechanical properties of crumpled graphene under hydrostatic and uniaxial compression using MD. In their study, using six bent graphene flakes to form a unit, and a total of 8 differently oriented units, as can be seen on Fig. 2.1, they applied a constant strain rate both in the hydrostatic and the uniaxial compression. They concluded that crumpled graphene under small compressive loadings behave like a non-Hookean elastic body, which means, that the model had a nonlinear stress-strain relation. The reason behind this phenomenon is the formation of new van der Waals and covalent bonds during compression.

Regarding the deformation upon the crumpled graphene, Baimova et al. (2015) found that for values above 1.25 g/cm^3 under hydrostatic compression, the deformation becomes inelastic. The same happens when the density reaches 1.5 g/cm^3 during uniaxial compression. Also, it was found that under uniaxial compression, the graphene flakes form highly anisotropic quasi-2D structures, while under hydrostatic compression, this flakes are prevented by the symmetry of the loading, to form such structures. Baimova et al. (2015) pointed out how important would be to understand the effect of shear strain and temperature in terms of application of crumpled graphene, thus letting such issues as a suggestion for future works.

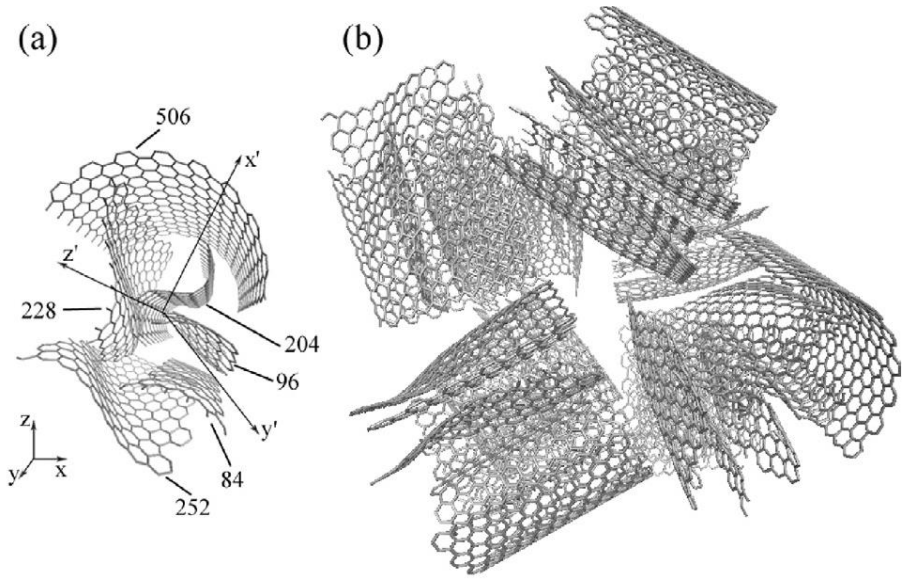

Figure 2.1: (a) unit of crumpled graphene consisting of six bent graphene flakes, (b) eight differently oriented, non-overlapping building units (Baimova et al. 2015).

On the experimental field, Ren et al. (2015) synthesized successfully a nickel-graphene composite by electrochemical deposition on a steel substrate. Unlike previous works (Kuang et al. 2013, Mahale et al. 2014) which used graphene oxide nanoflakes instead of graphene as the additive in the plating solution, the authors were aiming at measuring the resulting stronger mechanical properties graphene had to offer to this composite. In order to measure the composite samples properties, Ren et al. (2015) applied Raman spectroscopy, x-ray photoelectron spectroscopy, x-ray diffraction, energy dispersive spectrometry, scanning electron microscopy and nano indentation. With such a variety of devices to analyze the deposition process and resulting composite, they have found the graphene nanosheets dispersed uniformly over the nickel matrix surfaces and interfaces. As expected, graphene enhanced the mechanical properties of the nickel matrix by facilitating the formation of nickel crystalline in its (111) plane. Regarding the mechanical properties, an elastic modulus of 240 GPa was found along with a hardness of 4.6 GPa applying only 0.05 g/L of graphene on the nickel matrix, the strong interactions between the two materials are responsible for such improvement over its mechanical properties (Ren et al. 2015).

In its turn, Gong et al. (2015) investigated the influence of thickness on the mechanical properties of graphene oxide papers, once more, through an experimental method. Graphene oxide has a high affinity for water molecules, meaning it's hydrophilic and can be easily dispersed in water. Although having weaker mechanical properties than graphene itself (Liu et al. 2012), graphene oxide may have some technological applications, such as surface coatings (Yang et al. 2012), ionic and molecular sieving (Li et al. 2013, Joshi et al. 2014), hydrogen storage (Yang 2000), and nanocomposites (Ren et al. 2015). In this study, Gong et al. (2015) fabricated graphene oxide paper of various thicknesses, between 0.5 and 100 μm, by filtering solutions of various concentration of graphene oxide through filter membranes made of

aluminum oxide. The paper was then peeled off from the membranes and cut using laser. A in depth explanation of the experimental process is extensively explained in this article, and should be read, if one wishes to clearly understand the whole process. The paper resulting from the process roughly explained above, can be seen at Fig. 2.2.

To obtain the mechanical properties of this graphene oxide paper, Gong et al. (2015) used a tensile test device to test the thicker strips, while the thinner ones were test via a bulge test device. Also an electronic balance was used to measure its masses. A thin-film x-ray diffraction enabled the determination of the crystallinity and structural variations in the graphene oxide membranes. Atomic force microscopy was carried out to find the size of each graphene oxide flake. X-ray photoelectron spectroscopy was performed to show the different functional groups present on the paper. The functional groups in graphene oxide are sensitive to the humidity in the air, as a result, its mechanical properties vary accordingly. Gong et al. (2015) obtained Young's modulus ranging from 44.6 to 8.5 GPa and fracture strength, from 170.2 to 40 MPa. Both values decrease with thickness. They have found the most contributing factors to such behavior are the macro and microstructure, also the surface morphology, crack formation, roughness change and corrugation. As a footnote, these authors suggest that the modification of the fabrication process through a variation of the filtration speed, using another filter material and graphene oxide properties, can further enhance/control the mechanical properties of this graphene oxide papers, according to its application (Gong et al. 2015).

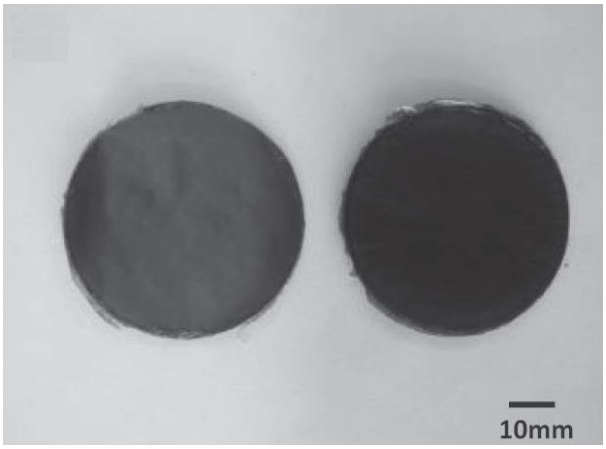

Figure 2.2: Free-standing thick graphene oxide papers with a diameter of 47mm (Gong et al. 2015)

Also very recently, Dang and Seppälä (2015) examined through an experimental process the mechanical and electrical properties within a range of temperatures for nanocellulose/graphene composites in high-moisture conditions. They prepared nanofibrillated cellulose (NFC) to receive either graphene oxide (GO) or reduced graphene oxides (RGO). The resulting nanocomposites were called NFC/GO and NFC/RGO papers. After which they measured and tested such materials using an atomic force microscope, a tensile testing device, to test sample papers at ambient temperature and a four point

probe method to measure the electrical conductivity of the composites. Using scanning electron microscopy these authors studied the surface morphology of the specimens. X-ray diffraction was also used, and dynamic mechanical analysis was carried out at different % of humidity. At last, thermogravimetric analysis were applied on the composite. With all this apparatus they were able to successfully prepare NFC/RGO composites. Besides, they observed that NFC/RGO showed enhanced mechanical, electrical and thermal properties compared to neat NFC. The Young's modulus of this composite paper is way higher than that of NFC, and it shows a huge improvement in mechanical performance in high-humidity mediums, being able to resist to temperatures up to 40 K higher than that of neat NFC. Dang and Seppälä (2015) also found it's possible to control the electrical conductivity on this composite by the amount of graphene loading in it (Dang and Seppälä 2015).

Wei et al. (2015) studied the thermo-mechanical properties of graphene integrated fluoroelastomer. On their article, it's explained how to experimentally prepare the (di-polymer of vinylidene fluoride and hexafluoropropylene) RGO/FKM and GO/FKM nanocomposites samples. These samples are then characterized using transmission electron microscopy for its morphology, an x-ray diffractometer to identify the GO and RGO patterns, Raman spectra, Fourier-Transform Infrared spectrum and a thermogravimetric analysis was run. Such measurements are carried out in order to understand the influence of RGO and GO on the thermo-mechanical properties of the obtained composites. To obtain the thermo-mechanical properties of the FKM samples, a universal tensile tester was used at several temperatures, 25, 75, 125 and 175 ºC. These authors concluded that RGO has a better interaction with FKM than GO does. A smaller steric effect during vulcanizing of RGO/FKM has a significant influence over the mechanical properties of such composites. Also, at higher temperatures, RGO/FKM shows a better performance as it's a thermal stable structure, while GO/FKM it's not. The RGO improves the working temperature on FKM by 50 ºC when just 2% of it is added (Wei et al. 2015). While GO/FKM can operate up to a temperature of 125ºC, RGO/FKM withstands 175ºC and still has better mechanical performance then pure FKM (Wei et al. 2015).

In brief, these very recent works show that graphene is a nanomaterial with very attractive mechanical and thermal properties.

2.2 Fullerenes

Regarding the fullerenes, there are many things to conclude from its mechanical properties. This year, Hu et al. (2015), applying MD to graphyne nanotubes, were surprised to find an unprecedentedly low thermal conductivity, below 10 W/mK at room temperature, on these nanotubes. Their study was focused on two types of structures, armchair and zigzag graphyne N nanotubes. Fig. 2.3 illustrates the previous statement. The nanotubes were designed based on *ab initio* calculations done to optimized graphyne sheets in a previous paper (Jing et al. 2013). According to their findings, the extremely low thermal conductivity comes from the acetylenic linkages in between the aromatic bonded hexagons. The disparity between the strength of such bonds provides a vibrational mismatch, inducing a highly inefficient

heat transfer along the tubes. Furthermore, Hu et al. discovered that even for close to infinite long tubes, all tested nanotubes were 500 nm long, and large diameters, being large ~18 nm the low thermal conductivity persists. Ultimately, these authors found that longer acetylenic chains drove to smaller thermal conductivity results, up to six times smaller, on a graphyne-10 nanotube, compared to a graphyne-1 nanotube (Hu et al. 2015).

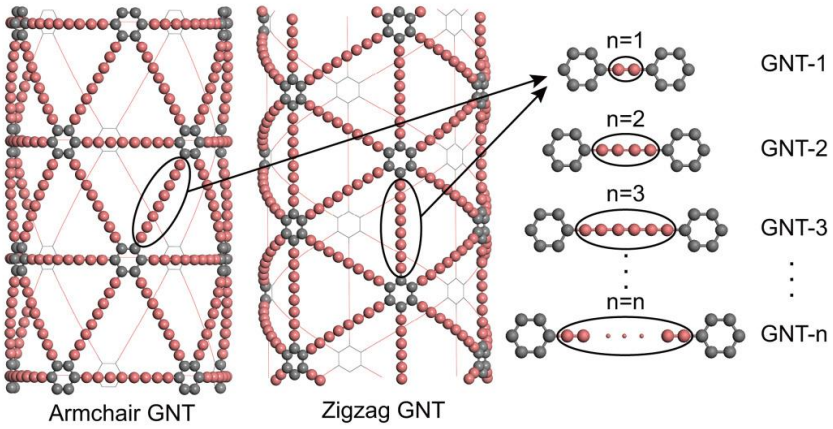

Figure 2.3: A representative armchair and zigzag graphyne n nanotube structure (Hu et al. 2015)

Zhao et al. (2015) dedicated a study on nanoarchitectured materials composed of fullerene-like spheroids and disordered graphene layers with tunable mechanical properties. Their research was focused on a special type of architectured materials composed of tailored functional building blocks. Those are more commonly known as mechanical metamaterials. Having a rather unusual skeletal nature, such materials yield uncommon mechanical properties, for example, negative Poisson's ratio (auxetic behavior), negative compressibility and so forth, while typically being lightweight. With that in mind, glass-like carbon (GC) Type-II, consisting of a disordered multilayer graphene matrix encasing numerous randomly distributed nanosized fullerene-like spheroids, was studied through MD simulations and experimental methods of sample material. An image to clarify how GC Type II looks like, is shown in Fig. 2-6. The yellow lines displayed at Fig. 2-6 represent the outer encase of GC Type II, which is done through disordered multilayers of graphene (DMLG). In this issue, Zhao et al. (2015) analyzed the hydrostatic compression behavior and elastic moduli of these "cubes" with sizes ranging from 5 to 10 nm in diameter. They concluded that GC Type II exhibits much higher volume compressibility and elastic recovery ability than most carbon materials, metals and even some organic polymers. This material displayed compressive strength above 1 GPa and was able to recover from linear strain of 6%, a value comparable to shape-memory alloys. Further studies were performed to understand the cause of such remarkable properties. It was then found that the average size and spatial distribution of the fullerene-like spheroids contribute to this behavior as well as the topological connectivity between the GC Type II and DMLG.

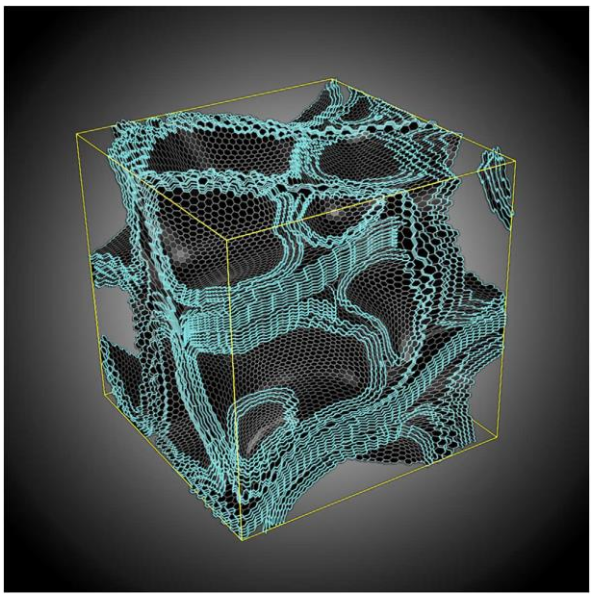

Figure 2.4: Fullerene-like spheroid in a disordered multilayer graphene matrix (Zhao et al. 2015)

Another remarkable property of this carbon allotrope is its ability to not structurally transform after the turn-over point, a common anomaly found on homogeneous materials. Thus, GC Type II can undergo large volume contractions without shape shifting at all. After this turn-over point, the materials experiences an increasing on Young's, bulk and shear modulus. By the end of their conclusions, Zhao et al. (2015) pointed out that the lack of orientated defects on the material is a very important factor in the determination of its superelastic behavior.

Finally, a very interesting issue arose this year through the paper by Lepore at al. (2015), which investigated silk reinforced with graphene or carbon nanotubes spun by spiders. They studied silk directly spun by spiders, produced after the exposure of those spiders to two variants of dispersions, the first being of carbon nanotubes (CNTs) and the second graphene (GS). However, two kinds of CNTs were used: CoMoCAT® single walled CNTs, named SWCNT-1, and electric arc discharge single walled CNTs, named SWCNT-2. After the silk is harvested, the presence of nanotubes and graphene inside it, is monitored by Raman spectroscopy. This technique is also used to measure the GS and CNTs samples. After this, nanotensile tests to find the desired mechanical properties were performed. The obtained results showed that CNTs improve Young's modulus, toughness and fracture strength of the silk, even beyond the improvements caused by GS. Thus, the silk experienced a fracture strength, Young's modulus and a toughness increment of 731%, 1183% and 663%, respectively. There was also a decrement of 41% of ultimate strain, caused by the SWCNT-1 dispersions. SWCNT-2 improved the fracture strength, Young's modulus and toughness of the silk by 350%, 330% and 204%, respectively, with a decrement of 36% on the ultimate strain value. At last, GS increase on mechanical properties had the smallest, but still significant value. With 151%, 142% and 250% for fracture strength, Young's modulus and toughness of silk, respectively. Unlike the previously mentioned dispersions, GS incremented the ultimate strain of the silk by 250%. Finally, this combination of increment in toughness

and decrement in ultimate strain experienced by the addition of CNTs dispersions to the silk, could prove useful on future application such as ballistic protection and flak jackets (Lepore et al. 2015).

These few but very recent investigations on the mechanical and thermal behavior of fullerenes also prove their ability for targeted solutions in which no other nanomaterial has better performance.

2.3 Graphyne

The mechanical properties of graphyne were always of the interest of many researchers, although it seems rather weak compared to graphene (Peng et al. 2014). However, with the addition of the acetylene links which are characteristic of graphyne, not only its mechanical properties change, but also its thermal, electric and optic properties. Although the thermal dependency of graphynes mechanical properties is yet to be fully understood and it's nowadays more commonly analyzed, it has been studied on the last few years by some researchers.

Shao et al. (2012) studied not only the temperature dependent elastic constants and ultimate strength of graphyne but also graphene. Their analysis were done based on the first principles calculation (DFT) combined with quasi-harmonic approximations (QHA). To do such analysis they utilized a lattice containing four atoms of carbon for graphene, and 24 atoms for graphyne. Therefore, the properties in study are dependent on the abovementioned two-dimensional lattices. The range of temperatures employed were between 0 and 1000K for both materials. Determining the thermal expansion coefficient (TEC) and temperature dependent ultimate strength in each case, the researchers were able to predict the behavior of the allotropes sheets in terms of its mechanical properties. Unlike many materials, graphene and graphyne have negative TEC values at low temperatures, being low in the range of 0 to ~350K. After which, the values increase in the positive region of TEC within the remaining range of temperatures. On the elastic properties, Shao et al. (2012) obtained a Young's modulus, E, value for graphene as high as 350.01 N/m, while the ultimate tensile strength, σ_{UTS}, reached 119.2 GPa at room temperature[1]. On the graphyne side, a Young's modulus of 250.91 N/m and ultimate tensile strength of 81.2 GPa were reported. Regarding the temperature dependency on these properties, the graphene was capable to keep its superior mechanical properties. Hence, from 0 to 1000K, graphene's E, only decreased by 2.2%, while its σ_{UTS} value felt by 4.03%. Graphyne for its turn, on the same temperature range, suffered a loss of 10.79% on its E value. As for σ_{UTS}, a decrease of 12.1% happens in its value. Therefore, the researchers conclude that graphyne's mechanical properties have a weaker resistance than graphene to the effects of higher temperatures (Shao et al. 2012).

Zhang et al. (2014) performed a somewhat similar study, since the objective of their work was to obtain the strain-rate and fracture strength dependency on temperature for α, β, γ and 6,6,12 graphynes. However, the analysis was done through the MD scope. With such a variety of graphyne structures, they

[1] Graphyne is a material of discrete (atomic) nature, hence its thickness cannot be considered conceptually. This is the reason why the elastic modulus is measured in N/m. However, a thickness can be given to the graphyne sheet, thus turning the unit of the elastic modulus into GPa.

were able to understand the overall influence of acetylenic percentage on mechanical properties of each of those nanomaterials. As a matter of comparison, a graphene sheet was also modeled. To better display the way the carbon atoms are organized within the different structures of graphyne, Fig. 2-5 is shown. To calculate the intended properties, diverse models were built for each graphyne structure. The simulations were run using approximately squared sheets with 20 nm on its sides. Periodic boundary conditions were applied. To perform the MD simulations, the software package LAMMPS (Plimpton 1995) was used. The interatomic forces acting on the carbon atoms were described recurring to the adaptive intermolecular reactive empirical bond order (AIREBO) potential (Stuart et al. 2000).

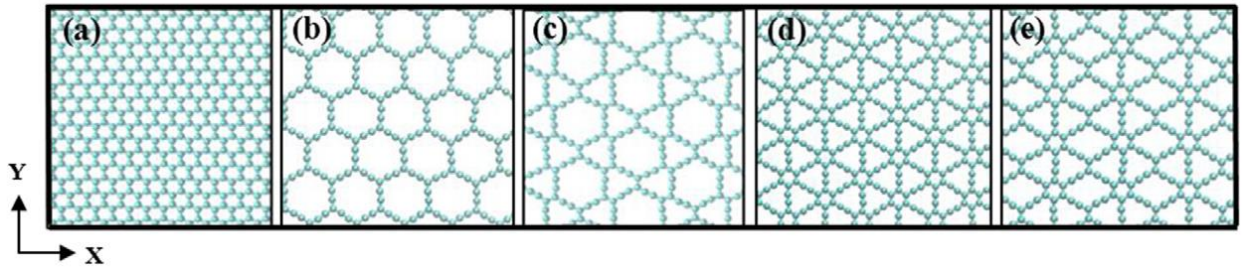

Figure 2.5: Atomistic structures of graphene and four different graphynes. (a) Graphene, (b) α-graphyne, (c) β-graphyne, (d) γ-graphyne, (e) 6,6,12 graphyne (Zhang et al. 2014)

The simulation results, though using a different method, were in agreement with Shao et al. (Shao et al. 2012), as Zhang et al. found both the fracture strength and the Young's modulus decrease with increasing temperature. In addition they agreed once more with Shao et al. on the fact that graphyne's mechanical properties decrease faster with the increasing in temperature than graphene does. However, an acetylene linkage percentage increase, causes a faster decay in mechanical properties. This is the same as saying that α-graphyne holds the largest loss in its mechanical properties for as long as the temperature augments. In their simulations, Zhang et al. (2014) looked upon a range of temperatures between 1 and 1200 K. When the temperature increases from 1 to 1200 K, the Young's modulus of graphene drops only by 10%, while the graphynes in analysis had its values drop ranging from 37.4% up to 76.7%, for γ and α-graphyne, respectively. The same pattern of results is repeated for fracture stress and strain, ergo, α-graphyne is the weaker structure of graphyne, speaking of its mechanical properties (Zhang et al. 2014).

This year, Hou et al. (2015) have chosen the analytical approach. They've built a molecular mechanics model to study the elastic properties of graphyne-n. The ultimate objective of this analysis is to compare the obtained results with other authors, whom studied the same properties with either MD (Cranford and Buehler 2011, Cranford et al. 2012, Zhang et al. 2012) or FDT simulations (Yang and Xu 2012, Peng and De 2012, Yue et al. 2013).

To do so, Hou et al. (2015) used a previously designed model, called stick-spiral. This model was of the authorship of Chang and Gao (2003) and it was firstly applied on the calculus of SWCNTs elastic

properties (Chang and Gao 2003). However, being a successful implemented model, it was applied on several other papers (Chang et al. 2005, Chang and Geng 2006, Chang 2010). Based on rather complex equations, the researchers studied and compared the in-plane stiffness of 10 distinct structures of graphyne, where they intended to capture the degradation of this property with increasing acetylenic linkages. Hou et al. extended their research to shear stiffness and Poisson's ratio. Having acquired their results from the developed equations, which they claim to be capable of linking macroscopic properties with graphyne-n atomic structure in a direct manner, after comparison, the predicted results matched the ones coming from MD and FDT simulations. As previously shown by Yang and Xu (2012) and later confirmed by Yue et al. (Yue et al. 2013), the decreasing value of in-plane stiffness happens with the increasing number of acetylenic links present on graphyne. Hou et al. (2015) obtained a similar trend of results but further extended the calculations up to graphyne-10, whereas other authors only went up to graphyne-5 on their simulations. On the shear stiffness values, with no other authors to compare with, these researchers achieved a trend much like the one obtained for in-plane stiffness. It should be reminded that both the shear stiffness and Poisson's ratio of graphynes are scarcely studied properties, but by no means, less important. With that in mind, this thesis will present results regarding both properties.

Hou et al. (2015) also obtained results for graphyne-n Poisson's ratio and although the trend in values along an increasing number of acetylenic linkages is believable, becoming higher, the results *per si*, as they mention, require further studies, especially regarding the temperature dependence of such property. These authors contribution on the reach of molecular mechanics is immense, not only for the development of an analytical model capable of obtaining graphyne-n mechanical properties, but also because it can be further extended to predict any kind of graphyne structure mechanical properties. (Hou et al. 2015)

Also very recently, Asadpour et al. (2015) studied the mechanical properties of γ-graphyne and two analogous systems of boron nitride (BN) sheets through DFT analysis. The 3 analyzed structures were a single sheet of γ-graphyne, another of BN where the atoms although being from different elements were displayed the same way, called BN-yne, and finally a single sheet composed by hexagonal rings of BN linked by carbon chains, or more commonly known as acetylene links. An image regarding such structures can be seen on Fig. 2-6, where the gray spheres represent the carbon atoms, while the blue and pink spheres represent the boron and nitride atoms. Through their simulations they've found that graphyne displays the largest value of in-plane stiffness among the three analyzed structures. Hence, the result for graphyne was 190.69 N/m, while BN-yne and the graphyne BN structures only achieved 162.451 and 163 N/m respectively. On the Poisson's ratio side, the graphyne BN structure got the highest value of 0.51. For this property, graphyne showed to have the smallest value. Regarding both the shear and bulk modulus, once again, graphyne displayed the highest values, compared to the other 2 structures. Therefore, the obtained graphyne bulk modulus was 122.725 N/m and its shear modulus was 77.043 N/m. In this case, the BN-yne structure displayed the smallest results. Finally, it was found by

Asadpour et al. (2015) that graphyne enters the plastic region of deformation with the highest magnitude of tension comparing with both BN-yne and graphyne BN structures.

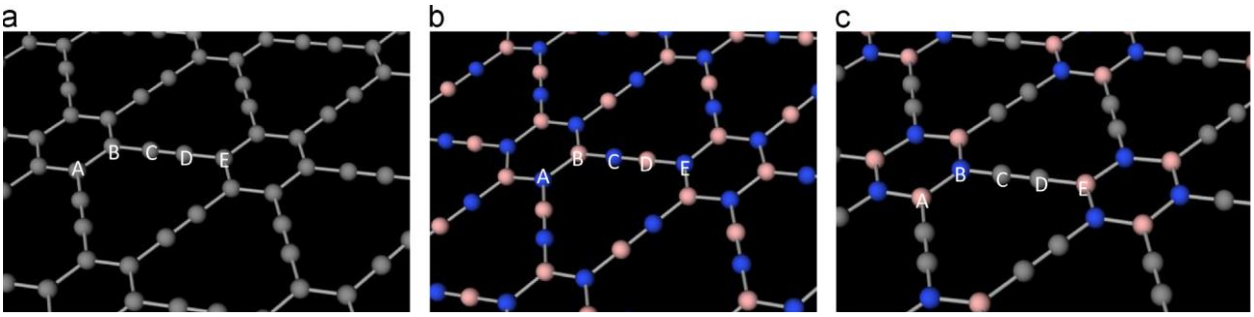

Figure 2.6: a) graphyne structure, b) BN-yne structure, C) graphyne BN structure (Asadpour et al. 2015)

As can be seen so far, the extent of studies on the mechanical properties of graphyne is small. Even though only a narrow range of properties are usually studied, it's well spread in terms of methods of calculations, from MD to FDT to molecular mechanics.

However, the scientific community has shown interest on its electrical (Coluci et al. 2004, Pan et al. 2011, Li et al. 2011, Srinivasu and Ghosh 2012, Jing et al. 2013, Perkgoz and Sevik 2014) and optical properties (Kang et al. 2011, Peng et al. 2014, Bhattachary et al. 2015), thus being more and more studied nowadays. With such a variety of studies, the range of possibilities of applications of this carbon allotrope increase. All this, while the material is still hard to synthesize. Much can be expected from both graphene and graphyne-n structures.

3. Finite Element Modeling of Graphyne

The previous chapter provided fully evidence that computational modelling carbon nanomaterials is deemed necessary because the assessment of their mechanical behavior needs rigorous experiments at nanoscale, which still are complex and too expensive. Among the computational methods, MD and DFT proved to be the most effective. They have been applied to evaluate the mechanical behavior of graphene, fullerenes and graphyne. However, these methods require computer intensive calculations, as they depend not only on the electron cloud of atoms (*ab initio*, DFT) but also on thermodynamic variables (MD), such as pressure, temperature and energy. In order to avoid such computational efforts and time consuming analyses, the finite element method has been applied to nanoscale structures to assess their mechanical behavior. The application of finite element to investigate the behavior of graphene and fullerenes has been very successful in the last decade (Tserpes and Papanikos 2013, Odegard 2002a). However, finite element method has not yet been applied to study the mechanical behavior of graphyne. This is the main objective of this thesis, and it is reached hereafter.

To achieve this goal, a squared graphyne sheet is built in order to study its elastic properties. The sheet resembles that investigated by Cranford and Buehler (2011) using MD: each side is approximately 10 nm long – see the sheet geometry studied by Cranford and Buehler (2011) in Figure 3.1. The software chosen was Ansys Mechanical APDL 14.0 (2013).

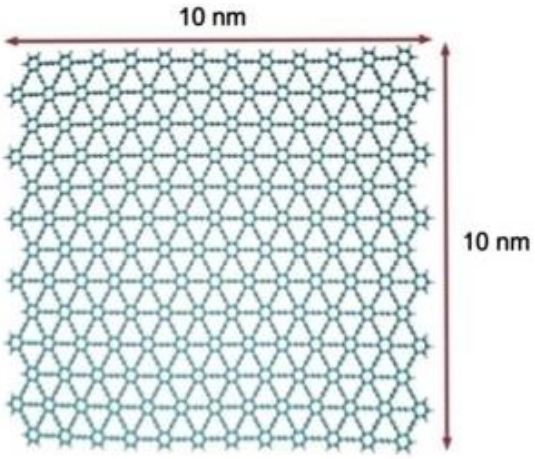

Figure 3.1 - Geometry of graphyne sheet studied by Cranford and Buehler (2011) using MD

3.1 Reference Finite Element Model

To accomplish the objective of develop a finite element model for this graphyne sheet, one must begin with the choice of suitable element types to simulate the interactions occurring between the carbon atoms. The base model, which is here designated as *Reference Model*, will account for three different types of covalent bonding, being them (i) aromatic, (ii) single and (iii) triple. The first type (aromatic)

occurs inside the hexagonal molecules of graphene, while the second (single) and third (triple) types occur on the acetylene links which forms the γ-graphyne. These three types of C-C bonds can be viewed in Figure 3.2.

Table 3.1 - Interatomic Bonds Length

Bond Type	**Length, L [Å]**
Aromatic	1.49
Single	1.48
Triple	1.19

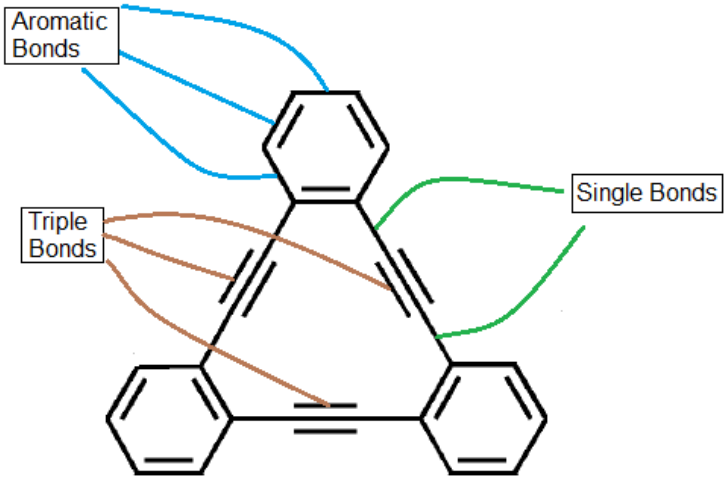

Figure 3.2 - Graphyne portion with interatomic bond description

To simulate such bonds in Ansys 14.0® (2013), the element Beam4 was chosen. This element was proven useful as it's a uniaxial element with tension, compression, torsion and bending capabilities. Also, this element is capable of translations and rotations on X, Y and Z directions, thus having 6 degrees of freedom per node. Another interesting particularity of this type of element is the amount of input data it lets the user controls. Hence, one can input cross-section area, 2nd moment of inertia about two principal axis of the beam cross-section, polar moment of inertia, angle of orientation of the beam, and some other real constants. The amount of options concerning input data is enlarged by material properties, body temperatures and some special features regarding stiffening and/or deflections, thought the latest aren't used for these simulations. The image belonging to Fig. 3.3 shows the geometry and coordinate system used by this element (Ansys 14.0® Help 2013). It shows a beam element with square cross-section for illustration, but the cross-section shape could be arbitrary.

Having the finite element selected, inputting the correct geometric properties is the following task. Therefore, in order to enable an accurate modelling of graphyne sheet, the length of the atomic bonds was assumed to be the same as those used by Cranford and Buehler (2011). Hence, Fig. 3-2 shows the aforementioned atomic bonds while Table 3.1 reveals the lengths of each bond (equilibrium distance between atoms).

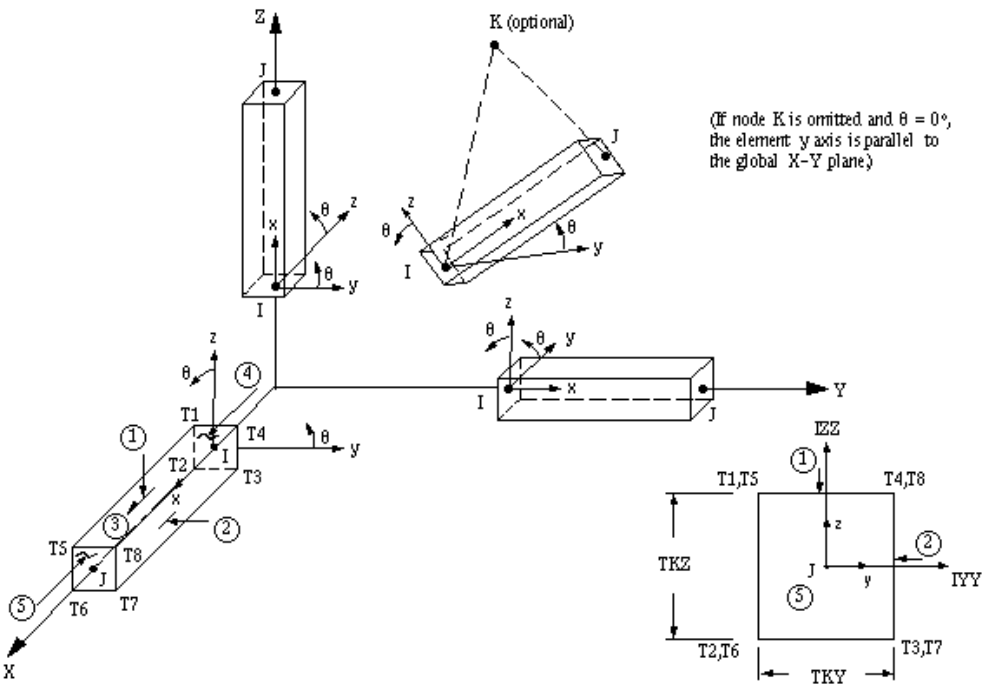

Figure 3.3 - Geometry of Beam4 (Ansys 14.0® Help (2013))

Now, we must characterize the geometrical properties of each beam cross-section. Because the formulation does not dependent on the shape of cross-section but only on its geometrical properties (e.g., area, 2nd moment of inertia), any cross-section shape could be chosen. With this in mind, the circular cross-section having diameter d was chosen.

To obtain the covalent forces being exerted by the interatomic bonds we follow the formulation proposed Odegard et al. (2002a), which was successfully implemented to evaluate the stiffness of CNTs and graphene. Hence, to calculate the bond-stretching interaction Young's Modulus, we follow

$$E^{\alpha}A = 2K^{\rho}L \tag{3.1}$$

which depends on bond length (L), cross-sectional area (A) and the stretching force constant (k^{ρ}). According to Odegard et al. (2002a), this constant has a value of k^{ρ}=469 Kcal/mol/Å^2. Besides the C-C bond-stretching interaction, the bond-angle variation interaction also should be taken into account when calculating the bond-angle interaction Young's Modulus, given by

$$E^{\beta}A = \frac{32K^{\theta}}{L}\left[\sin\frac{\Theta}{2}\right]^2 \tag{3.2}$$

This equation is applied to calculate bond-angle interaction Young's Modulus for each one of the three covalent bonds. In this equation, and besides the bond length (L) and cross-sectional area (A), it also depends on the undeformed bond angle (Θ) and the angle variation constant (k^{Θ}), which is k^{Θ}=63 Kcal/mol/rad^2, according to Odegard et al. (2002a). It should be noted that Θ is purely dependent on the angle between two adjacent covalent bonds, acting on the same carbon atom. The image present in Fig. 3-4 clarifies the previous sentence.

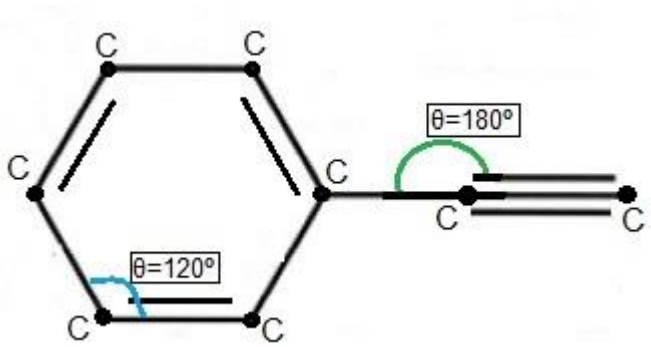

Figure 3.4: Graphyne fraction and undeformed bond angles

It is now important to mention that both equations (3.1) and (3.2) give the axial stiffness (EA) of a given C-C bond. Therefore, the calculation of E is dependent on the value of cross-section area while the opposite is also true (the value of A depends on the value of E). In conclusion, what really matters is the axial stiffness value (EA) and not the individual values of E and A. Therefore, we start by assuming that the cross-section area of the beam is equal to A=1 Å^2 (note that 1Å=0.1nm). Fixing this value, all the remaining cross-section properties are easily determined through the following basic formulas for the diameter d, moment of inertia I and polar moment J,

$$d = 2\sqrt{\frac{A}{\pi}} \qquad I = \frac{\pi d^4}{64} \qquad J = \frac{\pi d^4}{32} \tag{3.3}$$

Note that each aromatic and single covalent bond has a cross-sectional area of 1 Å^2 while the triple bonds should have 3 Å^2. Applying such equations, the cross-sectional properties for aromatic, single and triple covalent bonds, further implemented in Ansys APDL code, are given in Table 3.2.

Table 3.2 - Geometrical properties of cross-section for aromatic and single bonds (A=1Å^2) and triple bond (A=3Å^2)

Bound Type	**Single and Aromatic**	**Triple**
Diameter, d [Å]	1.12838	1.95441
Moment of Inertia, I [Å^4]	7.9578×10^{-2}	7.16197×10^{-1}
Polar Moment of Inertia, J [Å^4]	1.59155×10^{-1}	1.43239

With the geometrical properties calculated, we can now determine the Young's moduli to simulate the covalent forces being exerted by the interatomic bonds. This is done by using equations (3.1) and (3.2) and the cross-sectional areas for aromatic and single covalent bonds (A=1 Å^2) and triple bonds (A=3Å^2), as well as their lengths (Table 3.1). The values of (i) bond-stretching interaction Young's Modulus E^{α}, (ii) bond-angle interaction Young's Modulus E^{β} and (iii) total Young's Modulus E, are given in Table 3.3. Note that the triple bonds have a much smaller E value than both aromatic and single bonds, because their alignment (orientation) leads the bond-angle interaction Young's Modulus to $E^{\beta}=0$ (see Figure 3.4. For this very reason, one may expect graphyne to have a bigger elastic region than graphene, as this last allotrope is composed only by aromatic bonds. Furthermore, and because it has a negligible effect for the in-plane behavior of sheets, we assume a null Poisson's ratio for the bonds.

Table 3.3 - Young's modulus for aromatic and single bonds (A=1Å²) and triple bond (A=3Å²)

Bound Type	**Aromatic**	**Single**	**Triple**
E^{α} [nN/Å²]	97.1091	96.4573	25.8523
E^{β} [nN/Å²]	70.5076	70.5076	0
$E^{\alpha}+ E^{\beta} = E$ [nN/Å²]	167.617	167.441	25.8523

Finished the inputs of geometrical and mechanical properties of covalent bonds, we now proceed to the spatial modeling of the graphyne sheet. Hence, the images in Fig. 3.5 shows the evolution of the model in three steps, so one can glimpse how the graphyne sheet was built from scratch up to the point where all the carbon atoms and covalent bonds were in place. On a closer look we may see that, every image in Fig. 3.5 contains the chosen coordination system. Thus, the X-axis is aligned with the reclined chair or armchair direction of the graphyne sheet, while the Y-axis is aligned with the zigzag direction. To clarify the previous sentence, Fig. 3.6 is shown. The Z-axis is not yet used, as we're dealing with a bidimensional material (sheet in-plane behavior). However it could be considered as if it were aligned with the graphyne thickness direction.

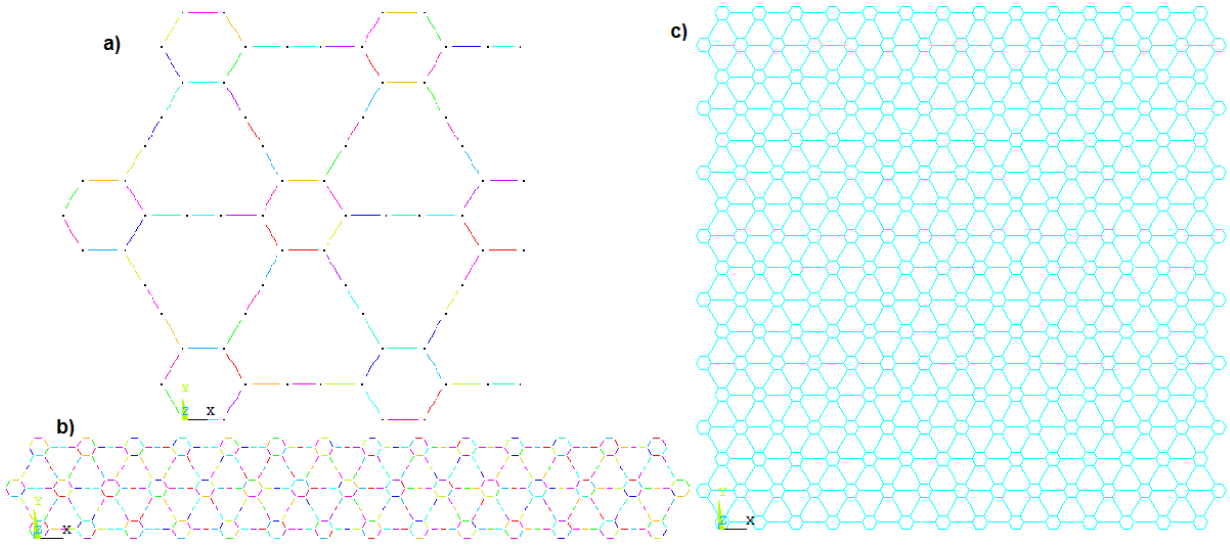

Figure 3.5: Evolution of the model built on Ansys 14.0® (2013): a) first steps into the construction of the graphyne sheet; b) replicating through the armchair direction; c) complete graphyne sheet

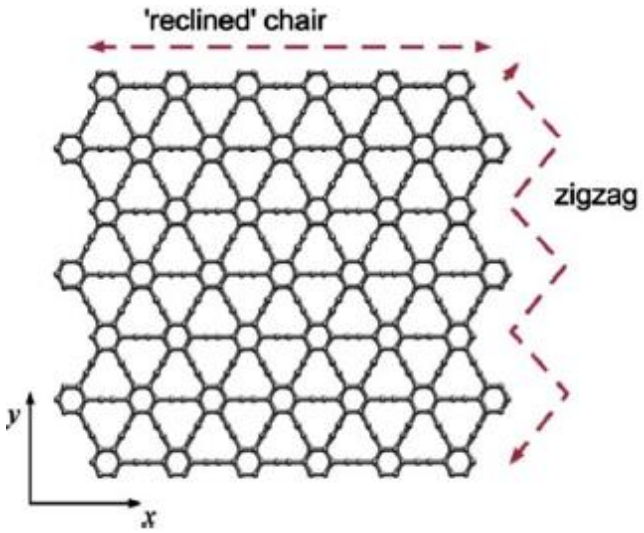

Figure 3.6 - Definition of the geometry of graphyne edges (Cranford and Buehler 2011)

3.2 vdW Finite Element Model

The finite element model previously described (*Reference Model*) accounted for bonded interactions between carbon atoms. However, it is known that forces exerted between atoms may also be due to non-bonded interactions. These forces are designated as *van der Waals* (vdW) forces and are due to the proximity between atoms, regardless of being bonded or not. The model we now present accounts not only for bonded interactions but also for non-bonded interactions. Because it will include the effect of *van der Waals* (vdW) forces, it is designated as *vdW Model*. vdW forces tend to be relatively weak compared to the forces due to the covalent bonds (Granta 2015). With this second model, we'll attest the veracity of this statement applied to the graphyne. The *vdW Model* was built following the same steps as before, but now vdW forces are added to the Reference Model (Fig. 3.7), being the starting point of this section.

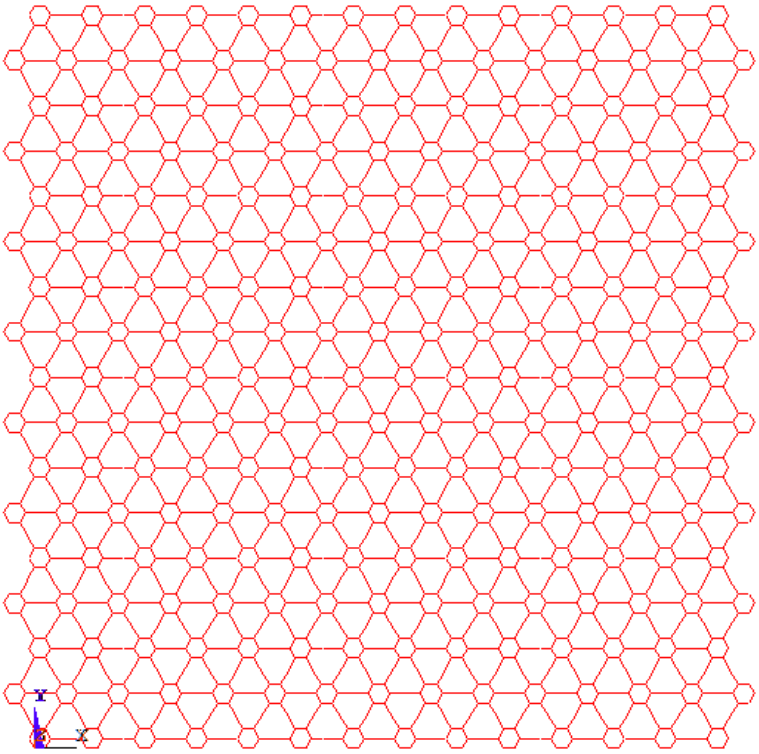

Figure 3.7 - Reference Model: graphyne sheet with covalent bonds

To do so, a new finite element was chosen specifically to simulate the effect of these forces, and how a carbon atom will interact with its neighbor carbon atoms on the presence of such vdW contribution. The finite element chosen in Ansys 14.0® (2013), is designated Link180. This is a tridimensional truss element used to simulate uniaxial tension-compression forces. It has three degrees of freedom per node, thus being capable of translation in X, Y and Z axes. Link180 is composed by two nodes in total, as the image shown in Fig. 3-8 confirms. In the same image it's also possible to see the coordinate system used by the element. Regarding input data, the user is able to control both the cross sectional area A and the material properties of the bar.

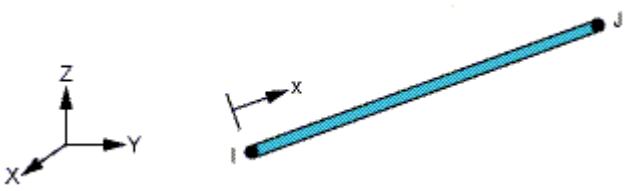

Figure 3.8 - Geometry of LINK180 (Ansys 14.0® Help (2013))

Having the element selected, some geometrical properties should be given. They are the cross section area A and Poisson's ratio. As for Poisson's ratio, once again it was assumed a value of zero. Regarding the calculation of mechanical properties, the bar axial stiffness due to vdW interaction is also

obtained from the formulation by Odegard et al. (2002a), following the well-known 12-6 potential of Lennard-Jones,

$$E^w A = \frac{2\rho^{ij} D^{ij}}{(\rho - \rho^{ij})^2}\left[\frac{1}{2}\left(\frac{\rho^{ij}}{\rho}\right)^{12} - \left(\frac{\rho^{ij}}{\rho}\right)^{6}\right] \tag{3.4}$$

$$D^{ij} = \sqrt{D^i D^j} \qquad\qquad \rho^{ij} = \sqrt{\rho^i \rho^j} \tag{3.5}$$

in which (i) the deformed interatomic distance is ρ, (ii) the well depth of interaction between carbon atoms i and j is D^{ij}, and (iii) the vdW equilibrium distance for interaction between carbon atoms i and j is ρ^{ij}. The aforementioned variables (defined via Eqs. 3.5) are quite useful in case the different interacting atoms. In this case, because only carbon atoms exist, $D^{ij}=D^i=D^j$ and $\rho^{ij}=\rho^i=\rho^j$. In the case of carbon, Odegard et al. (2002a) stipulate D^{ij} = 0.07 Kcal/mol and ρ^{ij} = 3.55 Å.

It should be noted that we start from the undeformed state on the graphyne sheet and don't know, at this point, how much displacement each atom will undergo. Therefore, we assumed the value of ρ as being equal to the interatomic distance before the loading is applied to the sheet. Fig. 3.9 shows the truss bars simulating vdW forces acting on carbons hexagons (Fig. 3.9a) and vdW forces acting on carbon atoms of acetylene linkages (Fig. 3.9b). Special attention should be taken regarding the value of ρ as it is the maximum distance a bond of this kind can take, once surpassed, the vdW interaction becomes negligible. This explains why not every pair of carbon atoms in Fig. 3.9 suffers the effect of vdW forces (not linked by truss bars). Thus, ρ^{IJ} can be considered the maximum operating distance between carbon atoms for non-negligible vdW forces. A closer look at Fig. 3.9 shows that there are three relevant interatomic distances in terms of calculation of the vdW interaction Young's Modulus. Regarding the variables name, present on both images from Fig. 3.9, ρ_c is the length of the crossed vdW bonds, while ρ_p is the length of the bonds perpendicular to the acetylene links.

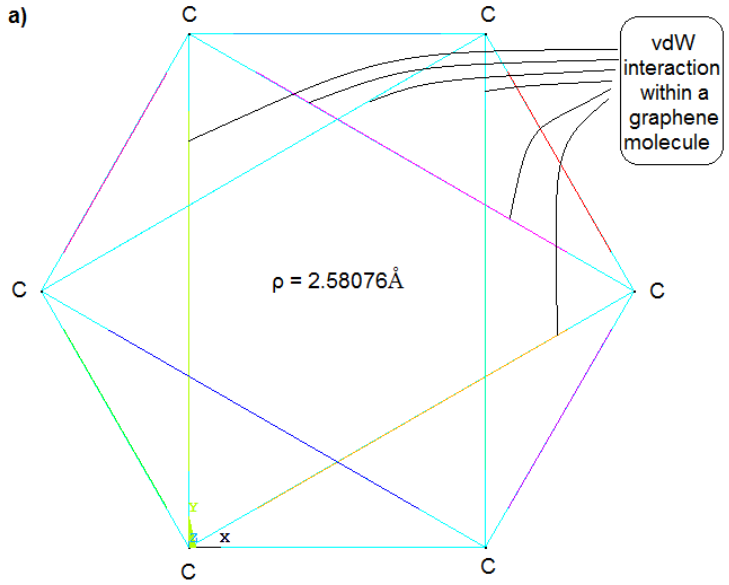

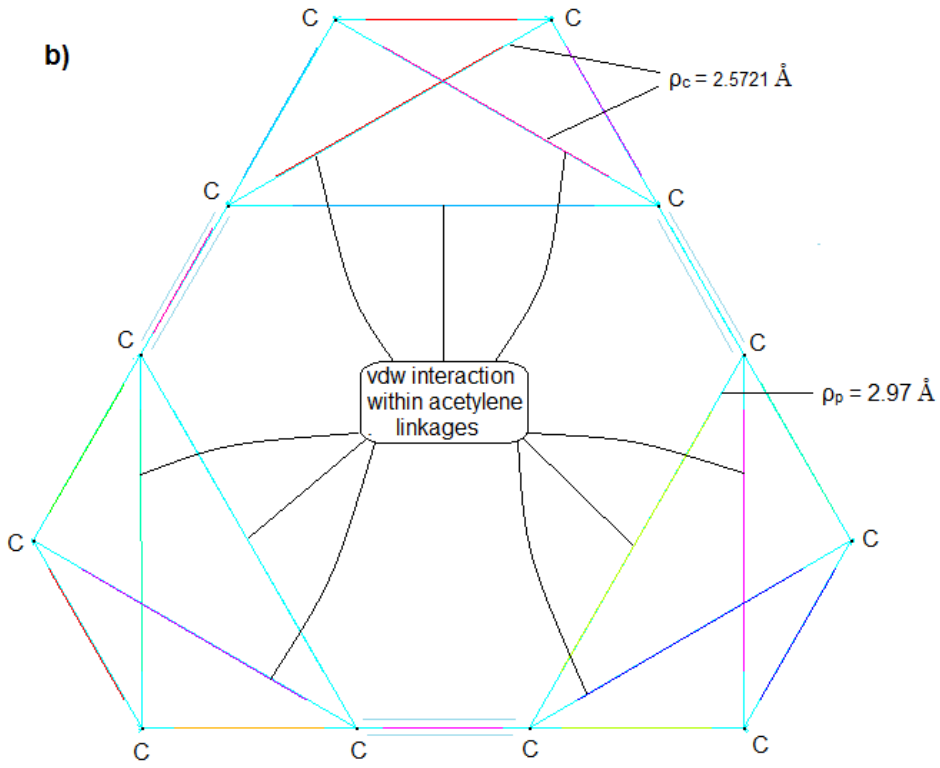

Figure 3.9: vdW interaction model; a) vdW forces acting on carbon hexagon, b) vdW forces acting on acetylene linkages

Again assuming A=1 $Å^2$ for each truss bar depicted in Fig. 3.9 with distinct lengths (ρ), the values of E^w calculated trough Eq. (3.4) are shown in Table 3.4.

Table 3.4 - Young's modulus for bars simulating vdW interactions

van der Waals Interaction Young's Modulus	**Units [nN/Å²]**
$E^{W}_{Hexagon}$	5.94507×10^{-1}
$E^{W}_{Perpendicular}$	1.37154×10^{-1}
$E^{W}_{Crossed}$	6.13147×10^{-1}

We started from the Reference Model depicted in Fig. 3.7 and included bars to account for vdW forces, thus having arrived at the vdW Model depicted in Fig. 3.10. Both models comprise 2830 carbon atoms, and display a total length L_i=10.28 nm and height H_i=10.14 nm. This was the graphyne shape closest to a square shape, respecting the covalent bonds length given by Cranford and Buehler (2011).

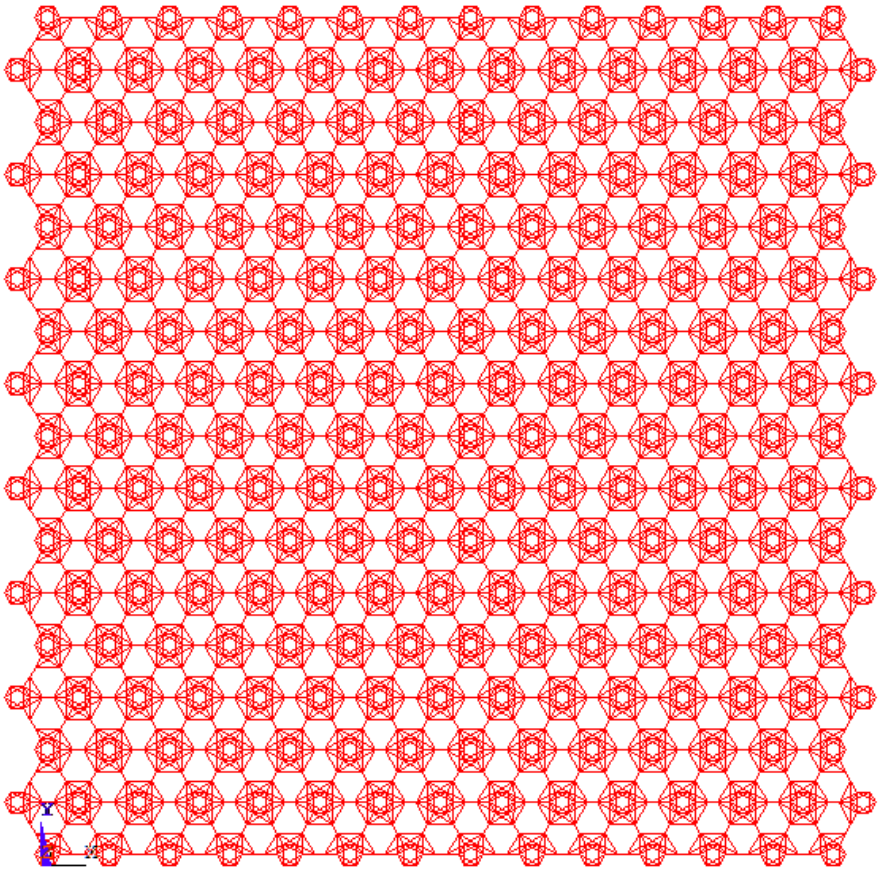

Figure 3.10 - vdW Model: graphyne sheet with both covalent and vdW bonds

The next step to fulfill will be the construction of the code that considers the proper boundary conditions and applied loading for both Reference and vdW Models.

3.3 Boundary and Loading Conditions

Now that the graphyne sheet was modeled on Ansys 14.0® (2013) within two main APDL codes, the next logical step will be to separate them in two different sets of calculations: one for the Reference Model and another for the vdW Model. However, in each case there are similar procedures regarding the imposition of boundary conditions and applied loading.

Since the purpose of this work is to evaluate the mechanical properties of graphyne, there are four main tests to be performed to the graphyne sheet:

- Uniaxial tensile test in the armchair direction (X-axis) – the graphyne elastic modulus E_x and Poisson's ratio ν_{yx} will be determined from this test.
- Uniaxial tensile test in the zigzag direction (Y-axis) – the graphyne elastic modulus E_y and Poisson's ratio ν_{xy} will be determined from this test.
- Biaxial tensile test (XY-plane) – the graphyne bulk modulus K will be determined from this test.
- Shear test (XY-plane) – the graphyne shear modulus G_{xy} will be determined from this test.

Such analyses must be done using the graphyne sheet with covalent bonds only (Reference Model, Fig. 3.7) and the graphyne sheet with both covalent bonds and vdW forces (vdW Model, Fig. 3.10). In total and after the APDL codes were written to every different case, we should had eight distinct programs.

Uniaxial tensile test in the armchair direction (X-axis)

The first analysis performed over the graphyne sheet was a uniaxial tensile test aligned with the armchair direction (X-axis), as depicted in Fig. 3.11. To do so, unit forces were applied to all the atoms on the right edge of the sheet, while the atoms on the left edge were restrained from displacement in X-axis but allowed to displace in Y-axis direction. To prevent any kind of (residual) bending behavior along the sheet, displacements along the Z-axis were totally restricted. To avoid any undesirable rigid-body movement that may appear during the solving process on Ansys 14.0® (2013), the carbon atoms at mid-height of the right and left edges of the sheet were fixed against displacements along Y-axis. Regarding the unit forces, they were applied in a total of 82 carbon atoms covering the right edge of the graphyne sheet, so a total force of F=82 nN was applied in this test. Fig. 3.11 shows how the boundary conditions and applied forces were imposed in the Reference Model (because the imposition in vdW Model is equal, it is nor shown here). The objective of this analysis was to extract the following displacements: (i) a, the displacement in zigzag direction (X-axis), and (ii) d, the displacement in armchair direction (Y-axis). With these values, we can later calculate the armchair elastic modulus, E_x and the Poisson's ratio v_{yx}.

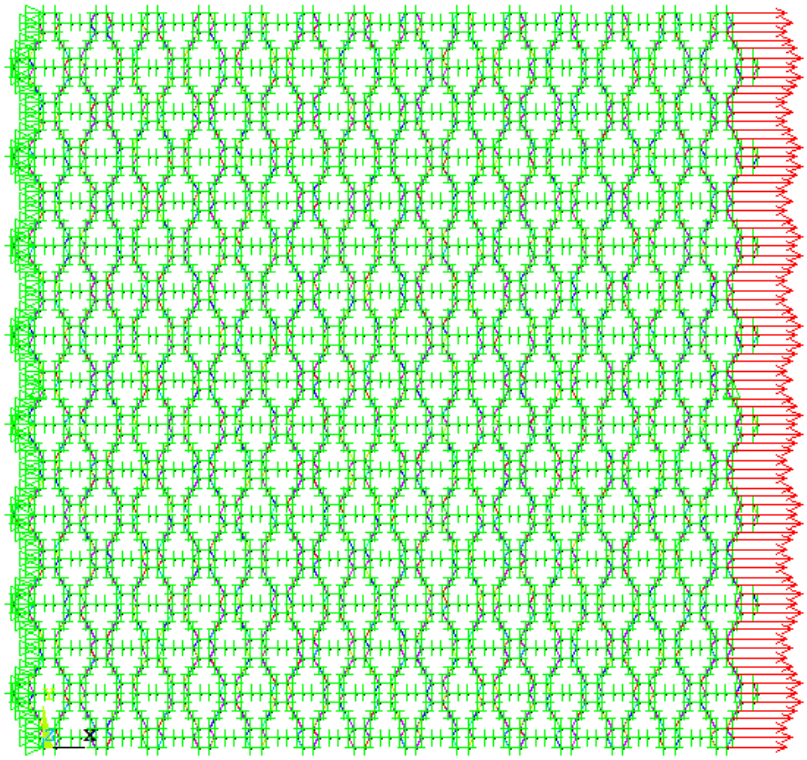

Figure 3.11: Uniaxial tensile test in the armchair direction (X-axis): boundary conditions and applied loading

Uniaxial tensile test in the zigzag direction (Y-axis)

The second analysis concerns the uniaxial tensile test aligned with the zigzag direction (X-axis) of the graphyne sheet (Fig. 3.12). Unit forces were applied to all the atoms on the top edge of the sheet, while the atoms on the bottom edge were restrained from displacement in Y-axis but allowed to displace in X-axis direction. As in the previous test, displacements along the Z-axis were totally restrained. The carbon atoms at mid-width of the top and bottom edges of the sheet were fixed against displacements along X-axis, in order to avoid any undesirable rigid-body movement of the sheet. Unit forces were applied in a total of 83 carbon atoms covering the top edge of the graphyne sheet leading to a total force of F=83 nN. Fig. 3.12 shows how the boundary conditions and applied forces were imposed in the Reference Model (because the imposition in vdW Model is equal, it is nor shown here). The objective of this analysis was to calculate the following displacements: (i) c, the displacement in zigzag direction (X-axis), and (ii) b, the displacement in armchair direction (Y-axis). After knowing these values, we are able to calculate the zigzag elastic modulus, E_y and the Poisson's ratio v_{xy}.

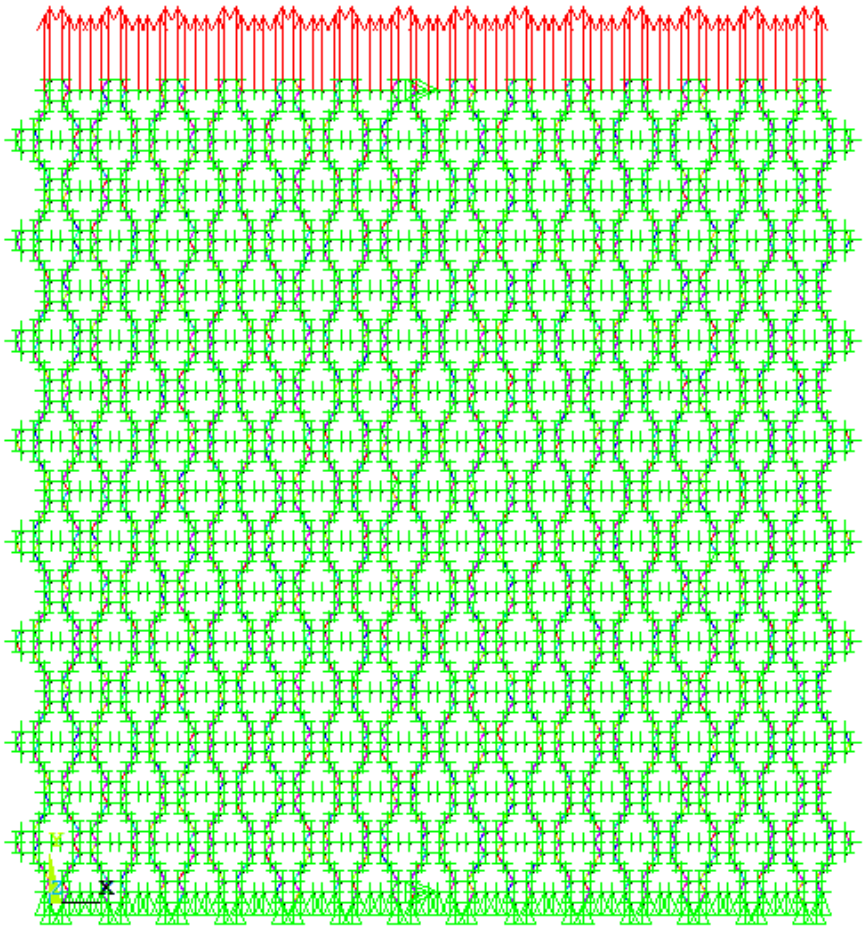

Figure 3.12: Uniaxial tensile test in the zigzag direction (Y-axis): boundary conditions and applied loading

Biaxial tensile test (XY-plane)

The third analysis is a biaxial tensile test. Such test must be simulated through the application of unit forces on each edge of the graphyne sheet, as depicted in Fig. 3.13. As before, bending was prevented by the restriction of displacement along the Z-axis. Also, to exclude any possibility of rigid-body movement during the simulation, the carbon atoms in the sheet center were restricted in terms of translation in both X-axis and Y-axis. The unit forces applied on each edge follow the rule of bulk modulus calculation: (i) unit forces were applied in the armchair direction (oppositely in right and left edges of the sheet), result in F_x=82 nN, and (ii) unit forces were applied in the zigzag direction (oppositely in top and bottom edges of the sheet), result in F_y=82 nN. This analysis aims at extracting the values of bulk modulus of this bidimensional sheet. In order to achieve this objective, one must get the length, L_f, and height, H_f, of the deformed sheet (after running the simulation). This procedure will enable the computation of the variation of area ΔA, needed for the calculation of bulk modulus, K_{xy}. Fig. 3.13 shows the Reference Model in this test.

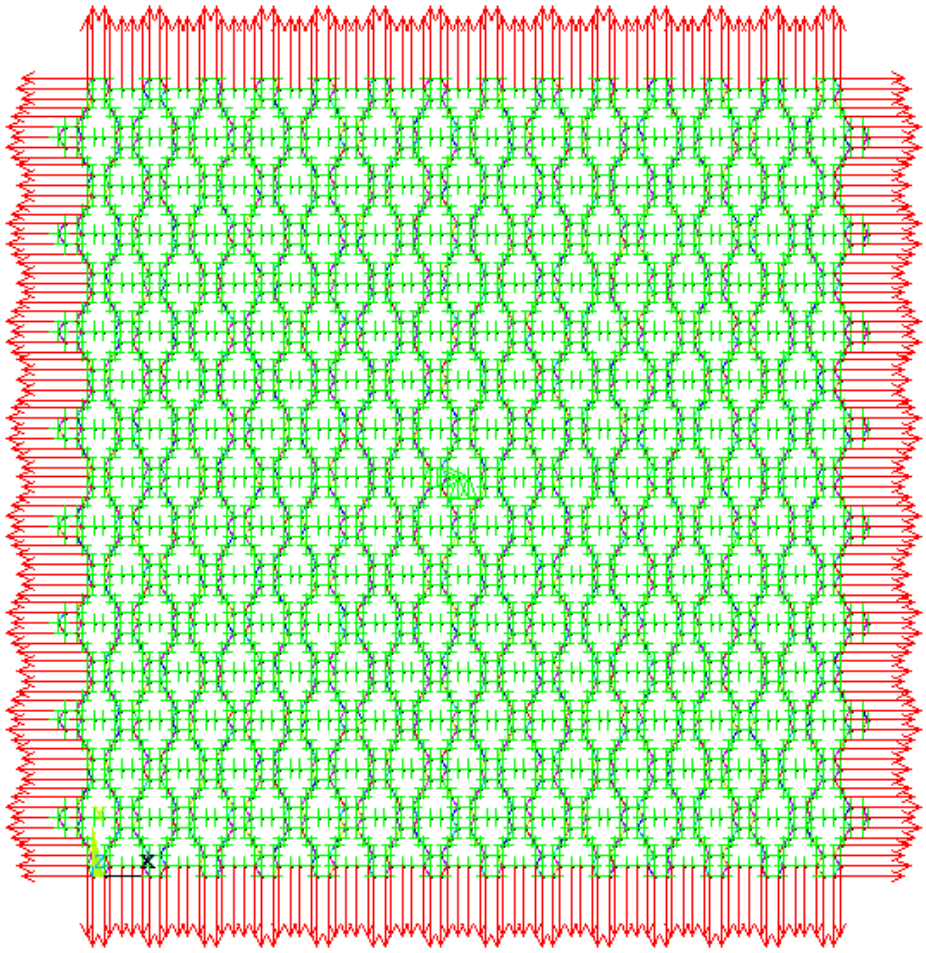

Figure 3.13: Biaxial tensile test (XY-plane): boundary conditions and applied loading

Shear test (XY-plane)

The fourth analysis is performed with the intent to obtain the shear stress, G_{xy}, of the graphyne sheet. To accomplish this task, the central carbon atoms in each edge were constrained, being the atoms at the top and bottom edges prevented to translate onto Y-axis direction, while the atoms at the left and right edge had their displacement restricted on X-axis direction. Likewise, to prevent the bending behavior over the graphyne sheet, we inhibited the displacement along the Z-axis. The unit forces follow the same principles as the previous analyses, regarding the point of application on the edges and its magnitude. The only change is the direction of the unit force: (i) the unit forces on the top and bottom edges apply a clockwise moment to the sheet and (ii) the unit forces on the right and left edges apply a anti-clockwise moment to the sheet. Because the total force is similar in all four edges (82nN), these opposite moments vanish but the sheet will distort. The image in Fig. 3-14 shows the boundary conditions and applied loading in this shear test. This analysis provides the displacements occurring in each corner of the graphyne sheet, which will later be used to compute the value of shear strain, γ, and finally obtain the shear modulus G_{xy}.

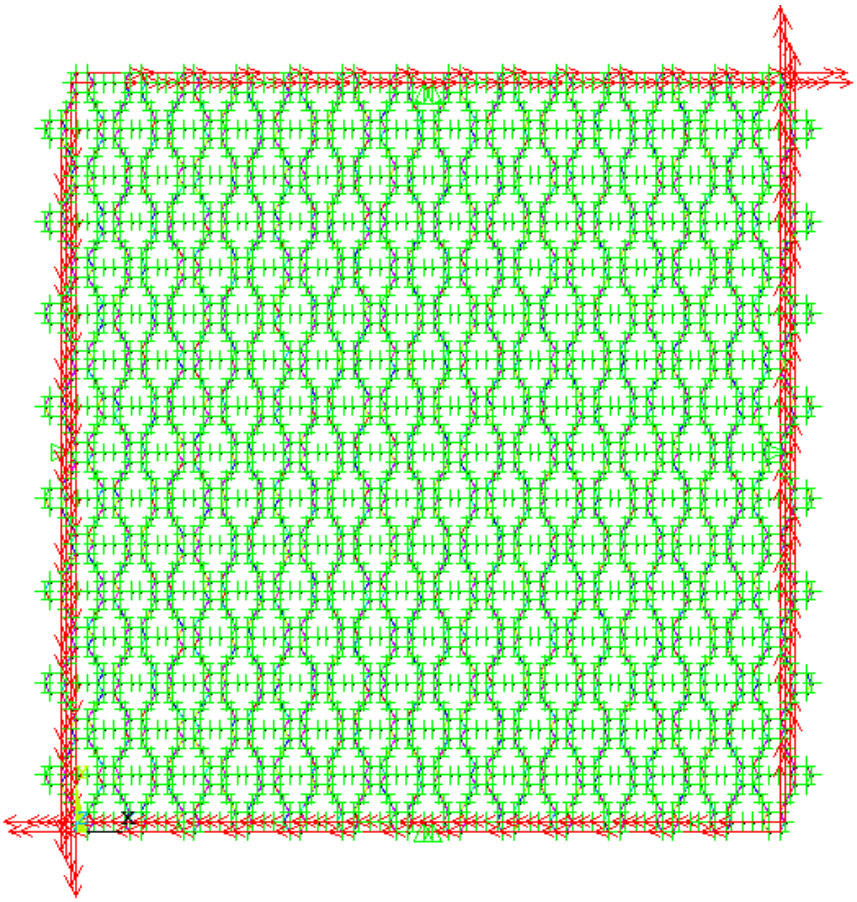

Figure 3.14: Shear test (XY-plane): boundary conditions and applied loading

The images seen in Fig. 3.11-14 regard the Reference Model, but similar images could be taken for the vdW Model. With all this data, the models were ready to run the eight simulations and obtain the aforementioned displacements for further calculus.

4 Elastic Properties of Graphyne

In this chapter, the results obtained from the finite element models will be presented and discussed.

4.1 Presentation of Results

Firstly, the best way to confirm if the simulations were running smoothly was to plot the graphyne sheet before and after being stretched/sheared by the applied forces. Such images, are presented in Fig 4.1 for the four tests (in case of Reference Model).

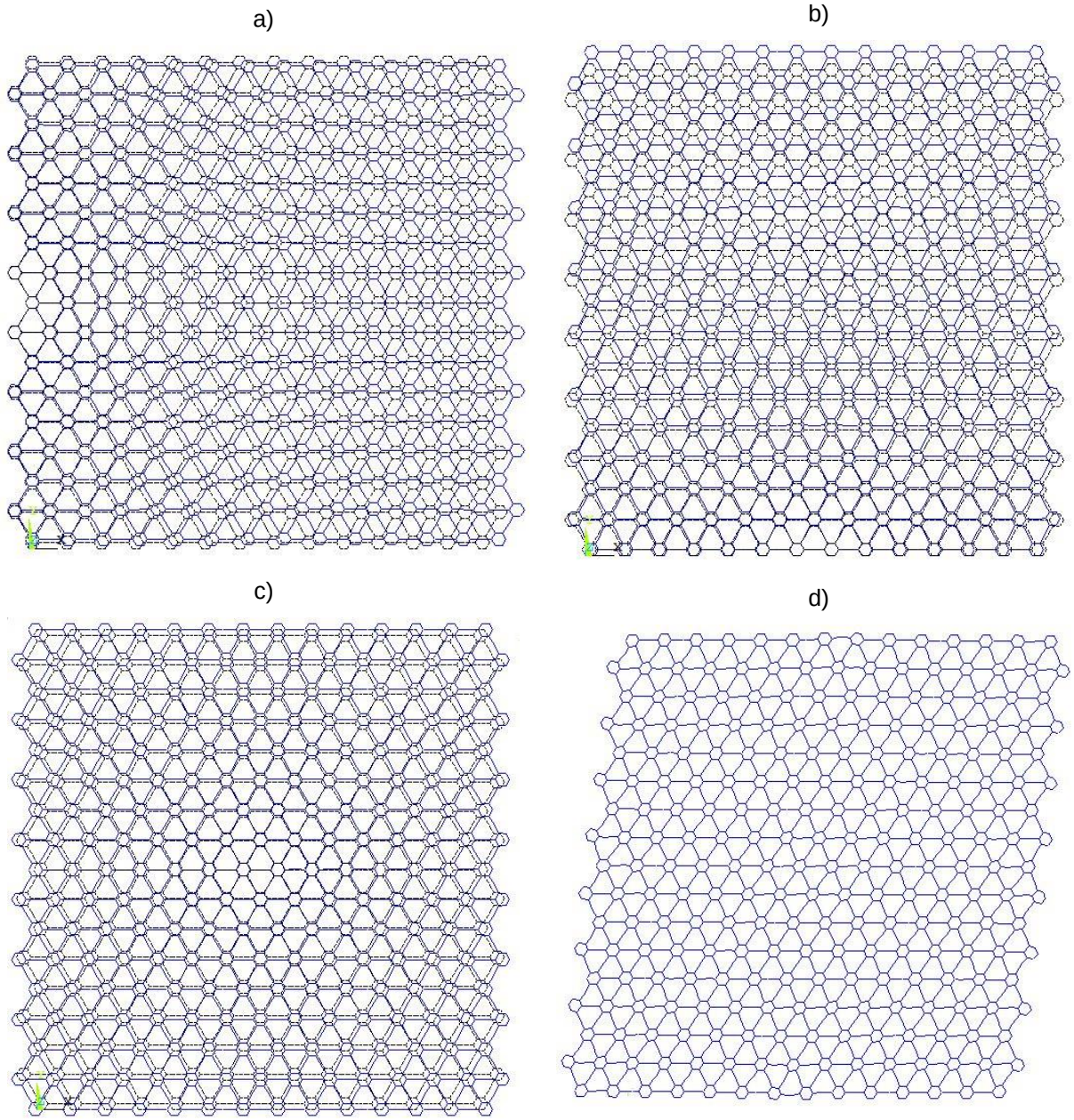

Figure 4.1: Initial and deformed shapes of graphyne sheet (Reference Model): a) uniaxial tensile test on armchair direction, b) uniaxial tensile test on zigzag direction, c) biaxial tensile test, d) shear test

The deformed shapes of the graphyne sheet can be drawn qualitatively as depicted in Figures 4.2 (uniaxial and biaxial tests) and 4.3 (shear test). These figures show the relevant displacements, deformed sheet size and positions of displaced nodes needed to calculate the graphyne elastic properties. In those images, the black square is equivalent to the graphyne sheet before any deformation takes place. The blue square is a representation of the deformation after the uniaxial tensile test was performed on armchair direction, whereas the red square is the equivalent for the uniaxial tensile test on zigzag direction. In turn, the green square shows the final dimensions the graphyne sheet after the biaxial tensile test is performed. Fig. 4.3 shows the corner position before and after the graphyne sheet is subjected to shear.

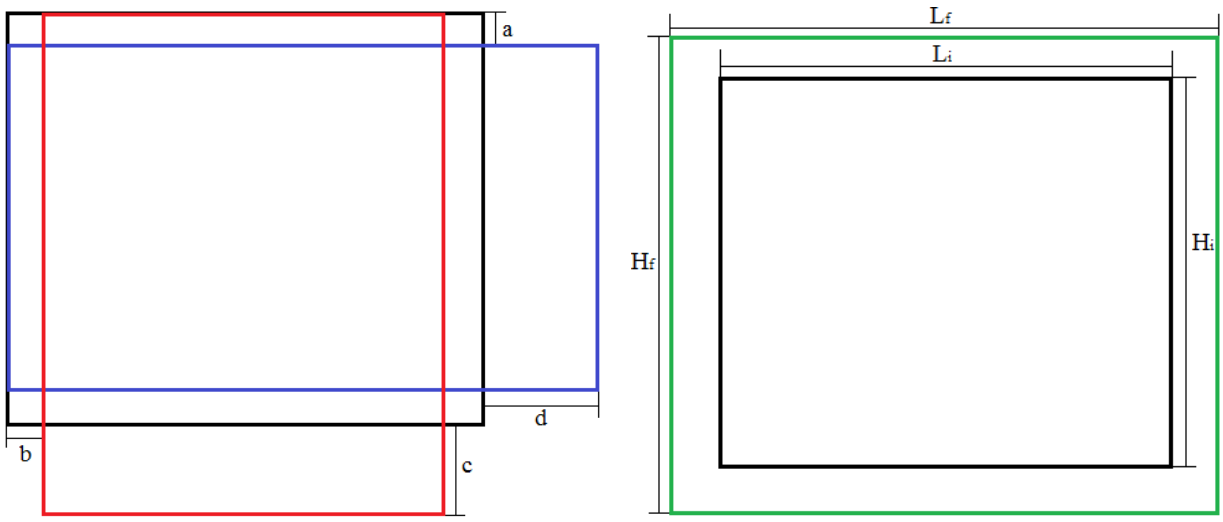

Figure 4.2: Displacements taking place on the graphyne sheet for uniaxial and biaxial tensile tests

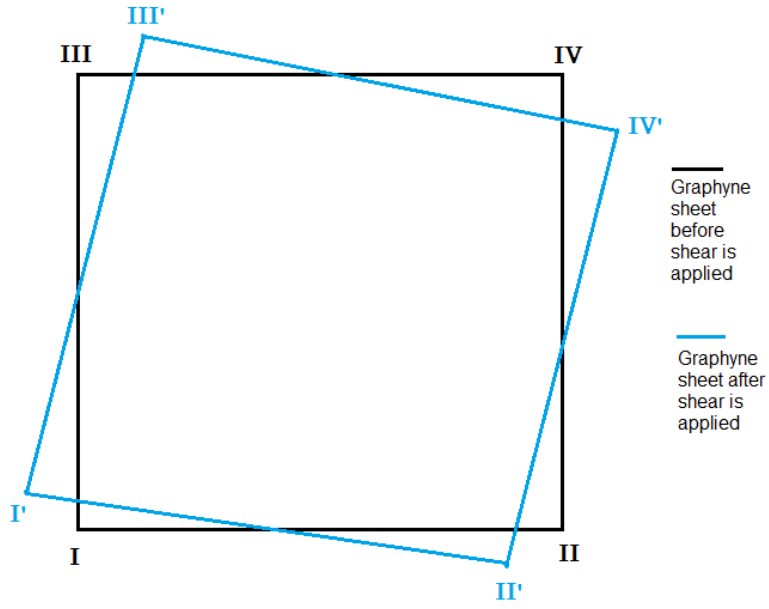

Figure 4.3 - Vertices position before and after shear is applied

Once the solving process on Ansys 14.0® (2013) was finished, we acquired the needed values: (i) a, b, c, d (uniaxial tests), (ii) L_f, H_f (biaxial test) and (iii) final position of corner nodes (shear test). Table 4.1 shows all the relevant values obtained from the uniaxial and biaxial tests, for both Reference and vdW Models. A separate table was built to show the displacement on the graphyne sheet due to the shear forces. The vertices were denoted with roman numerals so one can easily identify them (seen Fig. 4.13). Table 4.2 displays the values resulting from the shear tests on both Reference Model and vdW Model.

Table 4.1 - Displacements and sheet sizes after uniaxial and biaxial tensile tests

Analysis Type	**[Å]**	**Reference Model**	**vdW Model**
Uniaxial Tensile Test on X axis	a	-0.7562	-0.74988
	d	3.6405	3.6165
Uniaxial Tensile Test on Y axis	b	-0.7789	-0.77314
	c	3.8781	3.8539
Biaxial Tensile Test	H_f	104.008	103.992
	L_f	105.094	105.082

Table 4.2 - Coordinates before and after shear strength test

Corner	**Initial Coordinates**	**Corner**	**Reference Model**	**vdW Model**
I [Å]	(0;0)	I' [Å]	(-11.235;6.7624)	(-11.197;6.7578)
II [Å]	(94.18;0)	II' [Å]	(81.412;-4.9109)	(81.456;-4.9171)
III [Å]	(0;101.3769)	III' [Å]	(12.768;106.288)	(12.723;106.295)
IV [Å]	(94.18;101.3769)	IV' [Å]	(105,413;94.6145)	(105.378;94.6203)

4.2 Calculation of Elastic Properties

With all these results, we can finally achieve the main objective: to obtain the elastic properties of graphyne. Before that, we know that since graphyne is a discrete atomic structure, it has no real thickness (like continuous plates or shells have). In this case, the values of elastic modulus are given in N/m (Yang and Xu 2012). However, being a 2D material, some similarity with plates and shell exist. In this case, a thickness of 3.2 Å is usually adopted. With this, we are able to calculate the elastic modulus values in GPa (or TPa) and compare with those obtained by Cranford and Buehler (2011) and Zhang et al. (2012). To obtain the results of Young's Modulus in GPa, one must divide the stress σ (obtained in N/m) by the thickness t=3.2 Å. This value comes from adhesion energy results, presented in Cranford and Buehler (2011). With this in mind, a set of equations well-known from elasticity must be used.

Elastic modulus E_x and Poisson's ratio ν_{yx} (uniaxial tensile test in the armchair direction, X-axis)

$$E_x = \frac{\sigma_x}{\varepsilon_x} \qquad \varepsilon_x = \frac{d}{L_i} \qquad \sigma_x = \frac{F}{H_i} \tag{4.1}$$

$$\nu_{yx} = -\frac{\varepsilon_y}{\varepsilon_x} \qquad \varepsilon_y = \frac{2a}{H_i} \tag{4.2}$$

In these formulas, σ_x is the uniaxial stress in X-axis direction while ε_x and ε_y are the extensions in X and Y directions. The other variables (displacements, width and height) were given before (Table 3.5).

Elastic modulus E_y and Poisson's ratio ν_{xy} (uniaxial tensile test in the zigzag direction, Y-axis)

$$E_y = \frac{\sigma_y}{\varepsilon_y} \qquad \varepsilon_y = \frac{c}{H_i} \qquad \sigma_y = \frac{F}{L_i} \tag{4.3}$$

$$\nu_{xy} = \frac{-\varepsilon_x}{\varepsilon_y} \qquad \varepsilon_x = \frac{2b}{L_i} \tag{4.4}$$

In these formulas, σ_y is the uniaxial stress in Y-axis direction while ε_x and ε_y are the extensions in X and Y directions. The other variables (forces, displacements, width and height) were given before (Table 3.5).

Bulk modulus K (biaxial tensile test, XY-plane)

$$K = \frac{\theta}{2\Delta} \qquad \Delta = \frac{\Delta A}{A_0} \qquad \Delta A = A_f - A_0 \tag{4.5}$$

$$\frac{\theta}{2} = \frac{\sigma_1 + \sigma_2}{2} = \frac{F}{2H_i} + \frac{F}{2L_i} \tag{4.6}$$

In these formulas, $\theta/2$ is the average in-plane stress, A_0 is the sheet initial area, A_f is the sheet final area, ΔA is the variation of sheet area, and Δ is area extension. The other variables (forces, widths and heights, areas) were given before (Table 3.5). There aren't many studies done on the in-plane bulk modulus. In this specific case, the results obtained shall be presented in N/m, so we can better compare them with those obtained from Asadpour et al. (2015).

Shear modulus G_{xy} (shear test, XY-plane)

$$G_{xy} = \frac{\tau_{xy}}{\gamma} \qquad \tau_{xy} = \frac{F}{H_i} \qquad \gamma = \gamma_I - \gamma_{II} \tag{4.7}$$

As for shear strain, γ, since we are in presence of rotation coupled with translation of the atoms, as Fig. 4-3 show us, we must calculate two distinct angles and subtract them to later obtain the desired

shear strain result. Fig. 4.4 gives us a glimpse of the exact position of the required angles to subtract in order to obtain the shear strain.

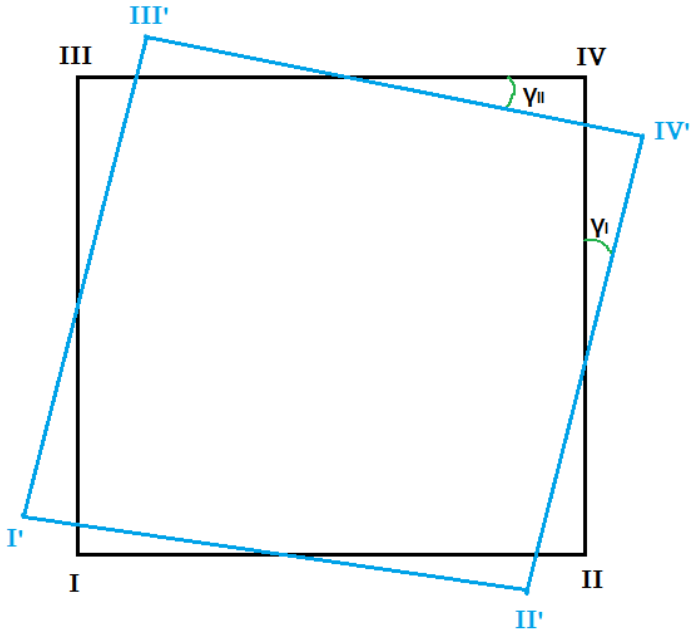

Figure 4.4 - Shear Strain angles

Whether we calculate these angles on corner I or IV, the shear strain should be the same, if the simulation is well defined on Ansys 14.0® (2013). Once more, the resulting in-plane shear modulus will be presented in N/m, which is very useful for later comparison with Asadpour et al. (Asadpour et al. 2015).

Finally, having all the necessary means and data, we shall present graphyne's mechanical properties. All the results are displayed in Table 4.3 for both models (Reference Model and vdW Model), as well as those elastic properties values obtained by other researchers using either MD or DFT simulations.

Table 4.3 - Mechanical Properties of Graphyne

Property	**Reference Model**	**vdW Model**	**Cranford and Buehler (2011)**	**Zhang et al. (2012)**	**Yang and Xu (2012)**	**Asadpour et al. (2015)**	**Units**
E_x	228.4 (713.7)	229.9 (718.5)	201.4 (629.4)	(508.0)	~155.0	190.69	N/m (GPa)
ν_{yx}	0.421	0.421				0.410	-
E_y	208.5 (651.6)	209.8 (655.7)	247.0 (772.0)	(505.0)	~150.0	-	N/m (GPa)
ν_{xy}	0.396	0.396	-	-	-	-	-
K	164.5	165.5	-	-	-	122.7	N/m
G_{xy}	70.5	71.0	-	-	-	77.0	N/m

4.3 Discussion of Results and Model Validation

After having obtained the main results (elastic properties of graphyne), we can describe some conclusions regarding those values and make a comparison between these values and those determined by other authors.

Influence of van der Waals forces

The first main remark regards the influence of non-bonded interatomic forces on the elastic properties of graphyne. From the comparison between the elastic properties (E_x, E_y, v_{yx}, v_{xy}, K, G_{xy}) obtained from the Reference Model (only bonded interatomic forces) and those coming from vdW Model (both bonded interatomic forces and van der Waals interatomic forces), we may easily conclude that the influence of van der Waals interatomic forces on the elastic behavior of graphyne is negligible because the maximum difference is about 0.6%. Regardless the direction we may choose, these forces effect is very weak, accounting only for 1 N/m of stiffness on the whole model. As for the Poisson's ratio, the influence is even smaller, and can't be found on our present results. The same happens for the in-plane bulk modulus. vdW forces have an even smaller influence on the in-plane shear modulus of graphyne.

However, one should not forget that our calculations were made assuming fixed interatomic distances for the calculation of bar elastic modulus (i.e. the equivalent stiffness of the bar was kept constant, as it did not depend on current interatomic distances). By having a closer look at the vdW distance of equilibrium between the atoms, which is 3.55 Å for carbon, we can estimate that such influence wouldn't be great unless the atoms were able to be much closer to each other. To witness such a remarkable event, we had to have some quite flexible covalent bonds, which is not the real case.

Therefore, we conclude that the consideration of van der Waals interatomic forces can be disregarded in the modelling of graphyne in-plane behavior. However, when studying the behavior of highly bended graphyne sheets (see Fig 2.4, for the case of graphene) or even the behavior of multi-layer graphyne, the consideration of van der Waals interatomic forces is mandatory because neighbor carbon atoms may not exhibit covalent bonds and can stay in equilibrium only due to van der Waals forces. Because of this evidence, we will now proceed by describing the value obtained from the Reference Model.

Orthotropic behavior

The observation of the results shown in Table 4.3 shows that we are in the presence of an orthotropic material, as the values of Young's modulus in armchair (X-axis) and zigzag (Y-axis) directions are not equal. Their difference is roughly 20 N/m, which corresponds to 9.5%. Comparing the graphyne Young's modulus with that of graphene which has around 325 N/m in armchair direction and 315 N/m in zigzag direction according to Yang and Xu (2012), we easily conclude that graphyne is a more flexible

(less stiff) material than graphene. Bearing in mind that graphene is also slightly orthotropic, the percentage difference is higher for graphyne than for graphene. It should also be highlighted that graphyne is stiffer in the armchair direction than in the zigzag one (E_x>E_y).

Regarding the Poisson's ratio, it can be concluded that graphyne exhibits a high transversal contraction in both directions, as the Poisson's ratio varies around 0.40. Because the Poisson's ratio becomes smaller for the zigzag direction of the graphyne sheet than for its armchair direction (ν_{yx}>ν_{xy}), one can conclude that graphyne has also orthotropic behavior regarding the transversal contraction. In this case, the percentage difference (about 6.5%) is even smaller than for the Young's moduli (about 9.5%).

Before going into details about the shear modulus (G_{xy}) and in-plane bulk modulus (K), it is useful to define the stress-strain relation for two-dimensional (2D) media. Let us consider a homogeneous 2D (without 3rd dimension) sheet which is isotropic. For such a 2D material, the relationship between the stress tensor and strain tensor is given by

$$\sigma_{ij} = 2G\varepsilon_{ij} + (K - G)\varepsilon_{kk}\delta_{ij} \qquad (i, j, k = 1,2) \tag{4.8}$$

This relation depends on the 2D bulk modulus K and shear modulus G. Similarly, the strain-stress relation is given by

$$\varepsilon_{ij} = \frac{1+\nu}{E}\sigma_{ij}\delta_{ij} - \frac{\nu}{E}\sigma_{kk}\delta_{ij} \qquad (i, j, k = 1,2) \tag{4.9}$$

where ν and E are the 2D Poisson's ratio and Young's modulus, respectively. Clearly, there are only two independent moduli. Comparing relations (4.8) and (4.9) yields the following relations,

$$G = \frac{E}{2(1+\nu)} \tag{4.10}$$

$$\nu = \frac{K-G}{K+G} \tag{4.11}$$

Replacing G (given by Eq. (4.10)) in Eq. (4.11) and solving this with respect to K, the following definition is obtained for the 2D bulk modulus

$$K = \frac{E}{2(1-\nu)} \tag{4.12}$$

This definition, obtained from 2D elasticity, differs from the usual one, derived from 3D elasticity, and given by

$$K = \frac{E}{3(1-2\nu)} \tag{4.13}$$

Using these 2D elasticity relations (Eqs. (4.10) and (4.12)), we should bear in mind that we are not dealing with either plane-strain or plane-stress elasticity. Such specifications only arise when one desires to deal with 3D elasticity. These relations were by Eischen and Torquato (1993) derived relations between 2D and 3D moduli for a 3D isotropic material. They proved, among other results, that the 2D shear modulus G (either in plane-strain or plane-stress) is equal to the 3D shear modulus. However, the bulk moduli relations are not so simple. The 2D bulk modulus K is related either to the bulk modulus $K_{PStrain}$ (for 3D plane-strain) or bulk modulus $K_{PStress}$ (for 3D plane-stress), by the relations

$$K_{PStrain} = K + \frac{G}{3} \qquad K_{PStress} = \frac{9KG}{3K+4G} \tag{4.14}$$

Concerning the shear modulus G_{xy}, it can be compared with that obtained from the assumption of "full-isotropy", in which the shear modulus depends on the Young's modulus and Poisson's ratio through the Eq. (4.10). If this formula were applied to the armchair direction (E_x=228.4 N/m, v_{yx}=0.421), one would obtain G=80.4 N/m. Likewise, the application of Eq. (4.10) to the zigzag direction (E_y=208.5 N/m, v_{yx}=0.396), one would obtain G=74.7 N/m. The shear modulus obtained from the Reference Model (G_{xy}=70.5 N/m) is much lower than the former "quasi-isotropic" prediction (14%) and lower than the latter "quasi-isotropic" prediction (6%). This evidence also shows the orthotropic nature of graphyne.

As before, the in-plane 2D bulk modulus can also be compared with that obtained from the assumption of "full-isotropy", in which the 2D bulk modulus depends on the Young's modulus and Poisson's ration through the Eq. (4.12). If we apply this formula to the armchair direction (E_x=228.4 N/m, v_{yx}=0.421), we obtain K=197.2 N/m. Likewise, the application of Eq. (4.12) to the zigzag direction (E_y=208.5 N/m, v_{yx}=0.396), one would obtain K=172.6 N/m. The bulk modulus obtained from the Reference Model (K=164.5 N/m) is much lower than the former "fully-isotropic" prediction (20%) and slightly lower than the latter "fully-isotropic" prediction (4.9%). This fact also proves the orthotropic behavior of graphyne.

Model validation

In order to validate our finite element model, we compare our results with those obtained by other researchers. These results comprise MD results using AIREBO potentials (Cranford and Buehler 2011, Zhang et al. 2012, Yang and Xu 2012, Hou et al. 2015), or using generalized gradient approximation (Asadpour et al. 2015). The few results available in the literature are more accurate than ours because these methods take into account many other parameters involved in atomic scale. Our model can be viewed as an approximation to these MD models. Nevertheless, it can be concluded, from the observation of Table 4.3, that the elastic properties of graphyne derived from our finite element model are fairly comparable to those more rigorous ones.

Furthermore, similarly to the results by Zhang et al. (2012) and Yang and Xu (2012), we also attained a Young's modulus for the zigzag direction slightly smaller than that for armchair direction. Yet, the results by Cranford and Buehler (2011) are in disagreement with ours and those by Zhang et al. (2012) and Yang and Xu (2012): the Young's modulus they obtained for the zigzag direction was higher than the value for the armchair direction. On the other hand, the absolute difference between both Young's moduli (armchair and zigzag) determined by Cranford and Buehler (2011) is higher than ours, but with opposite trend. The absolute difference between both Young's moduli (armchair and zigzag) determined by Zhang et al. (2012) and Yang and Xu (2012) is much lower than ours, but with the same trend.

Comparing the resulting in-plane bulk modulus of graphyne, we can observe that although being somewhat different, our value is of the same order of magnitude of that presented by Asadpour et al. (2015). Finally, the obtained shear modulus result is remarkably close to the one obtained by Asadpour et al. (2015). Furthermore, Hou et al. (2015) analyzed the shear behavior of several graphyne sheet configurations and got a value of around 75 N/m for shear modulus, which also agrees very well with the one obtained from our finite element model.

Finally, the scatter observed in the MD values presented in Table 4.3 could be due to several reasons. The most probable is the use of different computation parameters in MD simulations. Many MD parameters, like the displacement increment, time step, number of time steps, force field, equilibration phase, thermostat, MD ensemble or the cutoff function, could influence the response of the graphyne sheet. Additionally, the size of different sheets can also have some minor effects on the results. Effectively, the bigger the sheet is, the more accurate the results are.

5. Temperature effect on Graphyne

5.1 Model Description

To study the graphyne behavior under different temperatures, we use the Reference Model developed in the previous chapter with some adjustments. The number of atoms, covalent bonds and its bond types are exactly the same. This means that the beam elements (Beam4) simulating the forces between atoms are the same, as well the geometrical configuration of the model.

The calculation of the covalent forces acting between each pair of carbon atoms took place on Chapter 3 recurring to the molecular mechanics model proposed by Odegard et al. (2002a). However, the previously studied models confined our study of the mechanical properties to a constant value of temperature. Therefore, we shall develop a finite element model that can take into account the variation of temperature. To fulfill this task, we will apply the equations proposed by Zhang et al. (2007). In their work, they studied the effect temperature variation (from 0 to 600 K) on the mechanical properties of carbon nanotubes. Although their objective was not to study graphyne, their molecular mechanics model enables us to calculate the interatomic bond force constants depending on the temperature. Thus, such equations shall be presented next.

According to Zhang et al. (2007), the bond-stretching force constant can be obtained from

$$K_{ij}^{T} = 2G\frac{Z_i^* Z_j^*}{\left(r_{ij}^{T}\right)^3} \tag{5.1}$$

where G = 332.06, r_{ij}^{T} is the bond length between atoms i and j, and Z_i^* and Z_j^* are the nuclear effective charges of these atoms. According to Zhang et al. (2007), the bond-bending force constant is taken from

$$K_{ijk}^{T} = 2GZ_i^* Z_k^* r_{ij}^{T} r_{jk}^{T} \frac{\left[2\left(r_{ij}^{T}\right)^2 \cos\theta + r_{ij}^{T} r_{jk}^{T}(\cos 2\theta - 5) + 2\left(r_{jk}^{T}\right)^2 \cos\theta\right]}{2\left[\left(r_{ij}^{T}\right)^2 - r_{ij}^{T} r_{jk}^{T}\cos\theta + \left(r_{jk}^{T}\right)^2\right]^{5/2}} \tag{5.2}$$

where θ is the angle between C-C bonds and r_{jk}^{T} is the bond length between atoms j and k.

The superscript T means those variables that are dependent on temperature, whereas the others depend only on the position and geometry of the atoms and its inherent connections. The angle θ, depends solely on the position of the carbon atoms, but Z_i^*, $Z_j^*$and Z_k^* are described by the abovementioned force constant equations solved for environmental temperatures. This happens as a consequence of the small variation experienced by the nuclear effective charges even when there are large changes on the bond lengths (Badger 1935). As for the values of the bond-stretching and bond-bending force constants, both were obtained by Cornell et al. (1995).

Hence, considering room temperature as 300K, we have $K_{ij}^{300K} = 469\,Kcal/mol/\text{Å}^2$ and $K_{ijk}^{300K} = 63\,Kcal/mol/rad^2$.

To solve the required equations, we need the values of bond length and angles. Zhang et al. (2007) presented the needed values, but only for the aromatic bonds because they were studying only the mechanical properties on nanotubes. To adjust their model to our needs, we had to calculate the bond length of the single and triple bonds beforehand. In order to adapt these values, we brought back the bond lengths assumed on Chapter 3. Then, we sought for the difference between the length values of single and triple bonds, related to the aromatic bond length. Hence, single and triple bonds are smaller than aromatic bonds by 0.67% and 20.13%, respectively. As for the angles that can be seen on the single bonds, they are related to the ones present at the aromatic bonds, since both are linked as depicted on Chapter 3. The resulting bond lengths are presented in Table 5.1 along with the angles between C-C bonds. Bear in mind that the values for aromatic bonds are directly extracted from Zhang et al. (2007) for three distinct temperatures (0K, 300K and 600K).

Table 5.1 - Bond length variation with temperature

Bond Type	**Aromatic**			**Single**			**Triple**		
T. [K]	r_{ij} [Å]	r_{jk} [Å]	Θ [º]	r_{ij} [Å]	r_{jk} [Å]	Θ [º]	r_{ij} [Å]	r_{jk} [Å]	Θ [º]
0	1.45213	1.45241	120.541	1.44239	1.44267	119.730	1.15976	1.15998	180
300	1.45330	1.45330	120.260	1.44355	1.44355	119.870	1.16069	1.16069	180
600	1.45486	1.45328	120.251	1.44510	1.44353	119.875	1.16194	1.16067	180

Having access to each variable within Eq. 5.1 and 5.2, we can now obtain the effective nuclear charge by solving the aforementioned equations for a temperature of 300 K. Such calculations give rise to $Z_i^* = Z_j^* = 1.4723$ and $Z_k^* = 1.55275$. Then, the equations are solved the other way around to obtain the respective values of bond stretching and bond bending force constants for 0 and 600 K. Now, substituting the values given in Table 5.1 into Eq. 5.1 and 5.2, and also accessing to the results achieved by Cornell et al. (1995) for environment temperature, we obtain the set of values presented in Table 5.2. As expected, the results given in the Table 5.2 have small variations within the range of temperatures (0K<T<600K).

Table 5.2 - Bond stretching and bond bending force constants

Bond Type	**Aromatic**		**Single**		**Triple**	
T. [K]	K_{ij} [nN/Å]	K_{ijk} [nN.Å]	K_{ij} [nN/Å]	K_{ijk} [nN.Å]	K_{ij} [nN/Å]	K_{ijk} [nN.Å]
0	32.666	4.3547	33.332	4.4598	64.122	0
300	32.587	4.3773	33.252	4.4434	63.968	0
600	32.482	4.3759	33.145	4.4406	63.761	0

Now, with all the relevant properties affected by the temperature, we can apply once again the equations given by Odegard et al. (2002a) to obtain the Young's modulus for each beam element (interatomic bond). Accessing to Eq. 3.1 and 3.2 of the chapter 3, with certain modifications to better suit the current variables and constants designations, we obtain

$$E_s^T A = 2K_{ij}^T . r_{ij-jk}^T \tag{5.3}$$

$$E_b^T A = \frac{32K_{ijk}^T}{r_{ij-jk}^T}\left[\sin\frac{\Theta}{2}\right]^2 \tag{5.4}$$

Recurring to the newly written equations 5.3 and 5.4, we now possess the ability to obtain for each temperature (i) the bond-stretching interaction Young's modulus values, denoted by E_s^T, and (ii) the bond-angle interaction Young's modulus, denoted by E_b^T. Note that the cross-sectional area retains its original notation, A, while r_{ij-jk}^T is a mean value of the bond lengths r_{ij} and r_{jk}. The resulting values from such equations are presented in Table 5.3, along with the total value of Young's modulus, which accounts for the contribution of both interactions on the covalent bonds within the temperature range. Once more, the results have slight variations, even when comparing the values from 0 K with the ones given at 600 K. However, the variations follow a logical sequence, decreasing the covalent bond stiffness with the increase of bond length (dilatation).

Table 5.3 - Young's modulus of Covalent bonds for different temperatures

Bond Type	**Aromatic**			**Single**			**Triple**		
T. [K]	0	300	600	0	300	600	0	300	600
E_s [nN/Å^2]	94.879	94.717	94.463	96.165	96.001	95.743	49.582	49.498	49.365
E_b [nN/Å^2]	72.356	72.477	72.408	73.997	72.681	72.622	0	0	0
$E_s+E_b=E_T$	167.235	167.195	166.871	170.162	168.682	168.365	49.582	49.498	49.365

By now, we have all the geometrical and mechanical properties for each covalent bond and each temperature. With this information, we can now proceed to implement the computational model. Our first concern was towards the total sheet sizes and proportions, according to the variation they suffer for different temperatures. Yet, as already mentioned, the proportions between the different covalent bonds length are kept, even if the length of each one is now based on another author. An image attesting the aspect ratio of the sheet is shown in Fig. 5.1 (T=0K).

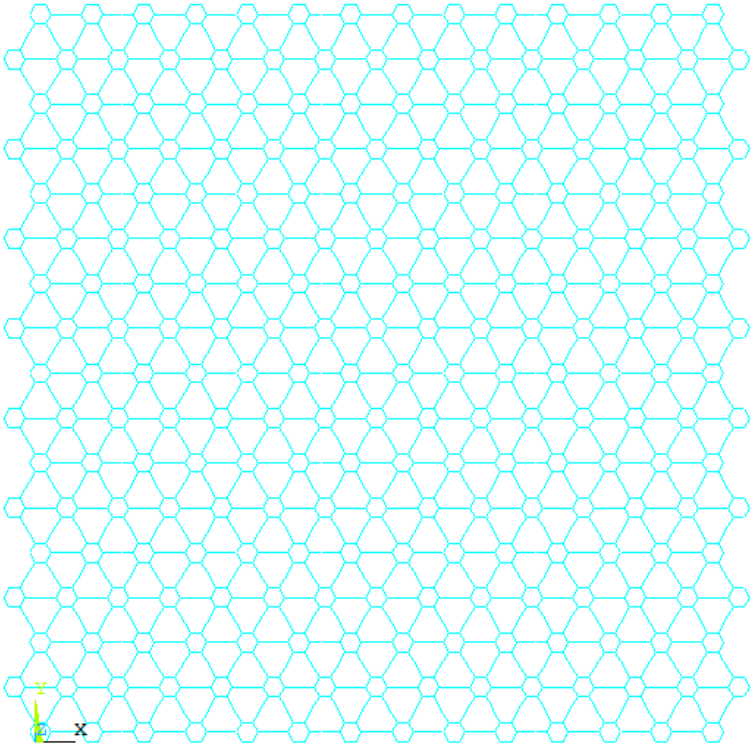

Figure 5.1: Graphyne sheet as modeled in Ansys 14.0® (2013) for a temperature of 0 K

The previous Fig. 5.1 is remarkably similar to the one present at Chapter 3, Fig. 3.7. Also, as we can see on the left bottom of the same figure, the axis system is kept for simplicity. Table 5.4 shows the sheets dimensions observed for the full range of temperature in study, where H_i and L_i refers to the initial height and width of the graphyne sheet at different temperatures, respectively. If we think about the results obtained so far, from Table 5.1 to Table 5.3, the small variation of overall sheet dimensions is readily expected.

Table 5.4 - Graphyne sheet sized at given temperatures

Size [Å] \ T. [K]	**0**	**300**	**600**
H_i	98.810	98.880	98.933
L_i	100.197	100.268	100.321

The next step to take must be the determination of correct boundary conditions, which allow us to correctly simulate the material. Unlike we've done in Chapter 3, we must now make 12 separated APDL codes in order to attain the desired results. These 12 codes, are divided in 3 sets (one for each temperature), each set consisting of 4 different codes, for the uniaxial tensile test in armchair (X) and zigzag (Y) direction, biaxial tensile test and finally the shear test. The boundary conditions will be applied the same way they were in the previous chapter. An image regarding the unit forces applied and the movement and/or rotation restrictions for each one of the 4 analyses can also be seen at Figs. 3.11–14. Note that the amount of unit forces will be exactly the same. After we impose the boundary conditions and

applied loading for each test, we must perform all the 12 analysis in Ansys 14.0® (2013). Carrying out both uniaxial tensile tests and also the biaxial test, their results are present in Table 5.5, in which the sizes and displacements taking place on the graphyne sheet now depend on the temperature. It won't be shown any visual of the deformations taking place on any analysis, since we're applying the same forces and supports on a model which has almost the same dimensions as the one presented at Chapter 4.

Table 5.5 - Sheet size and displacements within the temperature range

Analysis Type	**T. [K]**	**0**	**300**	**600**
Uniaxial Tensile Test on X axis	a [Å]	-0.6575	-0.6618	-0.6642
	d [Å]	3.0734	3.0898	3.0990
Uniaxial Tensile Test on Y axis	b [Å]	-0.6816	-0.6858	-0.6881
	c [Å]	3.2793	3.2963	3.3059
Biaxial Tensile Test	H_f	100.991	101.071	101.130
	L_f	102.113	102.184	102.242

The last analysis to be performed is the shear test. As previously shown in Chapter 4, Fig. 4.3, to express clearly how the displacements take place while testing the sheet in pure shear, we'll use the same notation. Table 5.6 shows the positions (coordinates) of sheet corners for each temperature.

The decision of making a separate table to show the behavior of graphyne with shear stresses applied on it, is taken because unlike the other simulations, we require the displacements on both armchair and zigzag directions to calculate the resulting shear modulus.

Table 5.6 - Sheet corner positions due to shear test at different temperatures

Corner position	**0 K**	**300 K**	**600 K**
I' [Å]	(-10.230;6.418)	(-10.265;6.432)	(-10.283;6.438)
II' [Å]	(-11.578;-4.806)	(-11.620;-4.811)	(-11.641;-4.812)
III' [Å]	(11.578;4.806)	(11.620;4.811)	(11.641;4.812)
IV' [Å]	(10.230;-6.418)	(10.265;-6.432)	(10.283;-6.438)

5.2 Temperature Influence on Elastic Properties

Knowing all the displacements and forces acting on the graphyne sheet at determined temperatures, one can finally calculate the mechanical properties of graphyne at different temperatures. To do so, we will apply once more Eq. 4.1-7, previously explained at Chapter 4. The results will be presented in N/m, and GPa (assumed sheet thickness t=3.35 Å, Shao et al. 2012, Zhang et al. 2014). At last, with all the data in our possession, we will display the mechanical properties of graphyne in Table 5.7. In the next section, we will discuss the results presented in Table 5.7 and, when possible, compare them with those

few results obtained by other authors, either through MD simulations (Zhang et al. 2014) and DFT solely and combined with quasi-harmonic approximation (Shao et al. 2012).

Table 5.7 - Mechanical Properties of Graphyne under Temperature Influence

Property	0	300	600	Units
E_x	270.550 (807.612)	269.115 (803.328)	268.315 (800.940)	N/m (GPa)
v_{yx}	0.4339	0.4344	0.4347	
E_y	246.592 (736.096)	245.320 (732.299)	244.609 (730.176)	N/m (GPa)
v_{xy}	0.4099	0.4103	0.4106	
K	198.032 (594.140)	197.541 (589.675)	196.99 (588.030)	N/m (GPa)
G_{xy}	78.772 (235.140)	78.329 (233.818)	78.087 (233.096)	N/m (GPa)

5.3 Results Discussion

When we first compare the obtained results from Chapter 3 with the ones we just got, we can conclude that even if the method to obtain such results is partially different, namely the equations used to calculate the interatomic bond force constants, the graphyne sheet shows a similar behavior. The armchair Young's modulus is still higher than the one on zigzag direction, now both values differ by ~25 N/m. Thus, graphyne it's an orthotropic material for this range of temperature at least.

Although the graphyne model presented on this chapter is stiffer, according to the results, than the one previously used on Chapter 3 and 4, it shows a bigger Poisson's ratio. On top of that, the shear modulus is only slightly bigger (~10%) than previously for any value of temperature. Which is an indicator of graphyne's elasticity. The reason for such difference in values comes from the assumed bond lengths. For this chapter analysis, we used the same bond lengths as Zhang et al. (2007), while in Chapter 3 and 4 the bond lengths were extracted from Cranford and Buehler (2011). Since Eqs. 5.3 and 5.4 use the same variables as Eqs. 3.1 and 3.2, even if the bond force constants are the same (which happens for environment temperature) the resulting bond stiffness will be increased, resulting in higher values of graphyne's elastic properties.

Regarding the small differences experienced by the different mechanical properties due to the change in temperature, we will show some graphics to better display how they vary in Fig 5.2.

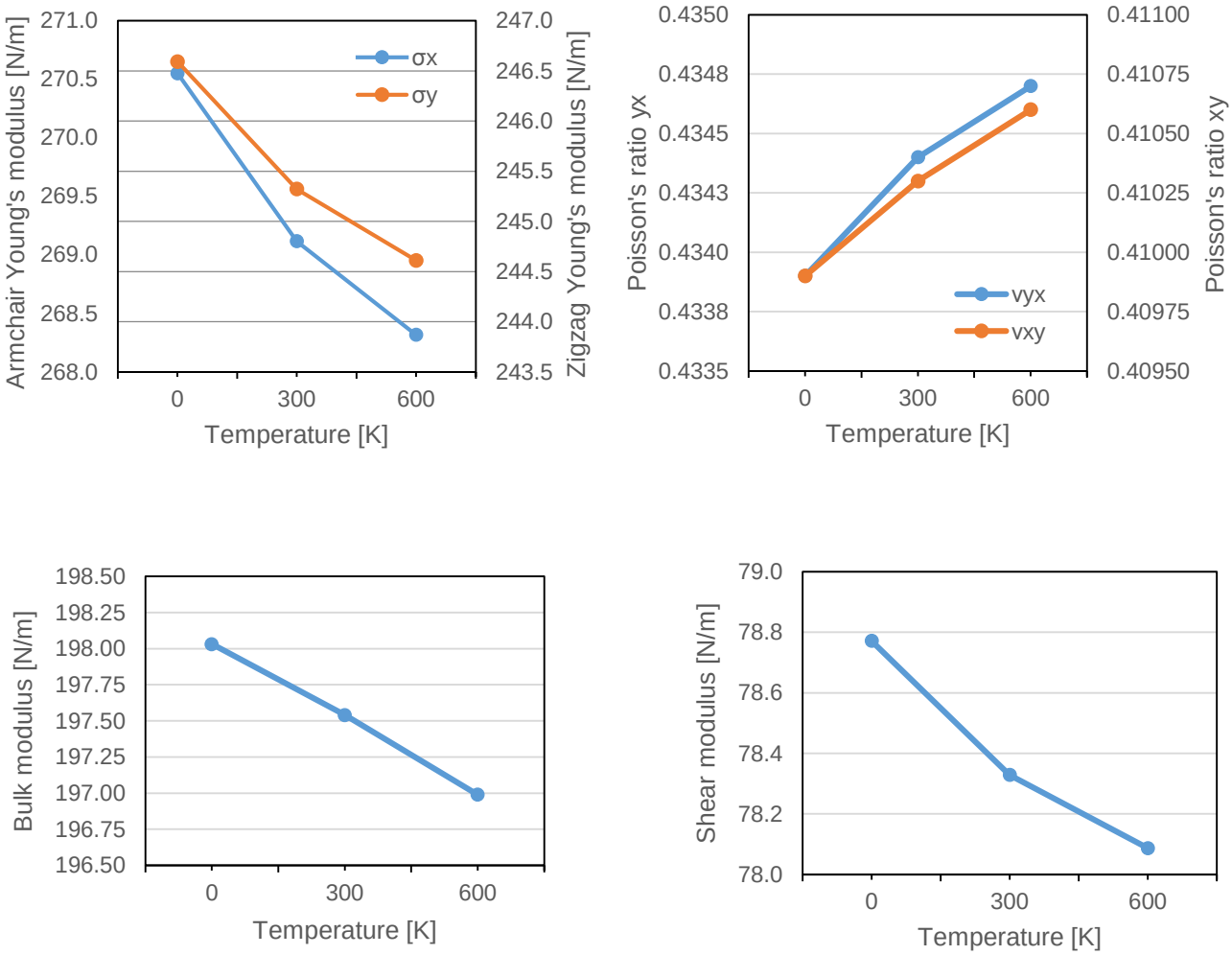

Figure 5.2: Graphyne mechanical properties variation within the range of temperatures: (a) Young's moduli, (b) Poisson's ratio, (c) Bulk modulus and (d) Shear modulus

While the sheet Young's modulus experience a steeper decrease between 0 and 300 K, in its values, behavior that is similar on the shear modulus, the Poisson's ratio increases accordingly. As for the in-plane bulk modulus, there's a faster decrease on its value between 300 and 600 K. However, the differences on every property are rather small and such event is supported by the fact that every bond length was calculated based on carbon nanotubes bond lengths (Zhang et al. 2007). Distinct bonds should have different behaviors within the same range of temperatures, which means the acetylenic linkages ought to have quite different deformations.

Even knowing this fact and since we're studying the graphyne sheet through the FEM scope, we either had to find/stipulate new equations to understand the behavior of each interatomic bond independently, or, like it was done, we assumed a relation between its deformations according to their initial size. Ergo, such decision culminated into a model that reflects the former behavior we obtained into

Chapter 4, although stiffer, but on the other hand, turned to be highly resistant to the effects of temperature.

Having access to the few results available from other authors, we'll now present their results so we can better compare with what we have. On Fig. 5.3 we have images regarding DFT calculations effectuated by Shao et al. (Shao et al. 2012). The right image shows the variation on the Young's modulus experienced by their simulation of a graphyne sheet, within a range of temperatures. As for the left image, it shows the elastic constants C_{11} and C_{12}, needed to obtain the values of Poisson's ratio, bulk and shear modulus.

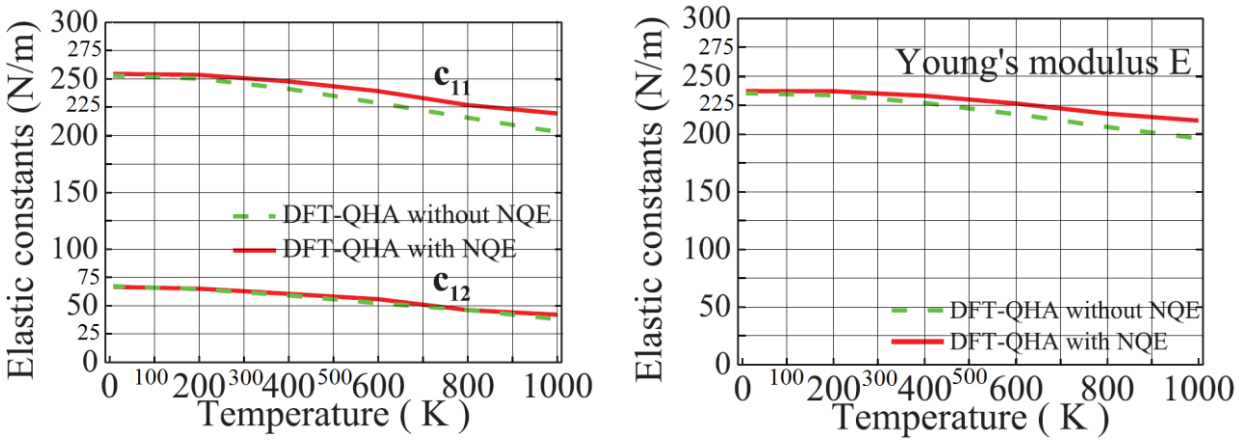

Figure 5.3: Elastic constants C_{11}, C_{12} and Young's modulus obtained by Shao et al. (Shao et al. 2012).

Comparing their results in terms of Young's modulus with ours, we're able to find the same pattern of events, with a slight decrease on its values from 0 to 600 K. Quantitatively, we can say that their Young's modulus is lower than ours for all range of temperatures. This fact corroborates the already mentioned distinct effect of temperature on the dilatation of the acetylenic linkages in relation with the aromatic bonds, all composing the graphyne. From the left image, values of bulk and shear modulus can be extracted, within the range of temperatures we're interested in, as well as Poisson's ratio. Through simple calculations the results were obtained and now will be shown on Table 5.8.

Table 5.8 - Mechanical Properties of Graphyne (Shao et al. 2012)

T [K]	**0**	**300**	**600**
v	0.22	0.2	0.19
K [N/m]	131.7	125	115.8
G_{xy} [N/m]	92.5	93.8	91.3

This author's results show some disparity, quantitatively speaking compared to ours in terms of Poisson's ratio and bulk modulus, the first value being half of ours, while the last is nearly 35% less. Following the logic of Young's modulus results, the material will become more flexible at higher temperatures. Qualitatively, the bulk modulus follows this logic, hence decreasing its value from 0 to 600 K. The same, however doesn't happen to the shear modulus, as it shows a peak for environment

temperature, 300 K. Oddly enough, the Poisson's ratio decrease, unlike ours. Sadly, this is the only source we've found with such results for comparison. Therefore, we have good agreement on the Young's and bulk modulus behavior with this author, even if the values itself are higher in our case.

Next, we will present the effect of temperature on the Young's modulus, studied by a MD approach (Zhang et al. 2014). This is the newest research we could find, in terms of mechanical properties of graphyne with the effect of temperature. We now introduce Fig. 5.4 to better compare such results with the ones we got from our FEM model.

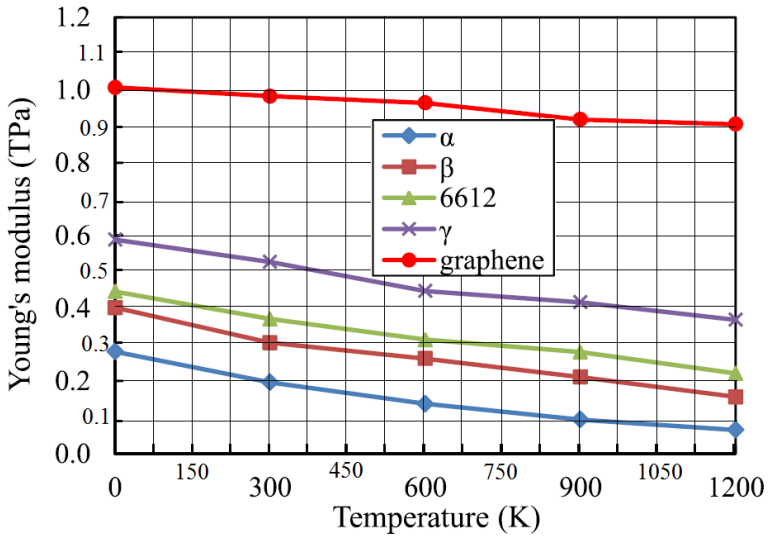

Figure 5.4: Young's modulus of graphene and the most common structures of graphyne (Zhang et al. 2014)

Zhang et al. obtained the smallest results, so far, on this property for γ-graphyne. The graphic in Fig. 5.4 also shows a larger reduction of the material Young's modulus, than Shao et al. did, for the same range of temperatures. There's also a small increase on the slope from 300 to 600 K, unlike we experienced on our model. According to Zhang et al. the bigger drop in mechanical properties of graphyne along with a temperature increase, happen due to the presence of acetylene links (Zhang et al. 2014). This reason could be a hint for our necessity to find or be able to calculate a better method to obtain the displacements suffered by the interatomic bonds within the graphyne sheet. Hence, we could say, there's space for improvement on our model, in order to further explore the sensitivity of graphyne to temperature. The present study shows how important is to take into account the effects of temperature on graphyne's mechanical properties. Even though we don't have a completely well-defined model that simulates the exact behavior of graphyne within the temperature range, we're giving the first steps on a much recognized software, Ansys 14.0® (2013) to carry out this complex study. Much improvements can be done in a near future on this model, given the amount time and effort it requires.

6. Conclusions and Future Developments

This thesis explored the mechanical properties of graphyne sheets through the development of suitable finite element models. The first two chapters seek to enlighten the importance of a wide variety of carbon allotropes, from graphene to fullerenes. Chapter 1 provided an overview of such allotropes and some general concepts that should be known, like mechanical, electrical or optic properties of those materials. Chapter 2 introduced the novel findings, new methods of calculation and latest results achieved within the last few years, for the newest topics on graphene, nanotubes and several structures of graphyne.

In Chapter 3, the definition and implementation of the computational model to study several mechanical properties of graphyne were accomplished. The steps involved in the construction of the model were described in depth. In order to extract the elastic properties (Young's moduli, Poisson's ratio, shear modulus, bulk modulus), different tests were performed and in each test a set of boundary conditions and applied loading were shown. The analyses in this chapter were made upon a squared graphyne sheet for two different possibilities: (i) only covalent bonds considered (Reference Model) and (ii) covalent bonds coupled with van der Waals atomic interactions (vdW Model). In Chapter 4, the main results were presented, discussed and validated through comparisons with available data obtained by other authors.

Chapter 5 aimed to investigate the effect of temperature on the elastic properties of the graphyne sheet (Young's moduli, Poisson's ratio, shear modulus, bulk modulus). In this chapter, we adapted both the equations used and the model developed in Chapter 3 to support the influence of temperature over graphyne's covalent bonds and bond forces. This was done with the support of a small amount of bibliography at our disposal, since it was rarely analyzed before by any means. Knowing beforehand the little effect of van der Waals interactions (from Chapters 3 and 4), we neglected its influence, which turned out the model as being easier to analyze. Finally, this chapter presents the conclusions and main findings of this thesis. In brief, they can be summarized:

- The influence of van der Waals interatomic forces on the elastic properties of graphyne is negligible and can be disregarded unless the covalent bonds undergo large deformations before breaking.
- The finite element models of graphyne developed in this work proved to be simple but fairly accurate. The mechanical properties (Young's modulus, Poisson's ratio, bulk modulus, shear modulus) obtained from the developed models were in agreement with those previously obtained by other authors using much more complex computational models (MD or DFT). Furthermore, the finite element model showed that graphyne exhibits orthotropic behavior, a fact that agrees with previous conclusions of other researchers.

- The present finite element model showed the temperature influence on the graphyne sheet had little impact on its elastic properties, hence it can be disregarded within the range of temperatures (0K to 600K).

As for the obtained results in Chapter 5, the present work agrees qualitatively well with the results available in the literature, showing a small decrease in graphyne's mechanical properties with a temperature increase. Quantitatively, our results showed to be higher than those found in the literature. The reason for this evidence has to do with the assumed bond lengths that were based on bond lengths acting on carbon nanotubes. As we know, the nanotubes in general, being made of graphene or graphyne, display shorter bond lengths than the plain sheet of the same material, and looking at the equations in Chapter 5, we can easily understand they are highly dependent on the bond length imposed.

After the presentation of this work, it is believed there are still many and interesting improvements to be done in these finite element models, as well as other future developments. These include:

- Incorporation of nonlinear stiffness variation with the interatomic distance in bar elements, so that van der Waals stiffness may vary with the distance between atoms and allow an exact representation of Leonard-Jones 12-6 potential.
- Development of similar models for sheets with increasing size and defining the optimum sheet dimensions, i.e. those that minimize the number of degrees of freedom and guarantee convergence of results.
- Development of similar models for sheets with chiral orientations, i.e. sheets for which the natural directions (armchair and zigzag) are not oriented with the directions of sheet edges.
- Introduction of failure criteria in bond material properties (elasticity limits) and find the strength properties of graphyne.
- Study of graphyne mechanical behavior for a larger range of temperatures.
- Implementation of a model to study the elastic properties of stacking sheets of graphyne, both with the same and different orientations

7. Bibliography

Asadpour M, Malakpour S, Faghihnasiri M, Taghipour B (2015) Mechanical properties of two-dimensional graphyne sheet, analogous system of BN sheet and graphyne-like BN sheet. Solid State Com 212 (2015) 46-52

Aykol M, Hou B, Dhall R, Chang SW, Branham W, Qiu J, Cronin SB (2014) Clamping Instability and van der Waals Forces in Carbon Nanotube Mechanical Resonators. Nano Lett. 14 (2014) 2426-2430

Baimova JA, Liu B, Dmitriev SV, Zhou Kun (2015) Mechanical properties of crumpled graphene under hydrostatic and uniaxial compression. J Phys D: Appl Phys 48 (2015) 095302

Baughman RH, Eckhardt H (1987) Structure-property predictions for new planar forms of carbon: Layered phases containing sp^2 and *sp* atoms. J Chem Phys 87 (11)

Bhattachary B, Singh NB, Sarkar U (2015) Pristine and BN Doped Graphyne Derivatives for UV Light Protection. Int J Quantum Chem 115 (2015) 820-829

Balasubramanian (2012) Reinforcement of poly ether sulphones (PES) with exfoliated graphene oxide for aerospace applications. Mat Sci Eng 40 (2012) 012022

Brenner DW, Shenderova OA, Harrison JA, Stuart SJ, Ni B, Sinnott SB (2002) A second-generation reactive empirical bond order (REBO) potential energy expression for hydrocarbons. J Phys: Condens. Matter 14 (2002) 783-802

Bunch JS, Verbridge SS, Alden JS, Zande AM, Parpia JM, Craighead HG, McEuen PL (2008) Impermeable Atomic Membranes from Graphene Sheets. Nano Lett. 8 (2008) 2458-2462

Bunch JS (2008) Mechanical and Electrical Properties of Graphene Sheets. Doctor of Philosophy. Faculty of the Graduate School of Cornell University

Buseck PR, Tsipursky SJ, Hettich R (1992) Fullerenes from the geological environment. Science **257**, 215– 217

Cami J, Salas JB, Malek SE, Peeters E (2010) Detection of C60 and C70 in a Young Planetary Nebula. Science 2010, 329 (5996) 1180-2

Choudhary V, Gupta A (2011). Polymer/Carbon Nanotube Nanocomposites, Carbon Nanotubes - Polymer Nanocomposites, Dr. Siva Yellampalli (Ed.), ISBN: 978-953-307-498-6, InTech, DOI: 10.5772/18423

Clementi E, Raimondi DL (1963) Atomic Screening Constants from SCF Functions. J Chem Phys 38, 2686 (1963)

Coluci VR, Braga SF, Legoas SB, Galvão DS, Baughman RH (2004) New families of carbon nanotubes based on graphyne motifs. Nanotechnology 15 (2004) S142-S149

Cornell WD, Cieplak P, Bayly CI. Gould IR, Merz KM, Jr., Ferguson DM, Spellmeyer DC, Fox T, Caldwell JW, Kollman PA (1995) A Second Generation Force Field for the Simulation of Proteins, Nucleic Acids and Organic Molecules. J Am Chem Soc 1995, 117, 5179-5197

Cranford SW, Buehler MJ (2011) Mechanical properties of graphyne. Carbon 49 (2011) 4111-4121

Cranford SW, Buehler MJ (2012) Selective hydrogen purification through graphdiyne under ambient temperature and pressure. Nanoscale 2012, 4, 4587

Dang LN, Seppälä J (2015) Electrically conductive nanocellulose/graphene composites exhibiting improved mechanical properties in high-moisture condition. Cellulose (2015) 22: 1799-1812

Duplock EJ, Scheffler, Lindan PJD (2004) Hallmark of Perfect Graphene. Phys Rev Lett 92.225502 (2004)

Elias DC, Nair RR, Mohiuddin TMG, et al. (2009) Control of Graphene's Properties by Reversible Hydrogenation: Evidence for Graphane. Science 2009, 323: 610-613

Eischen and Torquato (1993) Determining elastic behavior of composites by the boundary element method. J Appl Phys 74 (1) 1993

Fiori G, Lebègue S, Betti A, Michetti P, Klintenberg M, Eriksson O, Iannaccone G (2010) Simulation of hydrogenated graphene field-effect transistors through a multiscale approach. Phys Rev B 82, 153404 (2010)

Gong L, Kinloch IA, Young RJ, Riaz I, Jalil R, Novoselov KS (2010) Interfacial Stress Transfer in a Graphene Monolayer Nanocomposite. Adv Mater 2010, 22, 2694-2697

Gong T, Lam DV, Liu R, Won S, Hwangbo Y, Kwon S, Kim J, Sun K, Kim JH, Lee SM, Lee C (2015) Thickness Dependence of the Mechanical Properties of Free-Standing Graphene Oxide Papers. Adv Func Mater 2015, 25, 3756-3763

Haley MM, Brand SC, Pak JJ (1997) Carbon Networks Based on Dehydrobenzoannulenes: Synthesis of Graphdiyne Substructures. Angew Chem Int Ed Engl 1997, 36, No 8

Haley MM (2008) Synthesis and properties of annulenic subunits of graphyne and graphdiyne nanoarchitectures. Pure Appl Chem 80, (2008) 519-532

Haskins J, Kinaci A, Sevik C, Svinçli H, Cuniberti G, Çagin T (2011) Control of Thermal and Electronic Transport in Defect-Engineered Graphene Nanoribbons. ACS Nano 5 3779

Hou J, Yin Z, Zhang Y, Chang T (2015) An Analytical Molecular Mechanics Model for Elastic Properties of Graphyne-n. J App Mech 82 (2015) 094501-4

Hu M, Jing Y, Zhang X (2015) Low thermal conductivity of graphyne nanotubes from molecular dynamics study. Phys Rev B 91 155408 (2015)

Hussain T, Sarkar AD, Ahuja R (2012) Strain induced lithium functionalized graphane as a high capacity hydrogen storage material. Appl Phys Lett 101, 103907 (2012)

Iijima S (1991) Helical microtubules of graphitic carbon. Nature 1991;354: 56–58.

Jing Y, Wu G, Guo L, Sun Y, Shen J (2013) Electronic transport properties of graphyne and its family. Comp Mat Science 78 (0213) 22-28

Kang J, Li J, Wu F, Li SS, Xia JB (2011) Elastic, Electronic and Optical Properties of Two-Dimensional Graphyne Sheet. J Phys Chem C 2011, 115, 20466-20470

Katsnelson MI (2007) Graphene: carbon in two dimensions. Mater Today 10 (2007) 20-27

Kim Y, Lee J, Yeom MS, Shin JW, Kim H, Hone YJ, Jung Y, Jeon S, Han SM (2013) Strengthening effect of single-atomic-layer graphene in metal–graphene nanolayered composites. Nat. Commun. 4:2114

Krishnan A, Dujardin E, Ebbesen TW, Yianilos PN, Treacy MMJ (1998) Young's modulus of single-walled nanotubes. Phys Rev B 58:14013-14019

Kroto HW, Heath JR, O'Brien SC, Curl RF, Smalley RE (1985) C_{60}: Buckminsterfulleren. Nature 1985;318: 162-163

Kuang D, Xu L, Liu L, Hu W, Wu Y (2013) Graphene-nickel composites. App Sur Science 273 (2013) 484-490

Lazic P, Crljen Z (2015) Graphyne on metallic surfaces: A density functional theory study. Phys Rev B 91, 125423 (2015)

Lepore E, Bonaccorso F, Bruna M, Bosia F, Taioli S, Garberoglio G, Ferrari AC, Pugno NM (2015) Silk reinforced with graphene or carbon nanotubes spun by spiders. arXiv:1504.06751 (2015), (pdf)

Lee C, Wei X, Kysar JW, Hone J (2008) Measurement of the elastic properties and intrinsic strength of monolayer graphene. Science 2008;321:385-388

Li G, Li Y, Liu H, Guo Y, Li Y, Zhu D (2009) Architecture of graphdiyne nanoscale films. Chem Commun 2010, 46, 3256-3258

Li G, Li Y, Qian X, Liu H, Lin H, Chen N, Li Y (2011) Construction of Tubular Molecule Aggregations of Graphdiyne for Highly Efficient Field Emission. J Phys Chem C 2011, 115, 2611-2615

Liu L, Zhang J, Zhao J, Liu F (2012) Mechanical properties of graphene oxides. Nanoscale, 2012, 4, 5910

Los JH, Ghiringhelli LM, Meijer EJ, Fasolino A (2005) Improved long-range reactive bond-order potential for carbon. I. Construction. Phys Rev B 72, 214102 (2005)

Mahale NK, Ladhe RD, Atterde SB, Ingle ST (2014) Synthesis and the Structural Transformation of fcc to hcp in Ni-Graphene Nanocomposite by Simple Chemical Route via Sonication. J Nanoparticles 2014, 305637

Mak KF, Ju L, Wang F, Heinz TF (2012) Optical spectroscopy of graphene: From the far infrared to the ultraviolet. Solid Stat Com 152 (2012) 1341-1349

McCarthy MA, Byrne EM, O'Brien NP, Murmu T (2014) Improved Mechanical Performance of CNTs and CNT Fibres in Nanocomposites Through Inter-Wall and Inter-Tube Coupling. Modeling of Carbon Nanotubes, Graphene and their Composites 1-56

Min K, Aluru NR (2011) Mechanical properties of graphene under shear deformation. App Phys Lett 98, 013113 (2011)

Monetta T, Acquesta A, Bellucci F (2015) Graphene/Epoxy Coating as Multifunctional Material for Aircraft Structures. Aerospace 2015, 2, 423-434

Narita N, Nagai S, Suzuki S, Nako K (1998) Optimized geometries and electronic structures of graphyne and its family. Phys Rev B 58, 11009 (1998)

Njuguna and Pielichowski (2003) Polymer Nanocomposites for Aerospace Applications: Properties. Adv Eng Mat 2003, 5, 11

Novoselov KS, Geim AK, Morozov SV, Jiang D, Zhang Y, Dubonos SV, Grigorieva IV, Firsov AA (2004) Electric field effect in atomically thin carbon films. Science 2004;306 (5696): 666-9

Novoselov KS, Geim AK, Peres NMR, Guinea F, Neto AHC (2009) The electronic properties of graphene. Rev Mod Phys 81 (1) 109

Odegard GM, Gates TS, Wise KE, Park C, Siochi EJ (2002) Constitutive modeling of nanotube-reinforced polymer composites. Comp Science Tech 63 (2003) 1671-1687

Odegard GM, Gates TS, Nicholson LM, Wise KE (2002) Equivalent-continuum modeling of nano-structured materials. Comp Science Tech 62 (2002) 1869-1880

Pan LD, Zhang LZ, Song BW, Du SX, Gao HJ (2011) Graphyne and graphdiyne based nanoribbons: Density functional theory calculations of electronic structures. Appl Phys Lett 98, 173102 (2011)

Park C, Wise KE, Kang HJ, Kim JW et al. (2008) Multifunctional Nanotube Polymer Nanocomposites for Aerospace Applications: Adhesion Between SWCNT and Polymer Matrix

Pei Y (2012) Mechanical properties of graphdiyne sheet. Physica B 407 (2012) 4436-4439

Peng Q, Ji W, De S (2012) Mechanical Properties of Graphyne Monolayer: A First-Principles Study. Phys Chem Chem Phys 2012, 14, 13385-13391

Peng Q, De S (2012) Tunable band gaps of mono-layer hexagonal BNC heterostructures. Physica E 2012;223:2591-2596

Peng Q, De S. (2013) Mechanical properties and instabilities of ordered graphene oxide C6O monolayer. *RSC Adv* 2013;3:24337–24344

Peng Q, Chen XJ, Liu S, De S. (2013) Mechanical stabilities and properties of graphene-like aluminum nitride predicted from first-principles calculations. *RSC Adv* 2013;3:7083–7092

Peng Q, Dearden AK, Crean J, Han L, Liu S, Wen X, De S (2014) New materials graphyne, graphdiyne, graphone and graphane: review of properties, synthesis and application in nanotechnology. Nanotech Science and Appl 2014:7 1-29

Perkgöz NK, Sevik C (2014) Vibrational and thermodynamic properties of α-, β-, γ- and 6,6,12-graphyne strucutures. Nanotechnology 25 (2014) 185701

Plimpton S (1995) Fast Parallel Algorithms for Short-Range Molecular Dynamics. J Comp Phys 117, 1 (1995) 1-19

Poorsolhjouy A, Naei MH (2015) Effects of carbon nanotubes' dispersion on effective mechanical properties of nanocomposites: A finite element study. J Reinf Plast Comp 0 (0) 1-14

Pushparaj VL, Shaijumon MM, Kumar A, Murugesan S et al. (2007) Flexible energy storage devices based on nanocomposites paper. PNAS 104, 34, 13574-13577

Rasmussen K, Mast J, De Temmerman P-J, Verleysen E, Waegeneers N, Van Steen J, Pizzolon J-C: Multi-walled Carbon Nanotubes, NM-400, NM-401, NM-402, NM-403: Characterization and Physico-

Chemical Properties. JRC Repository: NM-series of Representative Manufactured Nanomaterials, 2014, Report EUR 26796 EN

Ren Z, Meng N, Shahxad K, Xu Y, Qu S, Yu B, Luo JK (2015) Mechanical properties of nickel-graphene composites synthesized by electrochemical deposition. Nanotechnology 26 (2015) 065706

Roman RE, Cranford SW (2014) Strength and Toughness of Graphdiyne/Copper Nanocomposites. Adv Eng Mat 2014, 16, 7

Scarpa F, Adhikari S, Phanti AS (2009) Effective elastic mechanical properties of single layer graphene sheets. Nanotechnology 20 (2009) 065709

Scarpa F, Adhikari SA, Gil AJ, Remillat C (2010) The bending of single layer graphene sheets: the lattice versus continuum approach. Nanotechnology 21 (2010) 125702

Seidel GD, Chatzigeorgiou G, Ren X, Lagoudas DC (2014) Multiscale Modeling of Multifunctional Fuzzy Fibers Based on Multi-Walled Carbon Nanotubes. Modeling of Carbon Nanotubes, Graphene and their Composites 135-176

Shao T, Wen B, Melnik R, Yao S, Kawazoe Y, Tian Y (2012) Temperature dependent elastic constants and ultimate strength of graphene and graphyne. J Chem Phys 137, 194901 (2012)

Sluiter MHF, Kawazoe Y (2003) Cluster expansion method for adsorption: Application to hydrogen chemisorption on graphene. Phys Rev B 68, 085410 (2003)

Srinivasu K, Ghosh SK (2012) Graphyne and Graphdiyne: Promising Materials for Nanoelectronics and Energy Storage Application. J Phys Chem C 2012, 116, 5951-5956

Stuart S J, Tutein A B and Harrison J A (2000) A reactive potential for hydrocarbons with intermolecular interactions. J Chem Phys 112 6472–86

Sundaram R (2011) Electrical Properties of Chemically Derived Graphene. Doctor ès Sciences. École Polytechnique Fédérale de Lausanne

Tan SM, Sofer Z, Pumera M (2013) Biomarkers Detection on Hydrogenated Graphene Surfaces: Towards Applications of Graphene in Biosensing. Electroanalysis 2013, 25, No. 3, 703-705

Tate JS, Gaikwad S, Theodoropoulou N, Trevino E, Koo JH (2013) Carbon/Phenolic Nanocomposites as Advanced Thermal Protection Material in Aerospace Applications. J Comp 2013, 403656

Tian Y, Li Zheng, Cai K (2015) Wrinkling Behaviour of Annular Graphynes under Circular Shearing Load Using Molecular Dynamics Simulations. Nanomater Nanotechnol, 2015, 5:9

Treacy MMJ, Ebesen TW, Gibson JM (1996) Exceptionally high Young's modulus observed for individual carbon nanotubes. Nature (London) 381:678-680

Tsai JL, Tu JF (2010) Characterizing mechanical properties of graphite using molecular dynamics simulation. Materials & Design 31, 1 (2010) 194-199

Tserpes and Papanikos (2013) Finite Element Modeling of the Tensile Behavior of Carbon Nanotubes, Graphene and Their Composites. Modeling of Carbon Nanotubes, Graphene and their Composites 303-329

Wei J, Zhang X, Qiu J, Weeks BL (2015) Thermal Kinetics and Thermo-Mechanical Properties of Graphene Integrated Fluoroelastomer. J Polym Sci B: Polym Phys 2015

WenXing B, ChangChun Z, WanZhao C (2004) Simulation of Young's modulus of single-walled carbon nanotubes by molecular dynamics. Physica B 352 (2004) 156-163

Wong EW, Sheehan PE, Lieber CM (1997) Nanobeam mechanics: elasticity, strength and toughness of nanorods and nanotubes. Science 277:1971-1975

Xue M, Qiu H, Guo W (2013) Exceptionally fast water desalination at complete salt rejection by pristine graphyne monolayers. Nanotechnology 24 (2013) 505720

Yang RT (2000) Hydrogen storage by alkali-doped carbon nanotubes-revisited. Carbon 2000, 38, 623

Yang Y, Xu X (2012) Mechanical properties of graphyne and its family – A molecular dynamics investigation. Comp Mat Science 61 (2012) 83-88

Zakharchenko KV, Katnelson MI, Fasolino A (2009) Finite Temperature Lattice Properties of Graphene beyond the Quasiharmonic Approximation. Phys Rev Lett 102, 046808 (2009)

Zhang YY, Pei QX, Wang CM (2012) Mechanical properties of graphynes under tension: A molecular dynamics study. Appl Phys Lett 101, 081909 (2012)

Zhang YC, Chen X, Wang X (2007) Effects of temperature on mechanical properties of multi-walled carbon nanotubes. Comp Sci Tech 68 (2008) 572-581

Zhang YY, Pei QX, Mai YW, Gu YT (2014) Temperature and strain-rate dependent fracture strength of graphynes. J Phys D: Appl Phys 47 (2014) 425301

Zhao J, Wei N, Fan Z, Jiang JW, Rabczuk T (2013) The mechanical properties of three types of carbon allotropes. Nanotechnology 24 (2013) 095702

Zhao Z, Wang EF, Yan H, Kono Y, Wen B et al. (2014) Nanoarchitectured materials composed of fullerene-like Spheroids and disordered graphene layers with tunable mechanical properties. Nat Comm 6, 6212 (2015)

Zhou J, Wang Q, Sun Q, Chen XS, Kawazoe Y, Jena P (2009) Ferromagnetism in Semihydrogenated Graphene Sheet. Nano Lett 9, 11 (2009)

Zhou J, Sun Q (2012) How to fabricate a semihydrogenated graphene sheet? A promising strategy explored. App Phys Lett 101, 073114 (2012)

Encyclopedia Britannica [Online] Available: http://www.britannica.com/science/fullerene [Accessed 4 August 2015]

Granta [Online] Available: http://www.grantadesign.com/education/datasheets/sciencenote.htm [Accessed 8 August 2015]

Graphenea [Online] Available: http://www.graphenea.com/ [Accessed 2 August 2015]

Pr Web [Online] Available: http://www.prweb.com/releases/carbon-nanotubes/market/prweb11141047.htm [Accessed 12 August 2015]

The University of Manchester [Online] Available: http://www.graphene.manchester.ac.uk/explore/the-story-of-graphene/ [Accessed 2 August 2015]

Ulloa E (2013) Fullerenes and their Applications in Science and Technology. [Online] Available: http://web.eng.fiu.edu/~vlassov/EEE-5425/Ulloa-Fullerenes.pdf [Accessed 15 September 2015]

ANSYS® Academic Research, Release 14.0, Help System, Coupled Field Analysis Guide, ANSYS, Inc.

A. Appendix

The following scripts refers to Mechanical APDL codes implemented on Ansys 14.0®. The 1st models the graphyne sheet with covalent bonds, while the 2nd adds the vdW interaction.

```
FINISH
/CLEAR, START
/prep7
/RGB,INDEX,100,100,100, 0
/RGB,INDEX, 80, 80, 80,13
/RGB,INDEX, 60, 60, 60,14
/RGB,INDEX, 0, 0, 0,15
/REPLOT
!------------------------
PI=4*ATAN(1.0)
ET,1,BEAM4
!Beam Properties (Single/Aromatic)
Ar=1
Iz=7.95775E-2
Iy=7.95775E-2
Tkz=1.12838
Tky=1.12838
Ix=1.59155E-1
R,1,Ar,Iz,Iy,Tkz,Tky,
RMORE,,Ix
!Beam Properties(Triple)
Ar1=3
Iz1=7.16197E-1
Iy1=7.16197E-1
Tkz1=1.95441
Tky1=1.95441
Ix1=1.43239
R,2,Ar1,Iz1,Iy1,Tkz1,Tky1,
RMORE,,Ix1
!Material Properties of Single Bounds
MPTEMP,1,0
MPDATA,EX,1,,167.441
MPDATA,PRXY,1,,0
NLGEOM,ON
!Circular Section Definition
SECTYPE,1,BEAM,CSOLID,SINGLE,
R=Tkz/2
SECDATA,R,,
!Material Properties of Triple Bounds
MPTEMP,1,0
MPDATA,EX,2,,25.8523
MPDATA,PRXY,2,,0
NLGEOM,ON
!Circular Section Definition
SECTYPE,2,BEAM,CSOLID,TRIPLE,
R=Tkz1/2
SECDATA,R,,
!Material Properties of Aromatic Bounds
MPTEMP,1,0
MPDATA,EX,3,,167.617
MPDATA,PRXY,3,,0
NLGEOM,ON
!Circular Section Definition
SECTYPE,3,BEAM,CSOLID,AROMATIC,
R=Tkz/2
SECDATA,R,,
!sin30
ANG1=SIN(PI/6)
!cos30
ANG2=COS(PI/6)
!Aromatic Bound
A=1.49
!Single Bound
S=1.48
!Triple Bound
T=1.19
AA=A*ANG2
AB=A*ANG1
A2=2*A
AC=(A2+S)*ANG2
AD=S*ANG1
AI=2*S+T
AE=(AI)*ANG1
AF=(A2+AI)*ANG2
AG=(A+S+T)*ANG2
AH=(A2+S+T)*ANG2
AJ=(4*A+3*S+2*T)*ANG2
AK=(3*A+3*S+2*T)*ANG2
AL=S+T
AM=AG+AC
AN=(A2+3*S+2*T)*ANG2
!Molecular Size in Armchair Direction
MSize=3*A+AI+2*AI*ANG1+2*AB
!Atom Coordinates
K,1,0,0
K,2,A,0
K,3,A+AB,AA
K,4,A,2*AA
K,5,0,2*AA
K,6,-AB,AA
K,7,A+AB+S,AA
K,8,A+AB+AL,AA
K,9,A+AB+AI,AA
K,10,A+2*AB+AI,2*AA
K,11,A+(A2-S)*ANG1+AI,AC
K,12,A+(A2-AL)*ANG1+AI,T*ANG2+AC
K,13,A2+AE,AF
K,14,A+AE,AF
K,15,A+AL*ANG1,T*ANG2+AC
K,16,A+AD,AC
K,17,-AD,AC
K,18,-AL*ANG1,T*ANG2+AC
K,19,-AE,AL*ANG2+AC
K,20,-(AI-A)*ANG1,AM
K,21,-(AI-A)*ANG1+S,AM
K,22,-(AI-A)*ANG1+AL,AM
K,23,-(AI-A)*ANG1+AI,AM
K,24,-AE-A,AL*ANG2+AC
K,25,-(AI+A)*ANG1-A,AM
K,26,-AE-A,AH+AC
K,27,-AE,AH+AC
K,28,-AL*ANG1,AF+AC
K,29,-AD,2*AG+AC
K,30,0,AN+AC
K,31,A,AN+AC
K,32,A+AD,2*AG+AC
K,33,A+AL*ANG1,AF+AC
K,34,A+AE,AH+AC
K,35,A+AB,AK+AC
K,36,A,AJ+AC
K,37,0,AJ+AC
K,38,-AB,AK+AC
K,39,A+AB+S,AK+AC
K,40,A+AB+AL,AK+AC
K,41,A+AB+AI,AK+AC
K,42,A+2*AB+AI,AN+AC
K,43,A+(A2-S)*ANG1+AI,2*AG+AC
K,44,A+(A2-AL)*ANG1+AI,AF+AC
K,45,A2+AE,AH+AC
K,46,A2+(AI+A)*ANG1,AM
K,47,A2+(AI+A)*ANG1+S,AM
K,48,A2+(AI+A)*ANG1+AL,AM
K,49,A2+(AI+A)*ANG1+AI,AM
K,50,A2+(AI+A2)*ANG1+AI,AH+AC
K,51,A2+(AI+A2)*ANG1+AI,AL*ANG2+
AC
K,52,A2+(AL+A2)*ANG1+AI,AF+AC
K,53,A2+(S+A2)*ANG1+AI,2*AG+AC
K,54,A2+2*AB+AI,AN+AC
K,55,A2+(AL+A2)*ANG1+AI,T*ANG2+A
C
K,56,A2+(S+A2)*ANG1+AI,AC
K,57,A2+2*AB+AI,2*AA
K,58,A+2*AB+AI,0
K,59,A2+2*AB+AI,0
K,60,A2+3*AB+AI,AA
K,61,A2+3*AB+AI,AK+AC
K,62,A2+2*AB+AI,AJ+AC
K,63,A+2*AB+AI,AJ+AC
K,64,A2+(AI+A2)*ANG1+AI+A,AH+AC
K,65,A2+(AI+A2)*ANG1+AI+A,AL*ANG
2+AC
K,66,A2+3*AB+AI+S,AA
K,67,A2+3*AB+AI+AL,AA
K,68,A2+3*AB+AI+S,AK+AC
K,69,A2+3*AB+AI+AL,AK+AC
!Carbon Linkages
L,1,2,1     !Aromatic 1
L,2,3,1     !Aromatic 2
L,3,4,1     !Aromatic 3
L,4,5,1     !Aromatic 4
L,5,6,1     !Aromatic 5
L,1,6,1     !Aromatic 6
LSEL,S,LINE,,1,6,1
LATT,3,1,1,,,,3
L,3,7,1     !Single  7
LSEL,S,LINE,,7
LATT,1,1,1,,,,1
L,7,8,1     !Triple  8
LSEL,S,LINE,,8
LATT,2,2,1,,,,2
L,8,9,1     !Single  9
LSEL,S,LINE,,9
LATT,1,1,1,,,,1
L,9,10,1    !Aromatic 10
LSEL,S,LINE,,10
LATT,3,1,1,,,,3
L,10,11,1   !Single  11
LSEL,S,LINE,,11
LATT,1,1,1,,,,1
L,11,12,1   !Triple  12
LSEL,S,LINE,,12
LATT,2,2,1,,,,2
L,12,13,1   !Single  13
LSEL,S,LINE,,13
LATT,1,1,1,,,,1
L,13,14,1   !Aromatic 14
LSEL,S,LINE,,14
LATT,3,1,1,,,,3
L,14,15,1   !Single  15
LSEL,S,LINE,,15
LATT,1,1,1,,,,1
L,15,16,1   !Triple  16
LSEL,S,LINE,,16
LATT,2,2,1,,,,2
L,16,4,1    !Single  17
L,5,17,1    !Single  18
LSEL,S,LINE,,17,18,1
LATT,1,1,1,,,,1
L,17,18,1   !Triple  19
LSEL,S,LINE,,19
LATT,2,2,1,,,,2
L,18,19,1   !Single  20
LSEL,S,LINE,,20
LATT,1,1,1,,,,1
L,19,20,1   !Aromatic 21
LSEL,S,LINE,,21
LATT,3,1,1,,,,3
L,20,21,1   !Single  22
LSEL,S,LINE,,22
LATT,1,1,1,,,,1
L,21,22,1   !Triple  23
LSEL,S,LINE,,23
LATT,2,2,1,,,,2
L,22,23,1   !Single  24
LSEL,S,LINE,,24
LATT,1,1,1,,,,1
L,23,14,1   !Aromatic 25
L,19,24,1   !Aromatic 26
L,24,25,1   !Aromatic 27
L,25,26,1   !Aromatic 28
L,26,27,1   !Aromatic 29
L,27,20,1   !Aromatic 30
LSEL,S,LINE,,25,30,1
LATT,3,1,1,,,,1
L,27,28,1   !Single  31
LSEL,S,LINE,,31
LATT,1,1,1,,,,1
L,28,29,1   !Triple  32
LSEL,S,LINE,,32
LATT,2,2,1,,,,2
L,29,30,1   !Single  33
LSEL,S,LINE,,33
LATT,1,1,1,,,,1
L,30,31,1   !Aromatic 34
LSEL,S,LINE,,34
LATT,3,1,1,,,,3
L,31,32,1   !Single  35
LSEL,S,LINE,,35
LATT,1,1,1,,,,1
L,32,33,1   !Triple  36
LSEL,S,LINE,,36
LATT,2,2,1,,,,2
L,33,34,1   !Single  37
LSEL,S,LINE,,37
LATT,1,1,1,,,,1
L,34,23,1   !Aromatic 38
L,31,35,1   !Aromatic 39
L,35,36,1   !Aromatic 40
L,36,37,1   !Aromatic 41
L,37,38,1   !Aromatic 42
L,38,30,1   !Aromatic 43
LSEL,S,LINE,,38,43,1
LATT,3,1,1,,,,3
L,35,39,1   !Single  44
LSEL,S,LINE,,44
LATT,1,1,1,,,,1
L,39,40,1   !Triple  45
LSEL,S,LINE,,45
LATT,2,2,1,,,,2
L,40,41,1   !Single  46
LSEL,S,LINE,,46
LATT,1,1,1,,,,1
L,41,42,1   !Aromatic 47
LSEL,S,LINE,,47
LATT,3,1,1,,,,3
L,42,43,1   !Single  48
LSEL,S,LINE,,48
LATT,1,1,1,,,,1
L,43,44,1   !Triple  49
LSEL,S,LINE,,49
LATT,2,2,1,,,,2
L,44,45,1   !Single  50
LSEL,S,LINE,,50
LATT,1,1,1,,,,1
L,45,34,1   !Aromatic 51
L,45,46,1   !Aromatic 52
L,46,13,1   !Aromatic 53
LSEL,S,LINE,,51,53,1
LATT,3,1,1,,,,3
L,46,47,1   !Single  54
LSEL,S,LINE,,54
LATT,1,1,1,,,,1
L,47,48,1   !Triple  55
LSEL,S,LINE,,55
LATT,2,2,1,,,,2
L,48,49,1   !Single  56
LSEL,S,LINE,,56
LATT,1,1,1,,,,1
L,49,50,1   !Aromatic 57
```

```
L,49,51,1    !Aromatic 58
LSEL,S,LINE,,57,58,1
LATT,3,1,1,,,,3
L,50,52,1    !Single  59
LSEL,S,LINE,,59
LATT,1,1,1,,,,1
L,52,53,1    !Triple  60
LSEL,S,LINE,,60
LATT,2,2,1,,,,2
L,53,54,1    !Single  61
LSEL,S,LINE,,61
LATT,1,1,1,,,,1
L,54,42,1    !Aromatic 62
LSEL,S,LINE,,62
LATT,3,1,1,,,,3
L,51,55,1    !Single  63
LSEL,S,LINE,,63
LATT,1,1,1,,,,1
L,55,56,1    !Triple  64
LSEL,S,LINE,,64
LATT,2,2,1,,,,2
L,56,57,1    !Single  65
LSEL,S,LINE,,65
LATT,1,1,1,,,,1
L,57,10,1    !Aromatic 66
L,9,58,1     !Aromatic 67
L,58,59,1    !Aromatic 68
L,59,60,1    !Aromatic 69
L,60,57,1    !Aromatic 70
L,54,61,1    !Aromatic 71
L,61,62,1    !Aromatic 72
L,62,63,1    !Aromatic 73
L,63,41,1    !Aromatic 74
LSEL,S,LINE,,66,74,1
LATT,3,1,1,,,,3
L,60,66,1    !Single  75
L,61,68,1    !Single  76
LSEL,S,LINE,,75,76,1
LATT,1,1,1,,,,1
L,66,67,1    !Triple  77
L,68,69,1    !Triple  78
LSEL,S,LINE,,77,78,1
LATT,2,2,1,,,,2
L,50,64,1    !Aromatic 79
L,65,51,1    !Aromatic 80
LSEL,S,LINE,,79,80,1
LATT,3,1,1,,,,3
LSEL,ALL
!Molecule 2 in Armchair Direction
LOCAL,11,0,2*A+AI+3*AB+AI/2,AJ+AC,
0,,,,1,1,
LSYMM,X,ALL, , , ,0,0
NUMMRG,ALL
NUMCMP,ALL
!Molecule 3 & 4 in Armchair Direction
LOCAL,12,0,2*A+AI+3*AB+AI/2+MSize,
AJ+AC,0,,,,1,1,
LSYMM,X,ALL, , , ,0,0
CSDELE,ALL, ,
K,261,A2+3*AB+AI+S+MSize,AK+AC
K,262,A2+3*AB+AI+AL+MSize,AK+AC
K,263,A2+3*AB+AI+S+MSize,AA
K,264,A2+3*AB+AI+AL+MSize,AA
L,107,261,1    !Single 313
LSEL,S,LINE,,313
LATT,1,1,1,,,,1
L,261,262,1    !Triple 314
LSEL,S,LINE,,314
LATT,2,2,1,,,,2
L,262,237,1    !Single 315
L,75,263,1     !Single 316
LSEL,S,LINE,,315,316,1
LATT,1,1,1,,,,1
L,263,264,1    !Triple 317
LSEL,S,LINE,,317
LATT,2,2,1,,,,2
L,264,205,1    !Single 318
LSEL,S,LINE,,318
LATT,1,1,1,,,,1
NUMMRG,ALL
NUMCMP,ALL
LSEL,ALL
!Molecule 5 to 7 in Armchair Direction
LOCAL,13,0,2*A+AI+3*AB+AI/2+3*MSi
ze,AJ+AC,0,,,,1,1,
LSYMM,X,ALL, , , ,0,0
CSDELE,ALL, ,
K,517,A2+3*AB+AI+S+3*MSize,AK+AC
K,518,A2+3*AB+AI+AL+3*MSize,AK+A
C
K,519,A2+3*AB+AI+S+3*MSize,AA
K,520,A2+3*AB+AI+AL+3*MSize,AA
L,168,517,1    !Single 625
LSEL,S,LINE,,625
LATT,1,1,1,,,,1
L,517,518,1    !Triple 626
LSEL,S,LINE,,626
LATT,2,2,1,,,,2
L,518,426,1    !Single 627
L,136,519,1    !Single 628
LSEL,S,LINE,,627,628,1
LATT,1,1,1,,,,1
L,519,520,1    !Triple 629
LSEL,S,LINE,,629
LATT,2,2,1,,,,2
L,520,394,1    !Single 630
LSEL,S,LINE,,630
LATT,1,1,1,,,,1
LSEL,ALL
LDELE,313,368,1,1
LDELE,371,390,1,1
LDELE,467,468,1,1
NUMMRG,ALL
NUMCMP,ALL
!Molecule 2 in ZigZag Direction
LOCAL,14,0,0,AK+AC,0, , , ,1,1,
LSYMM,Y,ALL, , , ,0,0
NUMMRG,ALL
NUMCMP,ALL
!Molecule 3 and 4 in ZigZag Direction
LOCAL,15,0,0,2*(AK+AC)-AA,0, , , ,1,1,
LSYMM,Y,ALL, , , ,0,0
NUMMRG,ALL
NUMCMP,ALL
!Molecule 5 to 8 in ZigZag Direction
LOCAL,16,0,0,4*(AK+AC)-3*AA,0,    ,    ,
,1,1,
LSYMM,Y,ALL, , , ,0,0
NUMMRG,ALL
NUMCMP,ALL
CSDELE,ALL, ,
LMESH,ALL
!----------------------
!Boundary Conditions and apllied forces
Fb=82/83
DK,ALL,UZ
!Left
KSEL,S,LOC,X,-AE,0
DK,ALL,UX
KSEL,ALL
!Right
KSEL,S,LOC,X,94.1,96.3
FK,ALL,FX,Fb
KSEL,ALL
!Central Left Kp
DK,796,UY
!Central Right Kp
DK,1111,UY
!Solution
FINISH
/SOL
/STATUS,SOLU
SOLVE
FINISH
!Displacement Plot
/POST1
PLDISP,2
!Displacement Lists in X and Y
PRNSOL,U,X
PRNSOL,U,Y
```

```
FINISH
/CLEAR, START
/prep7
/RGB,INDEX,100,100,100, 0
/RGB,INDEX, 80, 80, 80,13
/RGB,INDEX, 60, 60, 60,14
/RGB,INDEX, 0, 0, 0,15
/REPLOT
!------------------------
PI=4*ATAN(1.0)
ET,1,BEAM4
!Beam Properties (Single/Aromatic)
Ar=1
Iz=7.95775E-2
Iy=7.95775E-2
Tkz=1.12838
Tky=1.12838
Ix=1.59155E-1
R,1,Ar,Iz,Iy,Tkz,Tky,
RMORE,,Ix
!Beam Properties(Triple)
Ar1=3
Iz1=7.16197E-1
Iy1=7.16197E-1
Tkz1=1.95441
Tky1=1.95441
Ix1=1.43239
R,2,Ar1,Iz1,Iy1,Tkz1,Tky1,
RMORE,,Ix1
!Material Properties of Single Bounds
MPTEMP,1,0
MPDATA,EX,1,,167.441
MPDATA,PRXY,1,,0
NLGEOM,ON
!Circular Section Definition
SECTYPE,1,BEAM,CSOLID,SINGLE,
R=Tkz/2
SECDATA,R,,
!Material Properties of Triple Bounds
MPTEMP,1,0
MPDATA,EX,2,,25.8523
MPDATA,PRXY,2,,0
NLGEOM,ON
!Circular Section Definition
SECTYPE,2,BEAM,CSOLID,TRIPLE,
R=Tkz1/2
SECDATA,R,,
!Material Properties of Aromatic Bounds
MPTEMP,1,0
MPDATA,EX,3,,167.617
MPDATA,PRXY,3,,0
NLGEOM,ON
!Circular Section Definition
SECTYPE,3,BEAM,CSOLID,AROMATIC,
R=Tkz/2
SECDATA,R,,
!VdW Element
ET,2,LINK180
R,3,Tkz
!Material Properties VdW - Hexahedron
MPTEMP,1,0
MPDATA,EX,4,,5.94507E-1
MPDATA,PRXY,4,,0
NLGEOM,ON
!Material Properties VdW - Triangular (Parallel)
MPTEMP,1,0
MPDATA,EX,5,,1.37154E-1
MPDATA,PRXY,5,,0
NLGEOM,ON
!Material Properties VdW - Triangular (Crossed)
MPTEMP,1,0
MPDATA,EX,6,,6.13147E-1
MPDATA,PRXY,6,,0
NLGEOM,ON
!sin30
ANG1=SIN(PI/6)
!cos30
ANG2=COS(PI/6)
!Aromatic Bound
A=1.49
!Single Bound
S=1.48
!Triple Bound
T=1.19
AA=A*ANG2
AB=A*ANG1
A2=2*A
AC=(A2+S)*ANG2
AD=S*ANG1
AI=2*S+T
AE=(AI)*ANG1
AF=(A2+AI)*ANG2
AG=(A+S+T)*ANG2
AH=(A2+S+T)*ANG2
AJ=(4*A+3*S+2*T)*ANG2
AK=(3*A+3*S+2*T)*ANG2
AL=S+T
AM=AG+AC
AN=(A2+3*S+2*T)*ANG2
!Molecular Size in Armchair Direction
MSize=3*A+AI+2*AI*ANG1+2*AB
!Atom Coordinates
K,1,0,0
K,2,A,0
K,3,A+AB,AA
K,4,A,2*AA
K,5,0,2*AA
K,6,-AB,AA
K,7,A+AB+S,AA
K,8,A+AB+AL,AA
K,9,A+AB+AI,AA
K,10,A+2*AB+AI,2*AA
K,11,A+(A2-S)*ANG1+AI,AC
K,12,A+(A2-AL)*ANG1+AI,T*ANG2+AC
K,13,A2+AE,AF
K,14,A+AE,AF
K,15,A+AL*ANG1,T*ANG2+AC
K,16,A+AD,AC
K,17,-AD,AC
K,18,-AL*ANG1,T*ANG2+AC
K,19,-AE,AL*ANG2+AC
K,20,-(AI-A)*ANG1,AM
K,21,-(AI-A)*ANG1+S,AM
K,22,-(AI-A)*ANG1+AL,AM
K,23,-(AI-A)*ANG1+AI,AM
K,24,-AE-A,AL*ANG2+AC
K,25,-(AI+A)*ANG1-A,AM
K,26,-AE-A,AH+AC
K,27,-AE,AH+AC
K,28,-AL*ANG1,AF+AC
K,29,-AD,2*AG+AC
K,30,0,AN+AC
K,31,A,AN+AC
K,32,A+AD,2*AG+AC
K,33,A+AL*ANG1,AF+AC
K,34,A+AE,AH+AC
K,35,A+AB,AK+AC
K,36,A,AJ+AC
K,37,0,AJ+AC
K,38,-AB,AK+AC
K,39,A+AB+S,AK+AC
K,40,A+AB+AL,AK+AC
K,41,A+AB+AI,AK+AC
K,42,A+2*AB+AI,AN+AC
K,43,A+(A2-S)*ANG1+AI,2*AG+AC
K,44,A+(A2-AL)*ANG1+AI,AF+AC
K,45,A2+AE,AH+AC
K,46,A2+(AI+A)*ANG1,AM
K,47,A2+(AI+A)*ANG1+S,AM
K,48,A2+(AI+A)*ANG1+AL,AM
K,49,A2+(AI+A)*ANG1+AI,AM
K,50,A2+(AI+A2)*ANG1+AI,AH+AC
K,51,A2+(AI+A2)*ANG1+AI,AL*ANG2+
AC
K,52,A2+(AL+A2)*ANG1+AI,AF+AC
K,53,A2+(S+A2)*ANG1+AI,2*AG+AC
K,54,A2+2*AB+AI,AN+AC
K,55,A2+(AL+A2)*ANG1+AI,T*ANG2+A
C
K,56,A2+(S+A2)*ANG1+AI,AC
K,57,A2+2*AB+AI,2*AA
K,58,A+2*AB+AI,0
K,59,A2+2*AB+AI,0
K,60,A2+3*AB+AI,AA
K,61,A2+3*AB+AI,AK+AC
K,62,A2+2*AB+AI,AJ+AC
K,63,A+2*AB+AI,AJ+AC
K,64,A2+(AI+A2)*ANG1+AI+A,AH+AC
K,65,A2+(AI+A2)*ANG1+AI+A,AL*ANG
2+AC
K,66,A2+3*AB+AI+S,AA
K,67,A2+3*AB+AI+AL,AA
K,68,A2+3*AB+AI+S,AK+AC
K,69,A2+3*AB+AI+AL,AK+AC
!Carbon Linkages
L,1,2,1      !Aromatic 1
L,2,3,1      !Aromatic 2
L,3,4,1      !Aromatic 3
L,4,5,1      !Aromatic 4
L,5,6,1      !Aromatic 5
L,1,6,1      !Aromatic 6
LSEL,S,LINE,,1,6,1
LATT,3,1,1,,,,3
L,3,7,1      !Single 7
LSEL,S,LINE,,7
LATT,1,1,1,,,,1
L,7,8,1      !Triple 8
LSEL,S,LINE,,8
LATT,2,2,1,,,,2
L,8,9,1      !Single 9
LSEL,S,LINE,,9
LATT,1,1,1,,,,1
L,9,10,1     !Aromatic 10
LSEL,S,LINE,,10
LATT,3,1,1,,,,3
L,10,11,1    !Single 11
LSEL,S,LINE,,11
LATT,1,1,1,,,,1
L,11,12,1    !Triple 12
LSEL,S,LINE,,12
LATT,2,2,1,,,,2
L,12,13,1    !Single 13
LSEL,S,LINE,,13
LATT,1,1,1,,,,1
L,13,14,1    !Aromatic 14
LSEL,S,LINE,,14
LATT,3,1,1,,,,3
L,14,15,1    !Single 15
LSEL,S,LINE,,15
LATT,1,1,1,,,,1
L,15,16,1    !Triple 16
LSEL,S,LINE,,16
LATT,2,2,1,,,,2
L,16,4,1     !Single 17
L,5,17,1     !Single 18
LSEL,S,LINE,,17,18,1
LATT,1,1,1,,,,1
L,17,18,1    !Triple 19
LSEL,S,LINE,,19
LATT,2,2,1,,,,2
L,18,19,1    !Single 20
LSEL,S,LINE,,20
LATT,1,1,1,,,,1
L,19,20,1    !Aromatic 21
LSEL,S,LINE,,21
LATT,3,1,1,,,,3
L,20,21,1    !Single 22
LSEL,S,LINE,,22
LATT,1,1,1,,,,1
L,21,22,1    !Triple 23
LSEL,S,LINE,,23
LATT,2,2,1,,,,2
L,22,23,1    !Single 24
LSEL,S,LINE,,24
LATT,1,1,1,,,,1
L,23,14,1    !Aromatic 25
L,19,24,1    !Aromatic 26
L,24,25,1    !Aromatic 27
L,25,26,1    !Aromatic 28
L,26,27,1    !Aromatic 29
L,27,20,1    !Aromatic 30
LSEL,S,LINE,,25,30,1
LATT,3,1,1,,,,1
L,27,28,1    !Single 31
LSEL,S,LINE,,31
LATT,1,1,1,,,,1
L,28,29,1    !Triple 32
LSEL,S,LINE,,32
LATT,2,2,1,,,,2
L,29,30,1    !Single 33
LSEL,S,LINE,,33
LATT,1,1,1,,,,1
L,30,31,1    !Aromatic 34
LSEL,S,LINE,,34
LATT,3,1,1,,,,3
L,31,32,1    !Single 35
LSEL,S,LINE,,35
LATT,1,1,1,,,,1
L,32,33,1    !Triple 36
LSEL,S,LINE,,36
LATT,2,2,1,,,,2
L,33,34,1    !Single 37
LSEL,S,LINE,,37
LATT,1,1,1,,,,1
L,34,23,1    !Aromatic 38
L,31,35,1    !Aromatic 39
L,35,36,1    !Aromatic 40
L,36,37,1    !Aromatic 41
L,37,38,1    !Aromatic 42
L,38,30,1    !Aromatic 43
LSEL,S,LINE,,38,43,1
LATT,3,1,1,,,,3
L,35,39,1    !Single 44
LSEL,S,LINE,,44
LATT,1,1,1,,,,1
L,39,40,1    !Triple 45
LSEL,S,LINE,,45
LATT,2,2,1,,,,2
L,40,41,1    !Single 46
LSEL,S,LINE,,46
LATT,1,1,1,,,,1
L,41,42,1    !Aromatic 47
LSEL,S,LINE,,47
LATT,3,1,1,,,,3
L,42,43,1    !Single 48
LSEL,S,LINE,,48
LATT,1,1,1,,,,1
L,43,44,1    !Triple 49
LSEL,S,LINE,,49
LATT,2,2,1,,,,2
L,44,45,1    !Single 50
LSEL,S,LINE,,50
LATT,1,1,1,,,,1
L,45,34,1    !Aromatic 51
L,45,46,1    !Aromatic 52
L,46,13,1    !Aromatic 53
LSEL,S,LINE,,51,53,1
LATT,3,1,1,,,,3
L,46,47,1    !Single 54
LSEL,S,LINE,,54
LATT,1,1,1,,,,1
L,47,48,1    !Triple 55
LSEL,S,LINE,,55
LATT,2,2,1,,,,2
L,48,49,1    !Single 56
LSEL,S,LINE,,56
LATT,1,1,1,,,,1
L,49,50,1    !Aromatic 57
L,49,51,1    !Aromatic 58
LSEL,S,LINE,,57,58,1
LATT,3,1,1,,,,3
L,50,52,1    !Single 59
LSEL,S,LINE,,59
```

```
LATT,1,1,1,,,,1
L,52,53,1    !Triple  60
LSEL,S,LINE,,60
LATT,2,2,1,,,,2
L,53,54,1    !Single  61
LSEL,S,LINE,,61
LATT,1,1,1,,,,1
L,54,42,1    !Aromatic 62
LSEL,S,LINE,,62
LATT,3,1,1,,,,3
L,51,55,1    !Single  63
LSEL,S,LINE,,63
LATT,1,1,1,,,,1
L,55,56,1    !Triple  64
LSEL,S,LINE,,64
LATT,2,2,1,,,,2
L,56,57,1    !Single  65
LSEL,S,LINE,,65
LATT,1,1,1,,,,1
L,57,10,1    !Aromatic 66
L,9,58,1     !Aromatic 67
L,58,59,1    !Aromatic 68
L,59,60,1    !Aromatic 69
L,60,57,1    !Aromatic 70
L,54,61,1    !Aromatic 71
L,61,62,1    !Aromatic 72
L,62,63,1    !Aromatic 73
L,63,41,1    !Aromatic 74
LSEL,S,LINE,,66,74,1
LATT,3,1,1,,,,3
L,60,66,1    !Single  75
L,61,68,1    !Single  76
LSEL,S,LINE,,75,76,1
LATT,1,1,1,,,,1
L,66,67,1    !Triple  77
L,68,69,1    !Triple  78
LSEL,S,LINE,,77,78,1
LATT,2,2,1,,,,2
L,50,64,1    !Aromatic 79
L,65,51,1    !Aromatic 80
LSEL,S,LINE,,79,80,1
LATT,3,1,1,,,,3
L,1,3,1      !VdW[Hexahedron] 81
L,3,5,1      !VdW[Hexahedron] 82
L,5,1,1      !VdW[Hexahedron] 83
L,6,2,1      !VdW[Hexahedron] 84
L,2,4,1      !VdW[Hexahedron] 85
L,4,6,1      !VdW[Hexahedron] 86
L,9,59,1     !VdW[Hexahedron] 87
L,59,57,1    !VdW[Hexahedron] 88
L,57,9,1     !VdW[Hexahedron] 89
L,58,60,1    !VdW[Hexahedron] 90
L,60,10,1    !VdW[Hexahedron] 91
L,10,58,1    !VdW[Hexahedron] 92
L,24,20,1    !VdW[Hexahedron] 93
L,20,26,1    !VdW[Hexahedron] 94
L,26,24,1    !VdW[Hexahedron] 95
L,25,19,1    !VdW[Hexahedron] 96
L,19,27,1    !VdW[Hexahedron] 97
L,27,25,1    !VdW[Hexahedron] 98
L,14,46,1    !VdW[Hexahedron] 99
L,46,34,1    !VdW[Hexahedron] 100
L,34,14,1    !VdW[Hexahedron] 101
L,23,13,1    !VdW[Hexahedron] 102
L,13,45,1    !VdW[Hexahedron] 103
L,45,23,1    !VdW[Hexahedron] 104
L,30,35,1    !VdW[Hexahedron] 105
L,35,37,1    !VdW[Hexahedron] 106
L,37,30,1    !VdW[Hexahedron] 107
L,38,31,1    !VdW[Hexahedron] 108
L,31,36,1    !VdW[Hexahedron] 109
L,36,38,1    !VdW[Hexahedron] 110
L,41,54,1    !VdW[Hexahedron] 111
L,54,62,1    !VdW[Hexahedron] 112
L,62,41,1    !VdW[Hexahedron] 113
L,42,61,1    !VdW[Hexahedron] 114
L,61,63,1    !VdW[Hexahedron] 115
L,63,42,1    !VdW[Hexahedron] 116
LSEL,S,LINE,,81,116,1
LATT,4,3,2,
L,5,16,1     !VdW[Crossed] 117
LSEL,S,LINE,,117
LATT,6,3,2,
L,16,17,1    !VdW[Parallel] 118
LSEL,S,LINE,,118
LATT,5,3,2,
L,17,4,1     !VdW[Crossed] 119
L,15,23,1    !VdW[Crossed] 120
LSEL,S,LINE,,119,120,1
LATT,6,3,2,
L,22,15,1    !VdW[Parallel] 121
LSEL,S,LINE,,121
LATT,5,3,2,
L,22,14,1    !VdW[Crossed] 122
LSEL,S,LINE,,122
LATT,6,3,2,
L,21,18,1    !VdW[Parallel] 123
LSEL,S,LINE,,81,123
LATT,5,3,2,
L,18,20,1    !VdW[Crossed] 124
L,21,19,1    !VdW[Crossed] 125
L,20,28,1    !VdW[Crossed] 126
LSEL,S,LINE,,124,126,1
LATT,6,3,2,
L,28,21,1    !VdW[Parallel] 127
LSEL,S,LINE,,127
LATT,5,3,2,
L,21,27,1    !VdW[Crossed] 128
L,23,33,1    !VdW[Crossed] 129
LSEL,S,LINE,,128,129,1
LATT,6,3,2,
L,33,22,1    !VdW[Parallel] 130
LSEL,S,LINE,,130
LATT,5,3,2,
L,22,34,1    !VdW[Crossed] 131
L,31,29,1    !VdW[Crossed] 132
LSEL,S,LINE,,131,132,1
LATT,6,3,2,
L,29,32,1    !VdW[Parallel] 133
LSEL,S,LINE,,133
LATT,5,3,2,
L,32,30,1    !VdW[Crossed] 134
L,31,39,1    !VdW[Crossed] 135
LSEL,S,LINE,,134,135,1
LATT,6,3,2,
L,39,32,1    !VdW[Parallel] 136
LSEL,S,LINE,,136
LATT,5,3,2,
L,32,35,1    !VdW[Crossed] 137
L,40,42,1    !VdW[Crossed] 138
LSEL,S,LINE,,137,138,1
LATT,6,3,2,
L,40,43,1    !VdW[Parallel] 139
LSEL,S,LINE,,139
LATT,5,3,2,
L,43,41,1    !VdW[Crossed] 140
L,34,44,1    !VdW[Crossed] 141
LSEL,S,LINE,,140,141,1
LATT,6,3,2,
L,44,33,1    !VdW[Parallel] 142
LSEL,S,LINE,,142
LATT,5,3,2,
L,33,45,1    !VdW[Crossed] 143
L,43,54,1    !VdW[Crossed] 144
LSEL,S,LINE,,143,144,1
LATT,6,3,2,
L,43,53,1    !VdW[Parallel] 145
LSEL,S,LINE,,145
LATT,5,3,2,
L,53,42,1    !VdW[Crossed] 146
L,46,44,1    !VdW[Crossed] 147
LSEL,S,LINE,,146,147,1
LATT,6,3,2,
L,44,47,1    !VdW[Parallel] 148
LSEL,S,LINE,,148
LATT,5,3,2,
L,47,45,1    !VdW[Crossed] 149
L,50,48,1    !VdW[Crossed] 150
LSEL,S,LINE,,149,150,1
LATT,6,3,2,
L,48,52,1    !VdW[Parallel] 151
LSEL,S,LINE,,151
LATT,5,3,2,
L,52,49,1    !VdW[Crossed] 152
L,13,47,1    !VdW[Crossed] 153
LSEL,S,LINE,,152,153,1
LATT,6,3,2,
L,47,12,1    !VdW[Parallel] 154
LSEL,S,LINE,,154
LATT,5,3,2,
L,12,46,1    !VdW[Crossed] 155
L,49,55,1    !VdW[Crossed] 156
LSEL,S,LINE,,155,156,1
LATT,6,3,2,
L,55,48,1    !VdW[Parallel] 157
LSEL,S,LINE,,157
LATT,5,3,2,
L,48,51,1    !VdW[Crossed] 158
L,10,56,1    !VdW[Crossed] 159
LSEL,S,LINE,,158,159,1
LATT,6,3,2,
L,56,11,1    !VdW[Parallel] 160
LSEL,S,LINE,,160
LATT,5,3,2,
L,11,57,1    !VdW[Crossed] 161
L,9,11,1     !VdW[Crossed] 162
LSEL,S,LINE,,161,162,1
LATT,6,3,2,
L,11,8,1     !VdW[Parallel] 163
LSEL,S,LINE,,163
LATT,5,3,2,
L,8,10,1     !VdW[Crossed] 164
L,3,16,1     !VdW[Crossed] 165
LSEL,S,LINE,,164,165,1
LATT,6,3,2,
L,16,7,1     !VdW[Parallel] 166
LSEL,S,LINE,,166
LATT,5,3,2,
L,7,4,1      !VdW[Crossed] 167
L,15,13,1    !VdW[Crossed] 168
LSEL,S,LINE,,167,168,1
LATT,6,3,2,
L,15,12,1    !VdW[Parallel] 169
LSEL,S,LINE,,169
LATT,5,3,2,
L,12,14,1    !VdW[Crossed] 170
L,54,68,1    !VdW[Crossed] 171
LSEL,S,LINE,,170,171,1
LATT,6,3,2,
L,68,53,1    !VdW[Parallel] 172
LSEL,S,LINE,,172
LATT,5,3,2,
L,53,61,1    !VdW[Crossed] 173
L,60,56,1    !VdW[Crossed] 174
LSEL,S,LINE,,173,174,1
LATT,6,3,2,
L,56,66,1    !VdW[Parallel] 175
LSEL,S,LINE,,175
LATT,5,3,2,
L,66,57,1    !VdW[Crossed] 176
LSEL,S,LINE,,176
LATT,6,3,2,
LSEL,ALL
!Molecule 2 in Armchair Direction
LOCAL,11,0,2*A+AI+3*AB+AI/2,AJ+AC,
0,,,,1,1,
LSYMM,X,ALL, , , ,0,0
NUMMRG,ALL
NUMCMP,ALL
!VdW after Mirror
L,52,64,1    !VdW[Crossed] 349
LSEL,S,LINE,,349
LATT,6,3,2,
L,52,119,1   !VdW[Parallel] 350
LSEL,S,LINE,,350
LATT,5,3,2,
L,119,50,1   !VdW[Crossed] 351
LSEL,S,LINE,,351
LATT,6,3,2,
L,50,118,1   !VdW[Hexahedron] 352
L,118,51,1   !VdW[Hexahedron] 353
L,50,51,1    !VdW[Hexahedron] 354
L,49,64,1    !VdW[Hexahedron] 355
L,64,65,1    !VdW[Hexahedron] 356
L,65,49,1    !VdW[Hexahedron] 357
LSEL,S,LINE,,352,357,1
LATT,4,3,2,
L,65,55,1    !VdW[Crossed] 358
LSEL,S,LINE,,358
LATT,6,3,2,
L,55,122,1   !VdW[Parallel] 359
LSEL,S,LINE,,359
LATT,5,3,2,
L,122,51,1   !VdW[Crossed] 360
LSEL,S,LINE,,360
LATT,6,3,2,
LSEL,ALL
!Molecule 3 & 4 in Armchair Direction
LOCAL,12,0,2*A+AI+3*AB+AI/2+MSize,
AJ+AC,0,,,,1,1,
LSYMM,X,ALL, , , ,0,0
CSDELE,ALL, ,
K,261,A2+3*AB+AI+S+MSize,AK+AC
K,262,A2+3*AB+AI+AL+MSize,AK+AC
K,263,A2+3*AB+AI+S+MSize,AA
K,264,A2+3*AB+AI+AL+MSize,AA
L,107,261,1  !Single 721
LSEL,S,LINE,,721
LATT,1,1,1,,,,1
L,261,262,1  !Triple 722
LSEL,S,LINE,,722
LATT,2,2,1,,,,2
L,262,237,1  !Single 723
L,75,263,1   !Single 724
LSEL,S,LINE,,723,724,1
LATT,1,1,1,,,,1
L,263,264,1  !Triple 725
LSEL,S,LINE,,725
LATT,2,2,1,,,,2
L,264,205,1  !Single 726
LSEL,S,LINE,,726
LATT,1,1,1,,,,1
NUMMRG,ALL
NUMCMP,ALL
!VdW after Mirror
L,99,255,1   !VdW[Crossed] 715
LSEL,S,LINE,,715
LATT,6,3,2,
L,255,98,1   !VdW[Parallel] 716
LSEL,S,LINE,,716
LATT,5,3,2,
L,98,107,1   !VdW[Crossed] 717
L,256,223,1  !VdW[Crossed] 718
LSEL,S,LINE,,717,718,1
LATT,6,3,2,
L,256,222,1  !VdW[Parallel] 719
LSEL,S,LINE,,719
LATT,5,3,2,
L,222,231,1  !VdW[Crossed] 720
L,96,221,1   !VdW[Crossed] 721
LSEL,S,LINE,,720,721,1
LATT,6,3,2,
L,221,97,1   !VdW[Parallel] 722
LSEL,S,LINE,,722
LATT,5,3,2,
L,97,95,1    !VdW[Crossed] 723
L,88,217,1   !VdW[Crossed] 724
LSEL,S,LINE,,723,724,1
LATT,6,3,2,
L,217,87,1   !VdW[Parallel] 725
LSEL,S,LINE,,725
LATT,5,3,2,
L,87,93,1    !VdW[Crossed] 726
L,75,86,1    !VdW[Crossed] 727
LSEL,S,LINE,,726,727,1
```

```
LATT,6,3,2,
L,86,257,1    !VdW[Parallel] 728
LSEL,S,LINE,,728
LATT,5,3,2,
L,257,74,1    !VdW[Crossed] 729
L,216,205,1   !VdW[Crossed] 730
LSEL,S,LINE,,729,730,1
LATT,6,3,2,
L,216,258,1   !VdW[Parallel] 731
LSEL,S,LINE,,731
LATT,5,3,2,
L,258,204,1   !VdW[Crossed] 732
LSEL,S,LINE,,732
LATT,6,3,2,
LSEL,ALL
!Molecule 5 to 7 in Armchair Direction
LOCAL,13,0,2*A+AI+3*AB+AI/2+3*MSi
ze,AJ+AC,0,,,1,1,
LSYMM,X,ALL, , , ,0,0
CSDELE,ALL, ,
K,517,A2+3*AB+AI+S+3*MSize,AK+AC
K,518,A2+3*AB+AI+AL+3*MSize,AK+A
C
K,519,A2+3*AB+AI+S+3*MSize,AA
K,520,A2+3*AB+AI+AL+3*MSize,AA
L,168,517,1   !Single 1465
LSEL,S,LINE,,1465
LATT,1,1,1,,,,1
L,517,518,1   !Triple 1466
LSEL,S,LINE,,1466
LATT,2,2,1,,,,2
L,518,426,1   !Single 1467
L,136,519,1   !Single 1468
LSEL,S,LINE,,1467,1468,1
LATT,1,1,1,,,,1
L,519,520,1   !Triple 1469
LSEL,S,LINE,,1469
LATT,2,2,1,,,,2
L,520,394,1   !Single 1470
LSEL,S,LINE,,1470
LATT,1,1,1,,,,1
LSEL,ALL
LDELE,733,788,1,1
LDELE,791,810,1,1
LDELE,813,908,1,1
LDELE,983,984,1,1
LDELE,1075,1083,1,1
LDELE,1090,1092,1,1
NUMMRG,ALL
NUMCMP,ALL
L,160,447,1   !VdW[Crossed] 1273
LSEL,S,LINE,,1273
LATT,6,3,2,
L,447,159,1   !VdW[Parallel] 1274
LSEL,S,LINE,,1274
LATT,5,3,2,
L,159,168,1   !VdW[Crossed] 1275
L,157,346,1   !VdW[Crossed] 1276
LSEL,S,LINE,,1275,1276,1
LATT,6,3,2,
L,346,158,1   !VdW[Parallel] 1277
LSEL,S,LINE,,1277
LATT,5,3,2,
L,158,156,1   !VdW[Crossed] 1278
L,356,347,1   !VdW[Crossed] 1279
LSEL,S,LINE,,1278,1279,1
LATT,6,3,2,
L,347,448,1   !VdW[Parallel] 1280
LSEL,S,LINE,,1280
LATT,5,3,2,
L,448,348,1   !VdW[Crossed] 1281
L,149,342,1   !VdW[Crossed] 1282
LSEL,S,LINE,,1281,1282,1
LATT,6,3,2,
L,342,148,1   !VdW[Parallel] 1283
LSEL,S,LINE,,1283
LATT,5,3,2,
L,148,154,1   !VdW[Crossed] 1284
L,136,147,1   !VdW[Crossed] 1285
LSEL,S,LINE,,1284,1285,1
LATT,6,3,2,
L,147,449,1   !VdW[Parallel] 1286
LSEL,S,LINE,,1286
LATT,5,3,2,
L,449,135,1   !VdW[Crossed] 1287
L,330,341,1   !VdW[Crossed] 1288
LSEL,S,LINE,,1287,1288,1
LATT,6,3,2,
L,341,450,1   !VdW[Parallel] 1289
LSEL,S,LINE,,1289
LATT,5,3,2,
L,450,329,1   !VdW[Crossed] 1290
LSEL,S,LINE,,1290
LATT,6,3,2,
LSEL,ALL
NUMMRG,ALL
NUMCMP,ALL
!Molecule 2 in ZigZag Direction
LOCAL,14,0,0,AK+AC,0, , , ,1,1,
LSYMM,Y,ALL, , , ,0,0
NUMMRG,ALL
NUMCMP,ALL
!Molecule 3 and 4 in ZigZag Direction
LOCAL,15,0,0,2*(AK+AC)-AA,0, , , ,1,1,
LSYMM,Y,ALL, , , ,0,0
NUMMRG,ALL
NUMCMP,ALL
!Molecule 5 to 8 in ZigZag Direction
LOCAL,16,0,0,4*(AK+AC)-3*AA,0,    ,    ,
,1,1,
LSYMM,Y,ALL, , , ,0,0
NUMMRG,ALL
NUMCMP,ALL
CSDELE,ALL, ,
LMESH,ALL
!-----------------------
!Boundary Conditions and apllied forces
Fb=82/83
DK,ALL,UZ
!Left
KSEL,S,LOC,X,-AE,0
DK,ALL,UX
KSEL,ALL
!Right
KSEL,S,LOC,X,94.1,96.3
FK,ALL,FX,Fb
KSEL,ALL
!Central Left Kp
DK,796,UY
!Central Right Kp
DK,1111,UY
!Solution
FINISH
/SOL
/STATUS,SOLU
SOLVE
FINISH
!Displacement Plot
/POST1
PLDISP,2
!Displacement Lists in X and Y
PRNSOL,U,X
PRNSOL,U,Y
```